UNIVERSITY OF BELGRADE

FACULTY OF TECHNOLOGY AND METALLURGY

Danica V. Brzić

APPLICATION OF NONLINEAR FREQUENCY RESPONSE METHOD FOR INVESTIGATION OF EQULIBRIUM AND KINETICS OF GAS-SOLID ADSORPTION

Doctoral Dissertation

Belgrade, 2016

UNIVERZITET U BEOGRADU

TEHNOLOŠKO-METALURŠKI FAKULTET

Danica V. Brzić

PRIMENA NELINEARNE FREKVENTNE METODE NA ISPITIVANJE RAVNOTEŽE I KINETIKE ADSORPCIONIH SISTEMA GAS-ČVRSTO

Doktorska disertacija

Beograd, 2016

Graduation committee:

Supervisor:	dr Menka Petkovska, full professor University of Belgrade Faculty of Technology and Metallurgy
Members:	dr Nikola Nikačević, associate professor University of Belgrade Faculty of Technology and Metallurgy
	dr Radmila Garić-Grulović, senior research scientist Institute for Chemistry, Technology and Metallurgy Belgrade

Date of the defense: Belgrade, 24.06.2016.

Ackowledgements

The experimental part of this dissertation has been done in the frame of the collaborative project between Faculty of Technology and Metallurgy and R&D department of the German chemical company BASF SE "Experimental investigation of mass transport limitations in adsorption, based on the Nonlinear Frequency Response method". I would like to thank my supervisor prof. dr Menka Petkovska for providing me the opportunity to participate in this project. That was an important experience for me. Professor Petkovska had also always "the open door" for all my questions and doubts.

I am thankful to dr Frank Poplow for guiding my work in BASF SE Ludwigshafen and for his significant contribution in designing the experimental set-up. I also highly appreciate the technical support of Jürgen Brauch and Dieter Hibinger. With their experience and willingness to solve the problems, they contributed significantly to the construction of experimental set-up and were my strong daily support.

I would like to thank to my colleagues from the Department of Chemical Engineering, dr Nikola Nikačević for useful suggestions and encouragement as well as dr Nevenka Bošković-Vragolović and dr Milan Milivojević for their continious interest in progress of my work and willingness to hear my problems.

I am thankfull to my friends Emina, Ana, Dragan, Maja, Dubravka, Evangelia and Desislava, who were, each of them on his own way, the strong support for me.

I thank to my parents for their support during my whole education. My deepest thanks go to my sister Olivera and brother-in-low Milan for their love and understanding. And above all, I am thankfull to my little angel Nadja. Her comming on the world was a special motivation for me to finish this work.

Danica Brzić

Abstract

The understanding of complex kinetic mechanisms of gas-solid adsorption is a challenging issue. The Frequency Response (FR) method, which has commonly been used for studying the kinetics of adsorption, analyzes the frequency response of the system in a linear range, and therefore partly fails to identify and characterize the kinetics of nonlinear adsorption phenomena. In the frame of this thesis, the applicability of a new Nonlinear Frequency Response (NFR) method for characterization of kinetics and equilibria of gas adsorption, was investigated.

The NFR method is based on the analysis of the frequency responses for a rather large amplitude input excitation, named Nonlinear Frequency Responses, and determination of the higher-order frequency response functions (FRFs), by applying the Volterra series and generalized Fourier transform. The applicability of the NFR method for characterization of kinetics and equilibria of pure gas adsorption was investigated both theoretically and experimentally, for the case of a batch adsorber. The critical issue regarding the applicability of the NFR method was determination of the second-order FRF on the adsorbent particle scale. The theoretical investigation comprises two parts. The first part of investigation is based on the numerical simulations of the dynamic responses of a batch adsorption system, by using mathematical models on the adsorber scale and adsorbent particle scale. As a result, the procedure for designing the NFR experiments has been established. In the second part, the theoretical FRFs up to the second-order for nonisothermal macropore diffusion (NMD) model, as one of the common mechanisms of gas-solid adsorption, have been derived and analyzed. As a result, the methodology for estimation of the parameters of NMD model, based on the characteristics of the FRFs, was established. In order to validate the NFR method experimentally, a new experimental set-up was designed and constructed. The working principle of the apparatus is modulation of the volume of the closed cell in a sinusiodal way, with variable amplitude and frequency, and measuring the pressure, adsorbent temperature and gas temperature responses. The test system was CO_2/ zeolite 5A particles. The results showed that the NFR method can be applied for identification of the kinetic mechanism and estimation of equilibrium and kinetic data. It was also shown, that it is advantageous compared to the linear FR method in terms of reliability of identification of the kinetic model based on the second-order FRF, as well as in the possibility to estimate both kinetic and equilibrium data.

Since this work represents the first evidence of experimental application of the NFR method for investigation of gas adsorption, it opens significant new perspectives in this field.

Key words: Nonlinear frequency response, Gas adsorption, Second-order FRF, Model identification, Parameter estimation, Nonisothermal macropore diffusion

Scientific field: Chemistry and Chemical Technology
Scientific sub-field: Chemical Engineering
UDK number: 66.021.3.081.3:531.3:66.071.6

Izvod

Razumevanje složenih kinetičkih mehanizama adsorpcije gas-čvrsto predstavlja izazov u savremenom istraživanju. Klasična Frekventna metoda, koja se uobičajeno koristi za ispitivanje kinetike adsorpcije, analizira frekventni odziv sistema u linearnoj oblasti i zato ne može u potpunosti da okarakteriše kinetiku nelinearnih procesa adsorpcije. U okviru ove disertacije ispitivana je primenljivost metode Nelinearnog Frekventnog Odziva (NFO) za karakterizaciju kinetike i ravnoteže adsorpcije gas-čvrsto.

Metoda NFO se zasniva na analiziranju frekventnog odziva sistema na ulaznu pobudu relativno velike amplitude i određivanju frekventnih prenosnih funkcija (FPF) višeg reda, uz korišćenje Volterra redova i generalizovane Furijeove transformacije. Primenljivost metode NFO za karakterizaciju kinetike i ravnoteže adsorpcije čistih gasova je ispitivana teorijski i eksperimentalno u zatvorenom (šaržnom) sistemu. Ključno pitanje u pogledu primenljivosti metode NFO je mogućnost određivanja frekventne prenosne funkcije drugog reda na nivou čestice adsorbensa. Teorijsko istraživanje se sastoji od dva dela. Prvi deo se zasniva na numeričkim simulacijama dinamičkih odziva šaržnog adsorbera, uz korišćenje matematičkih modela na nivou adsorbera i na nivou čestice adsorbensa. Na osnovu dobijenih rezultata ustanovljena je procedura za planiranje nelinearnih frekventnih eksperimenata. U drugom delu, izvedene su i analizirane FPF prvog i drugog reda za model neizotermne difuzije kroz makropore, koji je jedan od čestih mehanizama adsorpcije gasova. Na osnovu rezultata ustanovljena je procedura za određivanje parametara pomenutog modela na osnovu karakteristika FPF. Da bi se metoda eksperimentalno potvrdila, projektovan je i izgrađen novi eksperimentalni sistem. Princip rada ovog sistema je promena zapremine sistema po sinusnom zakonu, sa promenljivom amplitudom i frekvencijom, i merenje odziva pritiska gasa, temperature adsorbensa i temperature gasa. Kao test sistem za eksperimente korišćen je adsorpcioni sistem CO_2/ zeolit 5A. Rezultati su pokazali da je moguće primeniti metodu NFO za utvrđivanje kinetičkog mehanizma adsorpcije gasova kao i za određivanje kinetičkih i ravnotežnih parametara. Takođe je pokazano da metoda NFO ima značajne prednosti u odnosu na klasičnu (linearnu) frekventnu metodu, i to u pogledu pouzdanosti utvrđivanja kinetičkog mehanizma na osnovu oblika FPF drugog reda kao i u pogledu mogućnosti određivanja i kinetičkih i ravnotežnih podataka iz istih eksperimentalnih podataka.

U ovom radu je prvi put eksperimentalno potvrđena mogućnost ispitivanja adsorpcije gas-čvrsto korišćenjem metode NFO, čime se otvaraju značajne nove perspektive u toj oblasti.

Ključne reči: Nelinearni frekventni odziv, Adsorpcija gas-čvrsto, Frekventna funkcija drugog reda, Identifikacija modela, Određivanje parametara, Neizotermna difuzija kroz makropore

Naučna oblast: Hemija i hemijska tehnologija
Uža naučna oblast: Hemijsko inženjerstvo
UDK broj: 66.021.3.081.3:531.3:66.071.6

CONTENTS

List of symbols

A amplitude of the input

a_p first-order concentration coefficient of the adsorption isotherm (Table 5.1.1)

a_q dimensionless first-order derivative of the inverse adsorption isotherm (Eq.4.1.6)

a_T first-order temperature coefficient of the adsorption isotherm (Table 5.1.1)

B amplitude of the output

b_p second-order concentration coefficient of the adsorption isotherm (Table 5.1.1)

b_{pT} second-order mixed coefficient of the adsorption isotherm (Table 5.1.1)

b_q dimensionless second-order derivative of the inverse adsorption isotherm

b_T second-order temperature coefficient of the adsorption isotherm (Table 5.1.1)

c_i dimensionless sorbate concentration in the pore (Table 5.1.1)

C_i sorbate concentration in the pore (mol/m^3)

c_{ps} heat capacity of the adsorbent (J/(kg·K))

D_p diffusion coefficient (m^2/s)

d_p particle diameter (m)

e parameter (Eq. (5.3.5))

e^* parameter (Eq. (6.7.4))

f parameter (Eq. (5.3.13))

$F_n(\omega_1, \omega_2, \ldots \omega_n)$ n-th order FRF relating adsorbed quantity to pressure

$G_n(\omega_1, \omega_2, \ldots \omega_n)$ n-th order FRF relating pressure to volume

$G_{nb}(\omega_1, \omega_2, \ldots \omega_n)$ n-th order FRF relating pressure to volume in a blank experiment

h heat transfer coefficient (W/(m^{2}K))

$H_n(\omega_1, \omega_2, \ldots \omega_n)$ n-th order FRF relating particle temperature to pressure

$I_n(\omega_1, \omega_2, \ldots \omega_n)$ n-th order FRF relating gas temperature to volume

$J_n(\omega_1, \omega_2, \ldots \omega_n)$ n-th order FRF relating adsorbed quantity to volume

$W_n(\omega_1, \omega_2, \ldots \omega_n)$ n-th order FRF relating particle temperature to volume

K_1 static gain due to compression (mol/(m^3)^2)

K_2 static gain due to adsorption (mol/(m^3)^2)

k_a mass transfer coefficient (s^{-1})

k_m modified mass transfer coefficient (Eq. 4.1.4)

m_p mass of the adsorbent (kg)

N number of data points

N_T number of periods of the time wave-form

p dimensionless pressure

P pressure (Pa)

q dimensionless sorbate concentration in the adsorbent particles

Q sorbate concentration in the adsorbent particles (loading) (mol/m^3)

q_i dimensionless sorbate concentration in the solid phase (Table 5.1.1)

Q_i sorbate concentration in the solid phase (mol/m^3)

R radius of the adsorbent particle (m)

r spatial coordinate

R_g universal gas constant (J/(molK))

T period of the time wave-form (s)

t time (s)

t_D diffusional time constant (Eq.5.4.2)

T_g gas temperature (K)

t_h heat transfer time constant (Eq. 5.4.3)

T_p particle temperature (K)

t_s sampling interval (s)

T_s temperature in the staedy-state (K)

v dimensionless volume of the adsorber

V volume of adsorber (m^3)

V_p volume of the adsorbent particles (m^3)

x input

X input harmonic

y output

Y_n Fourier transform of n-th harmonic of the pressure change (Pa)

Z_n Fourier transform of n-th harmonic of the particle temperature change (K)

Greek letters

$(-\Delta H)$	heat of adsorption (J/mol)
β	partition coefficient
β^*	parameter in Eqs.(6.5.3) and (6.5.4), ($Pa \cdot m^6$ /mol)
δ	nonisothermality coefficient (eq 5.4.4)
δK	relative deviation of the static gain from the linear value
ε_p'	modified porosity of the adsorbent particle (Table 5.1.1)
ε_p	porosity of the adsorbent particle
ζ	modified heat transfer coefficient (Table 5.1.1)
θ_g	dimensionless gas temperature (Table 5.1.1)
θ_p	dimensionless particle temperature (Table 5.1.1)
ξ	modified heat of adsorption (Table 5.1.1)
ξ^*	modified heat of adsorption ($\xi^*=(-\Delta H)/(\rho_p c_{ps})$)
ρ_p	bulk density of the adsorbent (kg/m^3)
σ	shape factor
τ	apparent time constant (s)
τ_D	diffusional time constant (s)
τ_F	time constant (s)(eq.(4.4.3))
τ_h	heat transfer time constant (s)
φ	phase shift
ω	frequency (rad/s)
ω^*	dimensionless frequency (eq. (4.3.3)

Abbreviations

FR	Frequency Response
FRF	Frequency Response Function
NFR	Nonlinear Frequency Response
PFG	Pulsed Field Gradient
NMR	Nuclear Magnetic Resonance
QENS	Quasi Elastic Neutron Scattering
ZLC	Zero Length Column

1. INTRODUCTION

1.1 State of the art and motivation

Separation processes play critical roles in a majority of process industries. Besides being the major operations (as in production of O_2 and N_2 from ambient air), separations are employed in pretreatment of raw materials, separation of recycle streams, purification of products and removal of pollutants from waste streams. The fact that separation processes account for 40-70% of both capital and operating costs (Humphrey and Keller, 1997) reflects how accuracy of the design of separation processes affects the revenue.

Adsorption is one of the most important technologies for separation processes in chemical, petrochemical, environmental and pharmaceutical industry. Production of H_2 from various gases, production of O_2 and N_2 enriched air from ambient air, gas drying, trace impurity removal from contaminated gases, CO_2 capture are the most important commercial gas phase adsorption separations. Different types of natural and synthetic zeolites and activated carbon are the most commonly used adsorbents for those separations. There are several hundred thousand adsorption units operated all over the world (Sircar, 2006).

Although adsorption has a long history, the adsorptive technologies are still the subject of intensive research and development, according to the increasing number of scientific articles and patents (Sircar, 2006). Besides the above mentioned processes, for which the adsorption is the state of the art technology, the new applications are continually being explored such as preventing of global warming and ozone layer depletion (Suzuki, 1996), nuclear waste processing (Tranter et al., 2003), etc. The new types of adsorbents are also being designed as cellulosic nanofibers, metal organic frameworks (MOFs), etc.

The adsorptive process design requires accurate data on three core adsorptive properties: equilibrium, kinetics and heat of adsorption. Adsorption equilibrium is defined by adsorption isotherm, i.e. the relation between solid-phase and fluid-phase concentrations of the adsorbate at a constant temperature, which is most often nonlinear and has to be determined experimentally. Adsorption kinetics defines the rate of adsorption and refers to identification of the most appropriate model equation that describes the dynamic of

accumulation of the adsorbate on the solid surface and estimation of the kinetic constant(s). Quantity of heat released during adsorption is important because it determines the degree of nonisothermality of the process. Since the molecules of adsorbate may have different sizes, polarities and polarizabilities and solid adorbents may have different structure and energetical heterogenities, the behavior of the mentioned adsorption features may be very complex. Therefore, the characterization of adsorption systems of commercial importance is often a challenging task. A variety of methods for measuring individual adsorptive properties have been developed and described in literature. Regarding the measurements of adsorption isotherms, gravimetric, volumetric and chromatographic methods are mainly employed. The kinetic data measurements (mostly measurements of diffusion coefficients) are divided into microscopic (PFG-NMR, QENS) and macroscopic methods (Wicke-Callanbach, ZLC, uptake rate and frequency response). The heats of adsorption are measured by microcalorimetry. Good reviews regarding those methods can be found in classical adsorption books (Rouquerol et al., 1999, Do, 1998, Kärger and Ruthven, 1992). The experimental determination of adsorption equilibria and heats of adsorption are mainly well established. However, in-depth understanding of the complex kinetic mechanism and reliable identification of the kinetic model, is still an open issue and needs more research. In most of the proposed methods, the kinetic parameters are obtained by fitting experimental data to an assumed model. Published data on diffusion coefficients, obtained by different methods, differ significantly (Kärger, 2003). A challenge is to develop a comprehensive technique, which could provide simultaneously consistent data for all three adsorptive properties with accuracy and reliability required for industrial design.

Up to now, the approach which has often been used for studying the kinetics of gas adsorption, is the Frequency response (FR) method (Yasuda, 1994; Song and Rees, 1997; Onyestyák et al., 1996; Sward and LeVan, 2003; Giesy et al., 2012; Bourdin et al., 1996, 1998), due to its ability to discriminate in the frequency spectrum between the rate constants of concurrent processes present in the complex adsorption process. The FR is based on measurement of a quasi steady-state responses of a system subjected to a periodic input modulation (usually sinusoidal) at different frequencies. If the input amplitude is kept small, the response contains a single harmonic (at the basic frequency),

which is directly proportional to the frequency response function (FRF) (first-order or linear FRF), which describes quasi-linear dynamic. The kinetic parameters are estimated by fitting the obtained FRF to a theoretical one, derived from a linearized model of the assumed kinetic mechanism. However, the fact that different kinetic models may have the same linearized forms and accordingly the same shape of the FRFs (Song and Rees, 1997), makes the linear FR method insufficient for characterization of nonlinear adsorption dynamics. It has been shown in literature that estimation of the model parameters from the linear FRF, especially for nonisothermal models is not straightforward (Sun and Bourdin, 1993).

Petkovska and Do (1998) have suggested the extension of the FR method to the nonlinear range, by applying larger input amplitudes. The response of the system to large amplitude excitation contains, besides the basic harmonic, also the second, third, etc. harmonic. This response is named nonlinear frequency response (NFR). The second and higher harmonics contain information regarding nonlinear dynamics of the system. One approach for analyzing complex NFR is the concept of higher order FRFs (Weiner and Spina, 1980). This concept is based on replacing the nonlinear model by a sequence of FRFs of different orders. It is applicable for stable, weakly nonlinear systems. This mathematical tool enables the second- and higher-order FRFs to be estimated experimentally from the individual harmonics of the system's response. It is to be expected that estimation of higher-order FRFs (besides the first-order FRF) can provide complete characterization of the kinetics of the nonlinear adsorption process. Petkovska and Do (2000) have derived the theoretical FRFs up to the second-order for several adsorption kinetic models: Langmuir model, linear driving force, micropore diffusion and pore-surface diffusion. Their study has shown that: 1) the second-order FRFs for different kinetic models have different shapes 2) the low frequency asymptotes of the FRFs corresponds to the equilibrium parameters. These findings make the NFR approach a promising tool for efficient dealing with characterization of adsorption systems, because it could provide: 1) direct unambiguous identification of the kinetic model based on the shape of the second-order FRF and 2) estimation of both kinetic and equilibrium parameters from the same experimental data.

This outstanding potential of the NFR approach was the motivation to implement this technique for characterization of kinetics and equilibria of gas adsorption within the frame of this thesis.

1.2 Scope and outline of the thesis

The objective of the research presented in this thesis is to explore the applicability of the NFR approach for characterization of kinetics and equilibria of adsorption of pure gases. The applicability of the NFR method will be evaluated through the possibility of experimental determination of accuarte second-order FRF for adsorption of pure gas on solid adsorbent.

Since the measuring NFRs of the adsorption systems has not been evidenced in the literature up to now, it was necesseary to construct the appropriate apparatus for NFR measurements. In order to design the functional apparatus and plan the efficient experiments, the applicability study based on numerical simulations have been performed. Based on the mathematical models of the batch adsorber and the film resistance control kinetics, NFRs have been simulated in MATLAB, and used as quasi-experimental data. The first- and second-order FRFs have been calculated using the concept of higher-order FRFs (Weiner and Spina, 1980). The influence of different parameters (mass of the adsorbent, input amplitude, frequency range, noise, sampling rate) on the accuracy of the estimation of the second-order FRF have been studied. The new apparatus was designed as the batch adsorber with sinusoidal volume change with the possibility to vary the amplitude. The gas pressure, particle temperature and, for the first time the gas temperature, are the measured responses. The applicability of the NFR method has been tested on the case of adsorption of CO_2 on commercial zeolite 5A particles. In the frame of the procedure for calculation of the FRFs from NFR experimental data, the concept of "blank" FRFs was developed as a new way for eliminating errors due to spurious effects. In order to identify the kinetic mechanism, it was necessary to compare the experimental FRFs with the theoretical ones for different possible kinetic models. Since the theoretical FRFs for nonisothermal macropore diffusion (NMD) model, which is one of the possible models for commercial biporous

adsorbents, do not appear in the literature, we have derived those FRFs (up to the second-order) in the frame of this thesis. In order to establish the methodology for estimation of the parameters of NMD model (kinetic constants, equilibrium data and heat of adsorption), the derived FRFs have been simulated and analyzed through parameter variation study. The thesis is organized in seven chapters as outlined below.

In Chapter 1 motivation, objectives and scope of the investigation presented in this work are given.

Chapter 2 gives some basic facts regarding gas adsorption. The existing methods for measurement of gas adsorption equilibria, kinetics and heats of adsorption are briefly reviewed. The basis of linear FR method for kinetic measurements is given together with a review of applications.

Chapter 3 deals with the theoretical basis of nonlinear dynamic analysis in the frequency domain. The concept of higher-order FRFs (Weiner and Spina, 1980) as a tool for analysis of the NFRs is described. The existing theoretical results regarding application of the concept of higher-order FRFs on adsorption systems are presented.

Chapter 4 contains the results of the simulation study regarding applicability of the NFR method for investigation of gas adsorption kinetics and equilibrium.

Chapter 5 contains derivation and analysis of the theoretical FRFs up to the second-order for NMD model.

Chapter 6 represents the experimental part of the work. It includes description of the experimental apparatus, measurement routine, procedure for data treatment as well as the results of the experimental measurements.

Chapter 7 summarizes the results of this research and points out the directions for further investigations.

2. GAS ADSORPTION ON POROUS SOLIDS

In this chapter the basic facts regarding gas adsorption, adsorbents and their applications will be given. Special attention is given to zeolites, since they are used in the experimental part of this work for testing the new method. Since the new method (NFR) for estimation of equilibrium, kinetics and heat of adsorption will be introduced, the existing methods for experimental measurements of those three properties in gas-solid systems will be briefly reviewed. The principle of linear FR method, which is the basis of the NFR method, together with its applications, will be given in detail.

2.1 Gas adsorption - basic facts, adsorbents and application

Adsorption is selective accumulation of substance(s) (adsorbate(s)) from the gaseous or liquid phase onto the surface of a solid phase (adsorbent). Physical adsorption is caused by weak van der Waals and electrostatic forces (polarization, field-dipol forces) between the adsorbate molecules and the atoms of adsorbent surface. Balancing of those forces leads to a dynamic equlubrium, as follows:

$$\text{Solid} + \text{Gas} \leftrightarrow \text{Gas/Solid} + \text{Heat} \qquad (2.1.1)$$

The heats released by adsorption are relatively low 10-40 kJ/mol. Adsorption is reversible and the reverse step is called desorption.

Adsorbents are mostly microporous solid materials. The features of those matherials, which charaterize them as adsorbents are: internal surface area, pore size distribution, and surface polarity. Internal surface area (mostly in the range 500 - 2500 m^2/g) is in direct correlation with adsorption capacity. Pore size distribution determines the assesibility of the adsorbate molecules of certain sizes to the internal adsorption surface, affecting thus the selectivity of the adsorbent. Surface polarity corresponds to the affinity towards polar or nonpolar substances. The nonpolar adsorbents (activated carbon, polymer adsorbents and silicalite) have high afinity for most organics and they are often described as hydrophobic. The polar adsorbents (zeolites, porous alumina, silica gel) are classified as

hidrophilic, since they have afinity for water and alcohols. The classification is conditional, since by oxidation of the activated carbon or variation of the Si/Al ratio of zeolites, the polarity can be changed.

Adsorption processes may be divided into purification processes (where trace contaminants are removed from a process stream), and bulk separation processes (if one or more components are recovered selectively from a mixture in high concentrations). Table 2.1.1 presents some representative commercial processes of each type, with typically used adsorbents.

Table 2.1.1 Gas adsorption industrial applications (IAS home page, 1999)

BULK SEPARATION PROCESSES	**Adsorbent**
Normal paraffins, isoparaffins, aromatics	zeolite
N_2/O_2	zeolite
O_2/N_2	carbon molecular sieve
CO, CH_4, CO_2, N_2 , NH_3 /H_2	zeolite, activated carbon
Acetone/vent streams	activated carbon
Ethylene/vent streams	activated carbon
Water/Ethanol	zeolite
PURIFICATION PROCESSES	**Adsorbent**
Organics/vent streams	activated carbon
Water/natural gas, air, synthesis gas	silica, alumina, zeolite
Sulfur compounds/natural gas, hydrogen, liquified petroleum gas	zeolite
Solvents/air	activated carbon
Odors/air	activated carbon
NOx/N_2	zeolite
SO_2/vent streams	zeolite

Adsorption processes are designed in practice as cyclic operations, with switching between unsteady-state acumulation of the adsorbate on the solid surface and regeneration of the adsorbent. The possible modes of operation are cyclic batch, continious counter-current and hromatographic. In a cyclic batch mode the adsorption is carried out in a fixed bed of the adsorbent as a discontinuous operation, consisting of adsorption and desorption steps. In the continious counter-current mode the adsorbent is circulated around two beds allowing adsorption and desorption steps to operate simultaneously. In a chromatographic mode the feed stream is introduced as a pulse, trying to reproduce the separation preformances of the laboratory hromatography on a

larger scale. Regarding the regeneration of the adsorbent two main concepts employed in industry are presure swing adsorption (PSA) and temperature swing adsorption (TSA).
In order to select an optimal adsorbent and process mode to achieve the desired separation, it is necessary to know three core adsorptive properties for systems of interest: equilibria, kinetics and heats of adsorption.

2.1.1 Zeolites

Zeolites are porous crystaline aluminosilicates which contain SiO_4 and AlO_4 tetrahedreal units (Fig. 2.1.1a), linked together through sharing of oxygen atoms into 4- 6- or 8-oxygen rings (Fig. 2.1.1b), which build polyedral units, such as, for example, sodalite cage (Fig. 2.1.c), which can form the different frameworks as A or X(Y) types (Fig.2.1.1d).

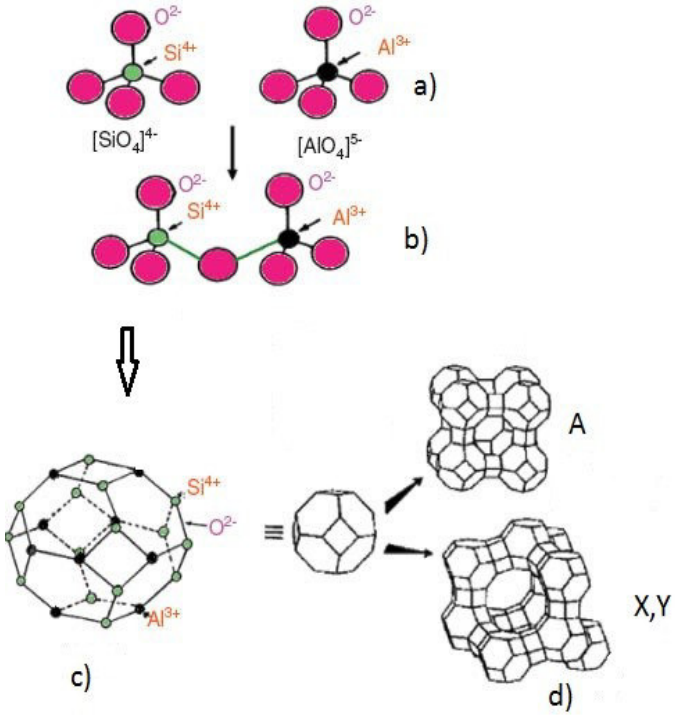

Fig. 2.1.1 Shematic representation of the framework structure of zeolites A and X (Y)

The obtained crystal lattice has regular channels (pores), which are of the molecular dimensions and into which adsorbate molecule can penetrate. This crystaline structure with uniforme pore sizes is a unique feature of zeolites that makes them one of the most often used type of adsorbents. Til nowadays, about 50 natural zeolites have been found and more than 100 synthetic types have been produced. The revised Atlas of Zeolite Framework Types (Baerlocher et al., 2007) gives comprehensive review regarding zeolite types.

The chemical composition of a zeolite can be represented by an empirical formula $M_{x/n}((AlO_2)_x(SiO_2)_y)_zH_2O$ (Staudt, 1994), where n is the valency of the exchangeable cation M (Na^+, K^+, Ca^{2+}, Mg^{2+}) and z is the number of water molecules in the zeolite unit cell. The numbers x and y are integers and the ratio y/x is equal or higher than one. It is evident from the above formula, that each aluminium atom present in the framework brings one negative charge which is balanced by that of the exchangeable cation. Zeolites A (which will be used in this work) have Si/Al ratio close to 1.0 and 12 univalent exchangeable cations per cell. Typical forms of zeolite A with respect to exchangeable cations are listed in Table 2.1.2. It can be seen from Table 2.1.2 that the sort of cations determines the effective pore diameter, affecting thus the selectivity of the zeolite.

Table 2.1.2 Typical forms of zeolite A (Thomas and Crittenden, 1998)

Type	Cations	Formula of typical unit cell	Effective pore diameter (nm)
4A	Na	$Na_{12}[(AlO_2)_{12}(SiO_2)_{12}]$	0.38
5A	Ca-Na	$Ca_5Na_2[(AlO_2)_{12}(SiO_2)_{12}]$	0.44
3A	K	$K_{12}[(AlO_2)_{12}(SiO_2)_{12}]$	0.29

Commercial zeolites are available in pellet forms where zeolite crystals (1-5 μm) are formed into particles of regular shapes (beads, pellets of 0.5-5 mm) using a binder material (clay, polymers). Some examples of commercial applications of zeolites are given in Table 2.1.1.

2.2. Adsorption equilibrium

2.2.1 Models for adsorption isotherms

Partition of the adsorbate molecules between the gas and the solid phase, when equilibrium defined by eq. 2.1.1 is established, is usually defined by adsorption isotherm (equilibrium relation). It defines the equilibrium loading (Q) for different pressures (P) at a constant temperature. The form of this relation depends on the nature and complexity of interactions between the adsorbate molecules and the surface of adsorbent. A general and well known classification of single solute isotherms of gases (Types I-V) is given by Braunauer et al. (1940). The adsorption isotherms of a pure gases on zeolites are most often of Type I by Braunauer classification (Young and Crowell, 1962). Different theoretical and empirical models (analytical equations) have been developed to describe the adsorption isotherms. Several models which describe Type I isotherms have been listed in Table 2.2.1 together with underlying assumptions.

Table 2.2.1 Models for adsorption isotherms

	Expression	Model parameters	Assumptions
Langmuir	$Q = Q_0 \frac{bP}{1+bP}$	Q_0, b	- energetically equal asdorption sites - no lateral interactions
Sips	$Q = Q_0 \frac{(bP)^{1/n}}{1+(bP)^{1/n}}$	Q_0, b, n	- energetically equal asdorption sites - no lateral interactions
Dual site Langmuir	$Q = Q_{01} \frac{b_1 P}{1+b_1 P} + Q_{02} \frac{b_2 P}{1+b_2 P}$	Q_{01}, b_1, Q_{02}, b_2	- energetically different adsorption sites - no lateral interactions
Toth	$Q = Q_0 \frac{P}{(b+P^t)^{1/t}}$	Q_0, b, t	- energetically different adsorption sites - no lateral interactions

2.2.2 Measurement of adsorption isotherms

A large number of methods for measuring adsorption isotherms have been developed and described in literature. The book "Gas Adsorption Equilibria- experimental methods and adsorption isotherms" by Keller and Staudt (2005) is one of the good contemporary

reviews. Here, a brief summary of the classical and some newer methods for measurements of adsorption isotherms will be given.

The developped methods can be divided into equilibrium and dynamic methods. Equilibrium methods analyze only equilibrium states, while dynamic methods consider concentration changes over time in order to determine adsorption isotherms. Classical equilibrium methods are volumetric and gravimetric and dynamic methods comprise different chromatographic methods.

In the **volumetric method** the adsorbed quantity is determined from measurements of: 1) pressure of a certain amount of gas contained in a storage vessel of known volume and 2) pressure after expansion of that amount of gas into an adsorption vessel of a known volume containing solid adsorbent (after equilibration at a constant temperature). The difference between the two pressure readings allows calculation of the adsorbed amount of gas based on the equation of state (EOS). In order to determine the whole isotherm, mesurements at different pressures have to be performed. The volumetric method is suitable due to the simplicity of the experimental measurements and availability of high precision pressure sensors. However, volumetric measurements are not useful at extremely low or high pressures, since the pressure measurements in these regions become difficult and accurate EOS of the sorptive gases are not always available. Examples of measurements of adsorption isotherms by volumetric metod can be found in (Riberio et al., 2014; Mofarahi and Bakhtyari, 2015; Zhu et al., 2015).

The **gravimetric method** is based on the measurement of the weight of the adsorbent before and after equilibration with the fluid phase containing the adsorbate, at given temperature and pressure, by a microbalance. The available microbalances (such as two beams balances and magnetic suspension balances) are highly accurate and operate with tiny amounts of adsorbents. On the other hand, the microbalances are complex systems, sensitive to electomagnetic and mechanical disturbances and very demanding regarding control and data processing. Examples of measurements of adsorption isotherms by gravimetric method can be found in (Camacho et al., 2015; Silva et al., 2015).

Besides those two classical equilibrium techniques, several newer ones have been developed, such as oscillometry (Keller, 1995) and impedance spectroscopy (Staudt et al., 1999).

Regarding the dynamic methods for measurements of adsorption isotherms, different **chromatographic methods** are established and described in detail in the literature (Kiselev and Yashin, 1969; Conder and Young, 1979; Katsanos, 1988; Grob and Barry, 2004; Poole, 2012): frontal analysis, frontal analysis by characteristic point, elution by characteristic point, perturbation method and inverse chromatography. Chromatographic methods are based on the measurement and mathematical analysis of breakthrough curves or dispersive fronts (concentration changes over time at the outlet of the chromatographic column) that correspond to different changes of the inlet concentrations. Chromatographic methods are generally faster and more accurate than the static methods, but a large amount of adsorbate is consumed in order to generate different inlet concentration changes. A good review paper regarding determination of isotherms by gas–solid chromatography is given by Roubani–Kalantzopoulou (2004).

2.3. Heat of adsoprption

The differential entalpy change for isothermal transfer of an infinitesimal amount of adsorbate from the adsorbed phase to the gas phase is called the isosteric heat of adsorption (Do, 1998). Adsorption is by nature an exothermic process and desorption is endothermic.

The isosteric heat ($-\Delta H$) can be measured directly as a function of loading and temperature using a microcalorimeter (Dunne et al., 1996; Siperstein et al., 1999). However, the isosteric heats are most often obtained from adsorption isotherms at different temperatures, by using Van't Hoff equation (Do, 1998), integrated under assumption that ($-\Delta H$) is independent of temperature:

$$\ln P = \frac{-\Delta H}{R_g T} + const. \qquad (2.3.1)$$

A plot of ln P against $1/T$ at constant loading has a slope equal to $-\Delta H/R_g$. In eq. (2.3.1) P is the pressure, T is the equilibrium temperature and R_g is the gas constant.

2.4. Adsorption kinetics

2.4.1. Transport processes in porous solids

The rates of adsorption of a gas molecule on a particular site inside the zeolite crystal, estimated by means of kinetic gas theory, are of the order of microseconds (Sircar and Myers, 2003). However, the experimentally observed rates are several orders of magnitude lower, which indicates that the overall rate is controled by diffusional resistance(s) associated with mass transfer to the adsorption site. If the adsorbent is in the form of individual crystals than the diffusion of adsorbate into the pores of crystal lattice (intracrystalline or micropre diffusion) determines the overall rate. However, as alraeady mentioned in Section 2.1.1, the adsorbents in the form of pellets are used for practical applications. The pellets are formed by binding crystals together using a binder, resulting in a biporous structure, as schematically presented in Fig. 2.4.1. The narrow chanels within the crystal lattice of the individual crystals are regarded as micropores, while the intercrystalline voids form larger macropores.

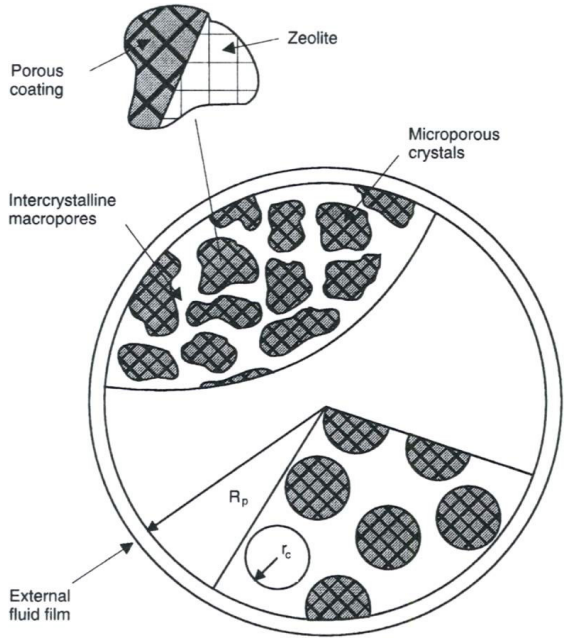

Fig. 2.4.1 Structure of the commercial zeolite pallet (from Thomas and Crittenden, 1998)

The overall rate of adsorption on such pellet may be controlled by the following resistances:

1. Resistence of the external fluid film surrounding the particle, which is present only for adsorption of gas mixtures. The transport mechanism through the film is gas-gas diffusion.
2. Resistence to transport through macropores/mesopores within the binder phase to the surface of the crystals. Transport of the adsorbing gas molecules through macropores takes place by bulk or Knudsen diffusion in the gas phase, in parallel with surface diffusion.
3. Resistance to diffusion through micropores of the crystals to the adsorption site. The transport mechanism is activated diffusion (jumping of the adsorbed molecules from site to site). Additionally, the outside surface of the crystal may cause resistance at the entrance of the micropore (surface barrier resistance).
Since adsorption is an exothermal process, the mentioned diffusional processes occur in the interplay with heat transfer through/from the particle.
The contribution of each of the possible resistances depends on the physicochemical properties of the adsorbent - adsorbate pair and the temperature and pressure conditions at which adsorption occurs. Experimental identification of the relative dominance of indivudual resistances is still a research challenge. However, different metods for measurements of the diffusion coefficients have been developed and descibed in the literature. A short review of those metods, with regard to principles and advantages/disadvantages will be given in Section 2.4.3.

2.4.2 Models for describng adsorption kinetics

The mathematical models which describe the kinetics of adsorption of a gas in a porous particle are generally based on the mass balance described by the Fickian diffusion equation, which has the following general form:

$$\frac{\partial Q(r,t)}{\partial t} = \frac{1}{r^{\sigma}} \frac{\partial}{\partial r}\left(r^{\sigma} D \frac{\partial Q}{\partial r} \right) \tag{2.4.1}$$

and heat balance (under assumption that tempertaure is uniform through particle):

$$(-\Delta H)\frac{d\overline{Q}}{dt} = \rho_p c_s \frac{dT_p}{dt} + ha(T_p - T_g) \tag{2.4.2}$$

In eqs. (2.4.1) and (2.4.2) Q(mol/m^3) is the local solid-phase adsorbate concentration, D(m^2/s) is the diffusion coefficient, σ is the shape factor (0 - for slab, 1- for cylinder and 2- for spherical geometry of particle), (-ΔH)(J/mol) is the hear of adsorption, c_s (J/kgK) is the heat capacity of the adsorbent, h(W/m^{2}K) is the heat transfer coefficient, a(m^2/m^3) is the specific surface of the particle, T_p(K) is the particle temeprtaure, T_g(K) is the gas temperature and $\overline{Q}$(mol/m^3) is the average solid-phase concentration in the particle defined as:

$$\overline{Q} = \frac{\sigma+1}{R^{\sigma+1}} \int_0^R r^{\sigma} Q(r,t) dr \tag{2.4.3}$$

2.4.3 Measurements of diffusion coefficients

A wide range of different experimental techniques have been applied in order to measure diffusion coefficients within microporous and bidispersed solids. It is convenient to distinguish between equilibrium techniques in which the self-diffusivity is measured (in absence of a concentration gradient) and non-equilibrium techniques which measure transport diffusivities. Regarding the scale of the measurements, the methods are divided into: microscopic (sub-crystal scale), mesocsopic (single-crystal scale) and macroscopic (an assembly of crystals). Comprehensieve review of those methods, containing detailed descriptions, critical analysis and examples, is provided by Karge and Weitkampf (2008). The most important methods are listed in Table 2.4.1 and briefly described below.

Microscopic techniques are based on the measurements of the mean square displacement of the gas molecules into the crystal micropores under equilibrium conditions, by either nuclear magnetic resonance (PFG NMR) or by neutron scattering (QENS). The obtained time-constants correspond to self-diffusivities (D_0). In order to get transport diffusivities (D), the gradient of the adsorption isotherm has to be taken into account, according to Darken's equation (Ruthven, 1984):

$$D = D_0 \frac{d \ln P}{d \ln Q} \tag{2.4.4}$$

Microscopic methods give accurate diffusivities for very fast micropore diffusion (when the diameter of the diffusing molecule is smaller than the micropore diameter), while the slower micropore diffusion (when the diameter of the diffusing molecule is equal or slightly larger than the micropore diameter) and macropore diffusion kinetics are inaccessible.

Table 2.4.1 Methods for measuring diffusion coeficients

Microcscopic methods	- NMR-PFG
	- QENS
Mesoscopic methods	- FTIR
	- Interference microscopy
Macrocsopic methods	- Wicke-Kallenbach
	- Uptake rate
	- Chromatographic
	- ZLC
	- Frequency response

Mesoscopic methods are newer and include using of infrared spectroscopy or interference microscopy. The Fourier transform infrared spectroscopy (FTIR) has been successfully employed by Niessen and Karge (1993) for measurements of diffusion of p-xylene in zeolite crystals. In FTIR spectroscopy the absorbance of an IR band of the adsorbate is monitored by scanning the spectra of pure adsorbent in inert atmosphere and after a step change of the partial pressure of the adsorbate. The intensity of absorbance (transmittance) is the measure of the adsorbent coverage. Since modern, high sensitivity spectrometers are available, FTIR is considered as a very accurate technique, with ability to measure the sorption of binary mixtures.

Another very promising technique for studying sorption kinetics is optical interference microscopy (IM), suggested by Schemmert et al. (1999). The technique is based on the analysis of the interference pattern generated by the superposition of two light beams, one passing through the adsorbing crystal and the other passing through the adsorbate. Since the optical density depends on the concentration of the guest molecules, changes in local

concentration appear directly as the corresponding changes in the interference pattern. Both FTIR and IM measurements are performed on single crystal scale and allow measurements in a wide range of temperature/pressure conditions.

Regarding the macroscopic methods, Wicke-Kallenbach method, uptake rate, chromatographic and frequency response method are the most important. The schematic representation of the apparatus for Wicke-Kallenbach method for measuring diffusivity is presented in Fig.2.4.2 (Ruthven, 1984).

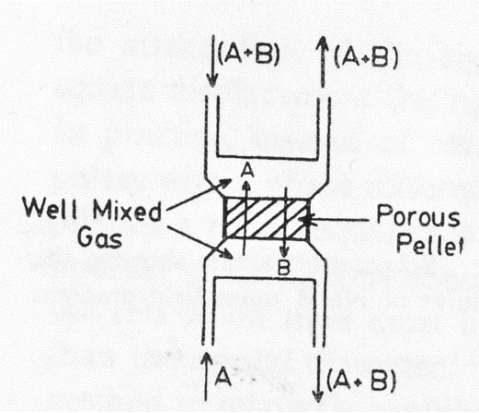

Fig. 2.4.2 Shematic representation of Wicke-kallanbach cell (Ruthven, 1984)

A cilyndrical adsorbent pellet is sealed within the cell. The inert gas is passed accros one face of the pellet and diluted mixture inert-adsorbate acrcross the opposite face of the pellet. By measuring the flowrates and concentrations of both streams in a quasi-steady state, the fluxes in both directions, and hence the effective macropore diffusivity can be calculated. The method could also be applied for measuring micropore diffusivities, but the difficulties of mounting and sealing of crystals make this application difficult.

The uptake rate method is based on direct measurement of the sorption rate (gravimetric or piezometric) on the adsorbent sample subject to a step-change in sorbate concentration in a closed volume (Ruthven, 1984). The diffusion coefficient can be estimated the by fitting the experimental uptake curve to the solution of diffusion equation (2.4.1). Generally, both adsorbent configurations (crystals and pellets) can be examined by uptake rate measurement. Micropore diffusivities in crystals can be determined accurately for slow diffusion, while for the faster diffusion the intrusion heat effects become significant. Although nonisothermal effects can be account for in the models,

they are not obvious from the shape of the uptake curve. Regarding the uptake rate measurements in biporous pellets, the effective macropore diffusivity can be determined accurately if micropore diffusion is significantly faster than the macropore diffusion. Experiments with different particle sizes are nedded in order to check whether this condition is fulfilled (Ruthven, 1984).

Chromatohraphy has already been mentioned in Section 2.2.2 as one of the methods for estimation of adsorption equilibrium. It is also possible to deduce the diffusion coefficient by analysis of the pulse response of the chromatographic column (in terms of the first and second moments of the pulse response). The main difficulty in the analysis of chromatographic data is to separate the axial-dispersion and diffusion contributions. The zero length column (ZLC) method, introduced by Eić and Ruthven (1988), which is a variant of the chromatographic method using an infinitezimal column, provides elimination of the axial dispersion effect.

The Frequency response (FR) method analyzes the responses to the periodic (usually sinusoidal) change of the input variable. It stands out from the other transient methods (step and pulse responses) due to the following features (Reyes and Iglesia, 1994):

1) An additional degree of freedom, introduced by frequency of periodic oscillation, provides direct examination of the time constants of concurrent processes within the adsorbing particle (each time constant corresponds to one critical frequency).

2) The analysis of the response data can be performed in the frequency domain, which is very convenient, since the kinetic models equations become algebraic equations in the frequency domain.

These features make the FR method a powerful and frequently used method for kinetic measurements of gas-solid adsorption systems. Since the FR method represents the basis for the NFR method, which is in the focus of this work, the concept and applications of the FR method will be discussed in the following section.

From the above given review, it can be concluded that reliable measurements of diffusion into porous solids is more difficult than it can be expected. Each method has certain limitations or requires experimental conditions to be adjusted so that the underlying assumptions are fulfilled. Moreover, diffusion coefficients derived from microscopic and macroscopic methods can differ substabntially (Kärger, 2003).

2.5 The FR method for measurement of adsorption kinetic data

The basic principle of FR method is that a system subject to a periodic perturbation of the input variable, produces a periodic response (output) that has a different amplitude and a phase lag with respect to the input. The magnitudes of the amplitude attenuation and the phase lag are related to the dynamics of the process(es) occuring within the system. If the amplitude of the input modulation is small, then the output is a quasi-linear response. The output to the input ratio in the frequency domain, measured over a range of frequencies, defines the frequency response function (FRF). This function is also called first-order FRF or linear FRF, and it is the function of frequency. Kinetic parameters are obtained by fitting the experimental FRF to the theoretical one, derived from the linearized form of the assumed kinetic model.

The FR method has been firstly applied for kinetic studies of adsorption by Naphtali and Polinski (1963), and since then, there have been a lot of applications of this method for different adsorption systems. Most investigators (Naphtali and Polinski, 1963; Yasuda, 1976; Rees and Shen, 1993, Onyestyak, 1996, Reyes et al.,1997) have performed the FR measurements in a batch adsorber with sinusoidal volume modulation and pressure as a measured output, as shematically presented in Fig. 2.5.1.

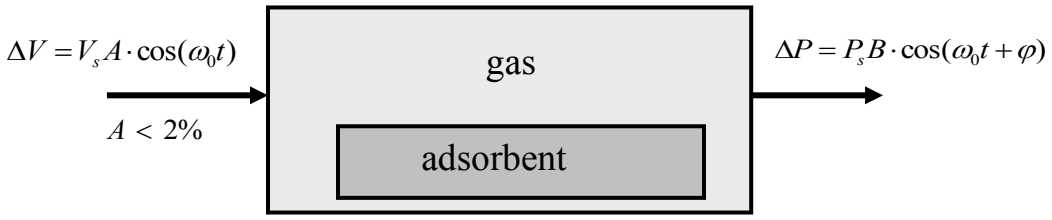

Fig. 2.5.1 Shematic representation of FR measurements in a batch adsorber (linearized case)

Based on the mass balance of the batch adsorber, Yasuda (1976) defined the so called "in-phase" (real) and "out-of-phase" (imaginary) components of the FRF, which can be calculated using the measured pressure responses. The experimental "in-phase" and "out-of-phase" functions can be used for estimating the kinetic data by fitting to the theoretical ones for an assumed model. Yasuda and co-workers have investigated the kinetics of adsorption/chemisorption of etylene on ZnO (Yasuda, 1976), hydrogenation of propylene

over $Pt/A1_2O_3$ catalyst (Yasuda, 1989), adsorption of CH_4, C_2H_6, and C_3H_8 on 5A zeolite pellets (Yasuda et al., 1991) and methanol conversion to olefins over HZSM-5 catalysts (Yasuda and Nomura, 1993). In order to interpret the FR experimental data, they have derived the theoretical FRFs for following kinetic models: adorption-desorption with one/several adspieces, adsorption-desorption during reaction, micropore diffusion with/without surface barrier (Yasuda, 1994). Jordi and Do (1994) have studied theoretically FR of isothermal diffusion into biporous solids. Sun et al. (1994) have extended the theoretical analysis to non-isothermal adsorption in biporous solids and deriverd and analyzed the in-phase and out-of-phase functions for non-isothermal micropore-macropore diffusion model. Sun and Bourdin (1993) have also derived theoretical FRF for isothermal diffusion-rearrangement model.

Rees and co-workers have used the FR experiments in order to investigate diffusion of different hydrocarbons within zeolites: benzene/NaX (Rees and Shen, 1993), n-butane and 2-butane/silicalite (Shen and Rees, 1991), propane/silicalite (Song and Rees, 1996) and n-hexane/silicalite (Song and Rees, 1997), using Yasuda's theoretical FRFs (Yasuda, 1994). Onyestyak and co-workers have examined the broad range of adsorption systems by the FR method: amonia, CO, CO_2, propane on activated carbon charcoal, silica gel and different zeolites (Onyestyak, 1996, 2011; Onyestyak and Rees, 1999).

A typical batch apparatus for FR adsorption measurements is usually a closed termostated cell, containing the adsorbate gas initially equilibrated with a small amount of the solid asdorbent. The sinusoidal modulation of the cell volume is typically performed by bellows coupled with a rotary motor and a suitable mechanism for converting circular into a linear motion (Yasuda, 1976; Reyes et al., 1997). Turner et al. (2001) improved the accuracy of the input sine wave approximation by using a servomotor with feedback control to drive the metal bellows. The pressure is measured with highly accurate, fast-response pressure sensors in order to obtain reliable amplitude attenuations and phase lags. Rees and Shen (1993) have designed a FR device with square-wave volume perturbation produced by electromagnetically driven bellows. This arrangement allows better long-term stability and working frequencies up to 10 Hz. Bourdin et al. (1998) have introduced the measurement of the adsorbent temperature (by an infra red thermometer) along with measurements of pressure response to the volume modulation

and they defined the in-phase and out-of-phase components of the temperature response function (TRF). The same group of authors have previously published a comprehensive theoretical study regarding the TRFs for the cases of non-isothermal diffusion in crystals and biporous pellets including surface barrier effects (Bourdin et al. 1996a, b). Their results show that frequency spectra of the TRF enable separation of heat transfer and diffusion time constants which is not possible from the pressure measurements only.

More recently, Jentys et al. (2005) have employed the IR spectroscopy in order to measure directly the surface concentration change due to the periodic pressure modulation in a batch system. This technique enables distinction between adsorption processes on different types of active sites.

Besides batch FR measurements, a continious FR apparatus have also been developed (Sward and LeVan, 2003; Wang et al., 2003; Liu et al., 2010), where the pressure is modulated periodically and the resulting changes in the outlet flowrate are measured by mass flow meter or mass spectrometer. Giesy et al. (2012) modified later the apparatus of Sward and and LeVan (2003), in such a way that it can operate in both continious and batch mode, in order to combine the advantages of both techniques. Theoretical considerations regarding FRs of the flow adsorber were treated by Park et al. (1998) and Sward and LeVan (2003). A summary of the existing FR devices together with their main characteristics is given in Table 2.5.1.

In spite of a broad field of applications, the FR method is limited by its inability to discriminate between kinetic models which have the same linearized forms and accordingly, the same shapes of the linear FRFs. For example, micropore diffusion, macropore diffusion and pore-surface diffusion models have the same shapes of the linear FRFs (Petkovska, 2006). Shen and Rees (1991) have reported that the FR experimental data for adsorption of n-butane on silicalite-1 fit equally well to three different models: non-isothermal micropore diffusion, two independent diffusion processes and diffusion-rearrangement process. Those facts gave rise to the extension of the FR method to the nonlinear range, suggested by Petkovska and Do (1998) and named Nonlinear Frequency Response (NFR) method, which will be applied in this work for studying the kinetics and equilibrium of gas adsorption.

Table 2.5.1 Summary of experimental FR devices

reference	configuration	modulated input/form	input amplitude	maximal frequency	measured output	investigated system
Naphtali and Polinski (1963)	batch	volume/ sinusoidal	no info		pressure/Pirani gauge	H_2/nickel
Yasuda (1976)	batch	volume/sinusoidal	± 3.8 %	0.25 Hz	pressure/Pirani gauge	ethylene/ZnO
Rees and Shen (1993)	batch	volume/square wave	± 1 %	10 Hz	pressure/ differential Baratron	benzene, etylbenzene, p-xylene/silicalite-1
Bourdin et al. (1998)	batch	volume/ sinusoidal	< 2 %	30 Hz	particle temperature/IR detector pressure/absolute Baratron	CO_2, propane/zeolite NaX
Reyes et al. (1997)	batch	volume/sinusoidal	± 1.4 %	10 Hz	pressure/ differential Baratron	N_2, Xe, isobutane/silica
Turner et al. (2001)	batch	volume/ sinusoidal	± 1.5 %	5 Hz	pressure/ differential Baratron	n-hexane , metanol/silicalite
Sward and LeVan (2003)	flow-through	pressure/ sinusoidal	± 5 %	0.2 Hz	mass flow rate/mass flowmeter	CO_2/BPL activated carbon
Jentys et al. (2005)	batch	volume/ square wave	< 5 %	1 Hz	concentration/ IR spectrometer pressure/absolute Baratron	bezene, tolene, o- and p-xylene /zeolite H/ZSM-5
Giesy et al. (2012)	combined batch/flow-through	volume pressure composition/ sinusoidal	< 2 %	10 Hz	pressure mass flow composition	CO_2/ zeolite 13X

3. NONLINEAR DYNAMIC ANALYSIS IN THE FREQUENCY DOMAIN - APPLICATION ON GAS ADSORPTION

Since this thesis deals with nonlinear analysis of gas adsorption, a short review of the methods for nonlinear analysis will be given in this chapter. The Volterra-Weiner concept of higher-order FRFs (Weiner and Spina, 1980), which represents one of the tools for analysis of NFRs and the theoretical basis of the NFR method, will be described in detail. The procedure for obtaining both experimental and theoretical higher-order FRFs, using the Volterra-Weiner concept higher-order FRFs, will be presented. The relevant theoretical results regarding the application of NFR method on the gas adsorption, which were already published, will be recalled. Also, a short review of the applications of the NFR method in other chemical engineering systems will be given.

3.1. Methods for dynamic analysis of nonlinear systems

The processes in chemical engineering (including adsorption which is the subject of this work) are generally nonlinear. Nonlinear systems are characterized by diverse and complex dynamic behavior. Till nowadays, there is no general theory for dealing with analysis of nonlinear systems. Depending on the complexity of the system and on the concrete purpose, the time and frequency domain approaches for studing the nonlinear phenomena are used in practice. In the time domain, the nonlinear systems are represented by mathematical models of different types of nonlinear differential equations, where the output-input relations are expressed implicitly. The explicit form of the output-input relation i.e., the exact solution exists only for a few specific types of nonlinear differential equations. It is usual in engineering practice to consider first the linearization of the nonlinear model, which may be sucessfull only in a very limited number of cases (when the changes of the variables do not vary too much from their equilibrium values). The graphical phase-plane analysis (Jordan and Smith, 2007) is a tool which may predict qualitative characteristics of the nonlinear system's behavior without solving the differential equations. Numerical techniques, such as finite element method, together with algorithms for numerical integration, are used for finding solutions of the PDEs numerically. However, numerical simulations may be time

consuming and they are approximate. The time domain techniques turned out to be only occasionaly usefull (stability theory is based on differential equations theory), but not suitable for most practical enginerring applications.

Regarding the nonlinear analysis in the frequency domain, the concept of higher-order FRFs (Weiner and Spina, 1980) is widely used in different fields of engineering. This concept is applicable for stable nonlinear systems with polynomial nonlinearities (weakly nonlinear systems), and it is based on the representation of the model of the system in the form of series of FRFs of different orders (theoretically indefinite). For practical purposes, the truncation to the third-order FRF is usually sufficient to characterize the system. Nonlinear analysis in the frequency domain has the following advantages: 1) the nonlinear models defined in the time domen as PDEs become ODEs, and those defined in the time domain by ODEs become algebraic equations 2) the insights gained from the linear FR analysis can be applied to analyze the nonlinear system dynamics. Although the concept of higher-order FRFs is known from the late 1950s, its applications are still very rare, since obtaining the FRFs for practical systems is difficult. Up to now, there has been no coherent method neither for calculation nor for measurement of the higher order FRFs. Two approaches regarding obtaining the FRFs for nonlinear systems have been reported in the literature. The first approach has been introduced by Peyton Jones and Billings (1989) and it is based on application of a recursive probing algorithm to the nonlinear autoregressive moving average with exogenous inputs model (NARMAX) (Leontaritis and Billings, 1985). Another approach for obtaining the FRFs is so called Voterra-Weiner concept of higher-order FRFs (Schetzen, 1980; Rough, 1981) and it is based on the representation of the frequency response of a nonlinear system in the form of Volterra series and application of multidimensional Fourier transform (Weiner and Spina, 1980). Since the latter approach represent the basis of NFR techique applied in this work, it will be presented in the following subsection.

3.2 Frequency response of the nonlinear system

3.2.1 Volterra-Weiner concept of higher-order FRFs

The Volterra-Weiner concept (Weiner and Spina, 1980) represents the generalization of the well known approach of convolutional integral and definition of the FRF, used in the linear frequency domain analysis. Namely, the dynamic response of a stable linear single-input single-output system to an arbitrary input signal $x(t)$ can be defined as a convolution integral:

$$y^{lin}(t) = \int_{-\infty}^{\infty} g(\tau)\, x(t-\tau)\, d\tau \qquad (3.2.1)$$

where $g(\tau)$ represents the impulse-response function of the system, or its kernel. By taking into account the definition of FRF (Weiner and Spina, 1980):

$$G(\omega) = \int_{-\infty}^{\infty} g(\tau)\, e^{-j\omega\tau}\, d\tau \qquad (3.2.2)$$

it is possible to relate the time domain response of the system, $y^{lin}(t)$, with its FRF $G(\omega)$ (which is the complex function of a single variable - frequency). The form of this relation depends on the form of input.

For the input in the form of idealized periodic function $x(t)=Ae^{j\omega t}$, (which can not be realized physically and will be called in the further text ideal single harmonic), the response defined by eq. (3.2.1) becomes:

$$y^{lin}(t) = Ae^{j\omega t} \int_{-\infty}^{\infty} g(\tau)\, e^{-j\omega\tau}\, d\tau \qquad (3.2.3)$$

which, considering the definition (3.2.2), becomes:

$$y^{lin}(t) = Ae^{j\omega t} G(\omega) \qquad (3.2.4)$$

From Eq. (3.2.4) it can be seen that the response of a linear system to a single harmonic input is also a single harmonic at the same frequency. Similarly, the response of a linear system for a single co-sinewave input $x(t)=A\cos(\omega t)=(A/2)e^{j\omega t}+(A/2)e^{-j\omega t}$, can be written as:

$$y^{lin}(t) = G(\omega)\frac{A}{2}e^{j\omega t} + G(-\omega)\frac{A}{2}e^{-j\omega t} \qquad (3.2.5)$$

By using the property of conjugate symmetry (Storer, 1991), eq. (3.2.5) becomes:

$$y^{lin}(t) = A\left|G(\omega)\right|\cos\left[\omega t + \arg(G(\omega))\right] \qquad (3.2.6)$$

Eq. (3.2.6) shows that the response of a linear system to a single sinewave is also a single sinewave of the same frequency. The response defined by eq. (3.2.5) can be written in a frequency domain as follows:

$$Y^{lin}(\omega) = G(\omega)X(\omega) \tag{3.2.7}$$

Eq. (3.7) shows that the FRF $G(\omega)$, which represents the model of the linear system in the frequency domain, can be simply determined from the response to a sinewave input.

When the nonlinear system with polynomial nonlinearities is the subject of the same arbitrary input $x(t)$, the response may be represented as an indefinite sum of multidimensional convolutional integrals (Volterra series):

$$y^{nonlin}(t) = \sum_{n=1}^{\infty} y_n(t) \tag{3.2.8}$$

$$y_n(t) = \int_{-\infty}^{\infty} \cdots \int_{-\infty}^{\infty} g_n(\tau_1, \cdots, \tau_n) \prod_{i=1}^{n} x(t-\tau_i) d\tau_1 \cdots d\tau_n \tag{3.2.9}$$

where $g_n(\tau_1,\ldots,\tau_n)$ is the generalized impulse response function of order n, or n-th order Volterra kernel. The first element of the series, $y_1(t)$, have the same form as $y^{lin}(t)$ (eq. 3.2.1), and represent the response of the linearized system, while each of the higher terms (n>1) represents the contribution of the nonlinearities of n-th order.

In analogy to the Fourier transform of the linear system's kernel, which defines the FRF (eq. 3.2.2), the multidimensional Fourier transform of the n-th order Volterra kernel defines the generalized n-th order FRF, as follows :

$$G_n(\omega_1, \cdots, \omega_n) = \int_{-\infty}^{\infty} \cdots \int_{-\infty}^{\infty} g_n(\tau_1, \cdots, \tau_n)\ e^{-j(\omega_1\tau_1 + \cdots \omega_n\tau_n)} d\tau_1 \cdots d\tau_n \tag{3.2.10}$$

which is a complex function of n variables (frequencies). In order to establish the relation between the response of the nonlinear system defined by eqs (3.2.8) and (3.2.9) and FRFs of the different orders defined by eq. (3.2.10), the concrete form of the input $x(t)$ has to be considered.

For better understanding of the concept, the input in the form of the ideal single harmonic $x(t)=Ae^{j\omega t}$ will be first considered. Namely, the n-th element of the response (eq. 3.9) to the ideal single harmonic will be (Storer, 1991):

$$y_n(t) = \int_{-\infty}^{\infty} \cdots \int_{-\infty}^{\infty} g_n(\tau_1, \cdots, \tau_n) \prod_{i=1}^{n} Ae^{j\omega(t-\tau_i)} d\tau_1 \cdots d\tau_n \tag{3.2.11}$$

or

$$y_n(t) = A^n e^{jn\omega t} \int_{-\infty}^{\infty} \cdots \int_{-\infty}^{\infty} g_n(\tau_1, \cdots, \tau_n) \prod_{i=1}^{n} e^{-j\omega\tau_i} d\tau_1 \cdots d\tau_n \tag{3.2.12}$$

which, considering the definition (3.2.10), becomes:

$$y_n(t) = A^n e^{jn\omega t} G_n(\omega, ..., \omega) \tag{3.2.13}$$

From this expression it may be seen that each element of the response to a single harmonic input is also a single harmonic at frequency $n\omega$, and the whole response is composed of a series of single harmonics at integer multiples of fundamental frequency:

$$y^{nonlin}(t) = \sum_{n=1}^{\infty} G_n(\omega, ..., \omega) A^n e^{jn\omega t} \tag{3.2.14}$$

Each of the output harmonics (eq. 3.2.13) has in the frequency domain following form:

$$Y(n\omega) = X(\omega)^n G_n(\omega, ..., \omega) \tag{3.2.15}$$

which shows that n-th harmonic defines uniquely the n-th order FRF $G_n(\omega, ..., \omega)$. If the ideal single harmonic input, $Ae^{j\omega t}$, could be realized physically, this would be the technique for straightforward determination of $G_n(\omega, ..., \omega)$ by simple separating the harmonics from the output spectra:

$$G_n(\omega, ..., \omega) = \frac{Y(n\omega)}{X(\omega)^n} \tag{3.2.16}$$

However, as already mentioned, the ideal single harmonic signal is not feasible. The nearest real signal is a single co-sinewave , which can be regarded as a sum of two ideal harmonics:

$$x(t) = A\cos(\omega t) = \frac{A}{2} e^{j\omega t} + \frac{A}{2} e^{-j\omega t} \tag{3.2.17}$$

By expanding the Volterra series (eq.3.9) for the single co-sinewave input, the first three elements will be:

$$y_1(t) = G_1(\omega) \frac{A}{2} e^{j\omega t} + G_1(-\omega) \frac{A}{2} e^{-j\omega t} \tag{3.2.18}$$

$$y_2(t) = \underbrace{G_2(\omega, \omega) \left(\frac{A}{2}\right)^2 e^{2j\omega t}}_{\substack{\text{second order term} \\ \text{of the response to} \\ \text{ideal single harmonic } (A/2)e^{j\omega t} \\ (eq.3.2.13)}} + \underbrace{2G_2(\omega, -\omega) \left(\frac{A}{2}\right)^2 e^{0}}_{\substack{\text{second order intermodulation} \\ \text{of input harmonics} \\ (A/2)e^{j\omega t} \text{ and } (A/2)e^{-j\omega t}}} + \underbrace{G_2(-\omega, -\omega) \left(\frac{A}{2}\right)^2 e^{-2j\omega t}}_{\substack{\text{second order term} \\ \text{of the response to} \\ \text{ideal single harmonics } (A/2)e^{-j\omega t} \\ (eq.3.2.13)}} \tag{3.2.19}$$

$$y_3(t) = G_3(\omega,\omega,\omega)\left(\frac{A}{2}\right)^3 e^{3j\omega t} + 3G_3(\omega,\omega,-\omega)\left(\frac{A}{2}\right)^3 e^{j\omega t} + 3G_3(-\omega,-\omega,\omega)\left(\frac{A}{2}\right)^3 e^{-j\omega t} + G_3(-\omega,-\omega,-\omega)\left(\frac{A}{2}\right)^3 e^{-3j\omega t} \quad (3.2.20)$$

The first element $y_1(t)$, is equal to the response of the linearized system to the single co-sinewave, $y^{lin}(t)$, (Eq. (3.2.5)), and it represents the sum of the responses to the individual harmonics contained in the co-sinewave input.

However, the second element of the response, $y_2(t)$, contains, besides the terms which characterize second order interactions of the individual harmonics ($(e^{j\omega t})^2$ and $(e^{-j\omega t})^2$), also the term which represents the second order intermodulations of two input harmonics (combined effect, $e^{j\omega t} \times e^{-j\omega t}$), resulting in a new (zero) frequency. Multiple interactions and intermodulations of input frequencies are characteristic only for the nonlinear systems. They are the reason for appearance of the frequencies different than fundamental in the output spectrum.

The third element, $y_3(t)$, shows that for the nonlinearities of the third order, the number of possible intermodulations increases (six intermodulation terms in eq. (3.2.20)). Generally, the n-th element of the response of a nonlinear system to a single co-sinewave input can be represented as:

$$y_n(t) = \sum_{i=0}^{n} {}_nB_i G_{n,i}\left(\frac{A}{2}\right)^n e^{j(n-2i)\omega t} \quad (3.2.21)$$

where ${}_nB_i$ is the binomial coefficient:

$${}_nB_i = \frac{n!}{i!(n-i)!} \quad (3.2.22)$$

and $G_{n,i}$ denotes the n-th order FRFs:

$$G_{n,i} = G_n(\underbrace{\omega,\ldots,\omega}_{(n-i)\ times},\underbrace{-\omega,\ldots,-\omega}_{i\ times}) \quad (3.2.23)$$

Unlike the response to the ideal single harmonic input, where each element is a single harmonic related to a single FRF (eq.3.15), in the response to a single co-sinewave input each element contains contributions of FRFs related to multiple interactions (Eq. 3.2.23 for i=0 and i=n) and FRFs related to intermodulations (Eq.3.23 for i(1,n-1)) of the two frequency

components (ω and $-\omega$). The overall response of the nonlinear system (Eq. 3.2.8) for the co-sinewave input - nonlinear frequency response (NFR)- can be written as follows:

$$y^{nonlin}(t) = \sum_{n=0}^{\infty}\sum_{i=0}^{n} {}_{n}B_i G_{n,i}\left(\frac{A}{2}\right)^n e^{j(n-2i)\omega t} \tag{3.2.24}$$

It is obvious from Eq. (3.2.24) that the relation of the NFR and the FRFs of different orders is complex and that extracting the individual FRFs from the response is a demanding task. The approximate procedure for obtaining the higher-order FRFs are described in the following subsection.

3.2.2 Estimation of higher-order FRFs from the nonlinear frequency response

After applying of the conjugate symetry property (Storer, 1991) on the individual terms of the NFR (eqs. (3.2.18), (3.2.19) and (3.2.20)), the overall response (Eq. (3.2.24)) can be written as follows:

$$\begin{aligned} y^{nonlin}(t) = y_1(t) + y_2(t) + y_3(t) + ... = {} & |G_1(\omega)|2\left(\frac{A}{2}\right)\cos(\omega t + Arg(G_1(\omega)) + \\ & |G_2(\omega,\omega)|2\left(\frac{A}{2}\right)^2 \cos(2\omega t + Arg(G_2(\omega,\omega)) + |G_2(\omega,-\omega)|2\left(\frac{A}{2}\right)^2 + \\ & |G_3(\omega,\omega,\omega)|2\left(\frac{A}{2}\right)^3 \cos(3\omega t + Arg(G_3(\omega,\omega,\omega)) + \\ & |G_3(\omega,\omega,-\omega)|6\left(\frac{A}{2}\right)^3 \cos(\omega t + Arg(G_3(\omega,\omega,-\omega)) + ... \end{aligned} \tag{3.2.24a}$$

From this expression it is evident that the response of a nonlinear system to a single sinewave will be composed of a series of sinewaves at integer multiples of the fundamental frequency ($n\omega$), with a possible component at zero frequency (DC shift). Each of those sinewaves at $n\omega$ is a complex sinewave and contains series of single sinewaves. For example, by collecting the terms at ω from eq. (3.2.24a), the first harmonic of the response is obtained:

$$\begin{aligned} y(\omega t) = {} & |G_1(\omega)|2\left(\frac{A}{2}\right)\cos(\omega t + Arg(G_1(\omega)) + \\ & |G_3(\omega,\omega,-\omega)|6\left(\frac{A}{2}\right)^3 \cos(\omega t + Arg(G_3(\omega,\omega,-\omega)) + ... \end{aligned} \tag{3.2.25}$$

The second harmonic, at 2ω is:

$$y(2\omega t)=|G_2(\omega,\omega)|2\left(\frac{A}{2}\right)^2\cos(2\omega t+Arg(G_2(\omega,\omega))+$$
$$|G_4(\omega,\omega,\omega,-\omega)|8\left(\frac{A}{2}\right)^4\cos(2\omega t+Arg(G_4(\omega,\omega,\omega.-\omega))+... \quad (3.2.26)$$

The third harmonic can be obtained analoguosly by collecting the terms at 3ω from eq. (3.2.24a) and so on. Eqs. (3.2.25) and (3.2.26) in the frequency domain have the following forms:

$$Y(\omega)=Y_I=G_1(\omega)X(\omega)+\frac{3}{4}G_3(\omega,\omega,-\omega)X(\omega)^2\overline{X}(\omega)+... \quad (3.2.27)$$

$$Y(2\omega)=Y_{II}=\frac{1}{2}G_2(\omega,\omega)X(\omega)^2+\frac{1}{2}G_4(\omega,\omega,\omega,-\omega)X(\omega)^3\overline{X}(\omega)+... \quad (3.2.28)$$

Individual harmonics $Y(\omega)$, $Y(2\omega)$,... can be estimated directly by harmonic analysis of the experimentally masured time domain NFR. Eq. (3.2.27) shows that first harmonic contains contributions of the first- and odd higher-order FRFs, while eq. (3.2.28) shows that the second harmonic contains the contributions of the second- and even higher-order FRFs. Since for weakly nonlinear systems, the contributions of higer-order FRFs decrease with the increase of their order, it arises that $G_1(\omega)$ corresponds to the dominant term of the first harmonic (eq. (3.2.27)) and $G_2(\omega,\omega)$ corresponds to the dominant term of the second harmonic (eq. (3.2.28)). All terms in Eqs. (3.2.27) and (3.2.28) depend on the input amplitude X. Taking those facts into account, it is possible to estimate approximately the FRFs by measuring the output harmonics. In the approach suggested by Lee (1997), each output harmonic ($Y(\omega)$, $Y(2\omega)$,...) is approximated by a sum of first k terms and the FRFs corresponding to those terms are estimated from the responses for k different input amplitudes by solving the system of algebraic equations. For example, if the first harmonic (eq. (3.2.27)) is approximated by first two terms:

$$Y_I=G_1(\omega)X(\omega)+\frac{3}{4}G_3(\omega,\omega,-\omega)X(\omega)^2\overline{X}(\omega) \quad (3.2.27a)$$

and measured for two different input amplitudes X_1 and X_2:

$$Y_{I,1}=G_1(\omega)X_1(\omega)+\frac{3}{4}G_3(\omega,\omega,-\omega)X_1(\omega)^2\overline{X_1}(\omega) \quad (3.2.27b)$$

$$Y_{I,2}=G_1(\omega)X_2(\omega)+\frac{3}{4}G_3(\omega,\omega,-\omega)X_2(\omega)^2\overline{X}_2(\omega) \quad (3.2.27c)$$

then the FRFs $G_1(\omega)$ and $G_3(\omega,\omega,-\omega)$ can be calculated by solving the system of eqs. (3.2.27b) and (3.2.27c). Similarly, the FRFs $G_2(\omega,\omega)$ and $G_4(\omega,\omega,\omega,-\omega)$ can be determined from the second harmonic measured for two different input amplitudes, and so on. The larger number of terms considered in individual harmonics provides higher accuracy of the obtained FRFs, but requires more measurements.

In the linear FR approach, (discussed in Section 2.5), very small input amplitudes (<2%) are used, such that contributions of all higher-order FRFs ($n\geq 2$) become negligible, and the response contains only the first harmonic in the form:

$$Y_I \approx G_1(\omega)X(\omega) \tag{3.2.29}$$

In that case $G_1(\omega)$ is directly calculated from eq. (3.2.29). Similarly, it can be assumed that for a somewhat larger input amplitude, it is possible to obtain the response where the contributions of FRFs of the third- and higher-order become negligible, and the response contains only the first harmonic (defined by eq. (3.2.29)) and the second harmonic as follows:

$$Y_{II} \approx \frac{1}{2}G_2(\omega,\omega)X(\omega)^2 \tag{3.2.30}$$

which would enable calculation of $G_2(\omega,\omega)$ form the experiments performed with only one input amplitude. The magnitudes of X for which eq. (3.2.30) is valid depends on the nonlinearity of the concrete system.

3.2.3 Theoretical derivation of FRFs

The procedures described in the previous subsection reffer to experimental estimation of higher-order FRFs. In order to obtain theoretical higher-order FRFs corresponding to a certain nonlinear model, the following general procedure has to be applied:

1) The first step in derivation of theoretical FRFs is setting the model of the nonlinear system in the time domain (generally set of PDEs).

2) In the second step, the input (x) and the output (y) variables have to be specified.

3) The specified input variable is expressed as a periodic function of the general form $x(t)=\sum_{k=1}^{N} A_k e^{j\omega_k t}$ and the output variable is expressed in the form of Volterra series

$y(t)=\sum_{n=1}^{\infty} y_n(t)$, with the *n*-th element in the form:

$$y_n(t)=\sum_{k_1=1}^{N}\sum_{k_2=1}^{N}\ldots\sum_{k_n=1}^{N} A_{k_1}A_{k_2}\ldots A_{k_n}G_n\left(\omega_{k_1},\omega_{k_2},\ldots,\omega_{k_n}\right)e^{j\left(\omega_{k_1}+\omega_{k_2}+\ldots+\omega_{k_n}\right)t} \qquad (3.2.31)$$

The previously defined input and output are then substituted into the time domain model equation(s).

4) In this step the method of *harmonic probing* (Weiner and Spina, 1980) is applied. Namely, the coefficients of $A_{k_1}A_{k_2}\ldots A_{k_n}e^{j\left(\omega_{k_1}+\omega_{k_2}+\ldots+\omega_{k_n}\right)t}$ on each side of the model equation obtained in the previous step are equated, thus giving the expressions which defines the *n*-th order FRF $G_n\left(\omega_{k_1},\omega_{k_2},\ldots,\omega_{k_n}\right)$ as a function of frequency.

5) By solving the equation obtained in the previous step, the *n*-th order FRF $G_n\left(\omega_{k_1},\omega_{k_2},\ldots,\omega_{k_n}\right)$ is obtained. It should be emphasized that the solution procedure is recursive. Namely, for solving the equation which defines *n*-th order FRF, the equations which define the FRFs of all orders lower than *n*-th have to be solved previously.

For illustration, in order to obtain the first-order FRF, the specified input variable is expressed as a single periodic input $x(t)=Ae^{j\omega t}$ and the corresponding output in the form of Volterra series will be:

$$y(t)=G_1(\omega)Ae^{j\omega t}+G_2(\omega,\omega)Ae^{2j\omega t}+\ldots \qquad (3.2.32)$$

By substitution of the previously defined input and output into the time domain model equation and equating the coefficients of $Ae^{j\omega t}$ on each side of the obtained expression, the equation which defines first-order FRF $G_1(\omega)$ is obtained.

In order to obtain the second-order FRFs, the input variable is expressed as a periodic function of two frequencies $x(t)=A_1e^{j\omega_1 t}+A_2e^{j\omega_2 t}$, and the corresponding output will be:

$$\begin{aligned} y(t)&=G_1(\omega_1)A_1e^{j\omega_1 t}+G_1(\omega_2)A_2e^{j\omega_2 t}+\\ &G_2(\omega_1,\omega_1)A_1^2e^{2j\omega_1 t}+2G_2(\omega_1,\omega_2)A_1A_2e^{j(\omega_1+\omega_2)t}+G_2(\omega_2,\omega_2)A_2^2e^{2j\omega_2 t}+\ldots. \end{aligned} \qquad (3.2.33)$$

Again, after substitution of the input and output into the time domain model equation and equating the coefficients of $A_1A_2e^{j(\omega_1+\omega_2)t}$, the expression which defines $G_2(\omega_1,\omega_2)$ is obtained. For the case $\omega_1=\omega_2$, the FRF $G_2(\omega,\omega)$, which corresponds to second-order interactions of input frequency is obtained. The expressions for the third- and higher-order FRFs can be derived in an analogous way.

3.3 Adsorber vs. particle higher-order FRFs for the case of a nonisothermal batch adsorber

At the end of 90s, Petkovska and Do (1998) have proposed the utilization of the previously described general concept of higher-order FRFs for investigation of the gas-solid adsorption. In the frame of their comprehensive theoretical studies, they have defined the higher-order FRFs for general nonisothermal adsorption system and established the procedure as well as the theoretical basis for practical application of the NFR for characterization of equilibrium and kinetics of adsorption (Petkovska, 2001). The excerpts from their theoretical work, concerning the nonisothermal batch adsorber will be given below. The FRFs up to the second-order will be considered.

3.3.1 Definitions of FRFs

In Fig.3.3.1 a batch adsorber of a volume V (which can be modulated), containig a certan amount of solid adsorbent is shematically presented. It is assumed that the gas (at temperature T_g and pressure P) is ideally mixed, that the adsorbent particles (at loading Q and temperture T_p) are equally exposed to the gas and that the system is in temperature and concentration equilibrium in the initial state ($Q=Q_s(P)$, $T_p=T_g$ at t=0).

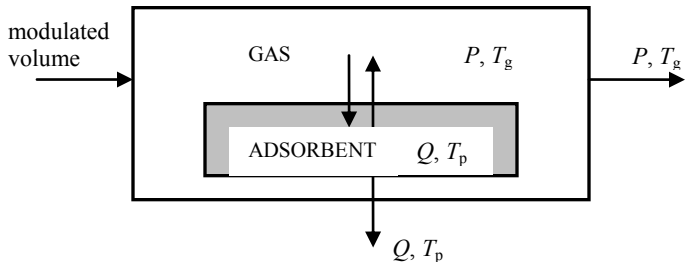

Fig. 3.3.1 Shematic representation of an ideally mixed batch adsorber

When the volume is modulated periodically, in the general nonisothermal case, all four output variables (P, T_g, Q, T_p) change, and in the quasi steady-state become periodic functions of time as well. Each output is related to the input through an indefinite sequence of FRFs, as shown in block diagram given in Fig.3.3.2. These functions are named the adsorber FRFs.

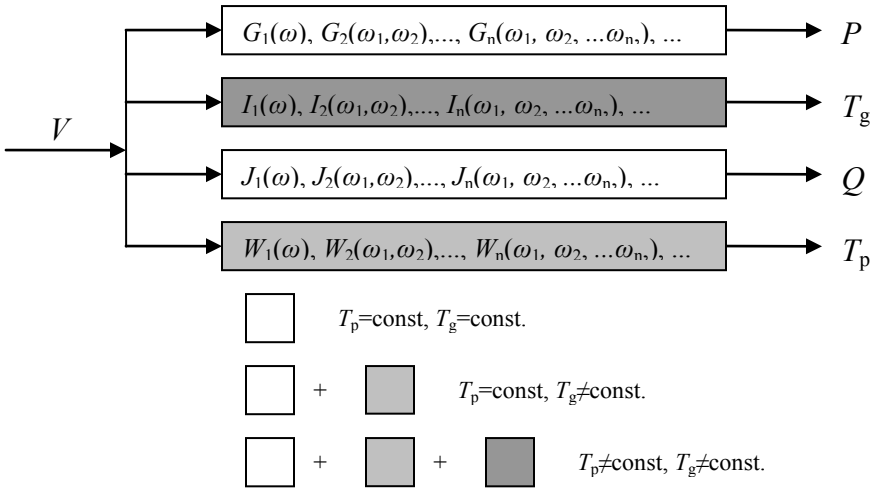

Fig.3.3.2 A general block diagram of a batch adsorber and definitions of adsorber FRFs (Petkovska, 2001)

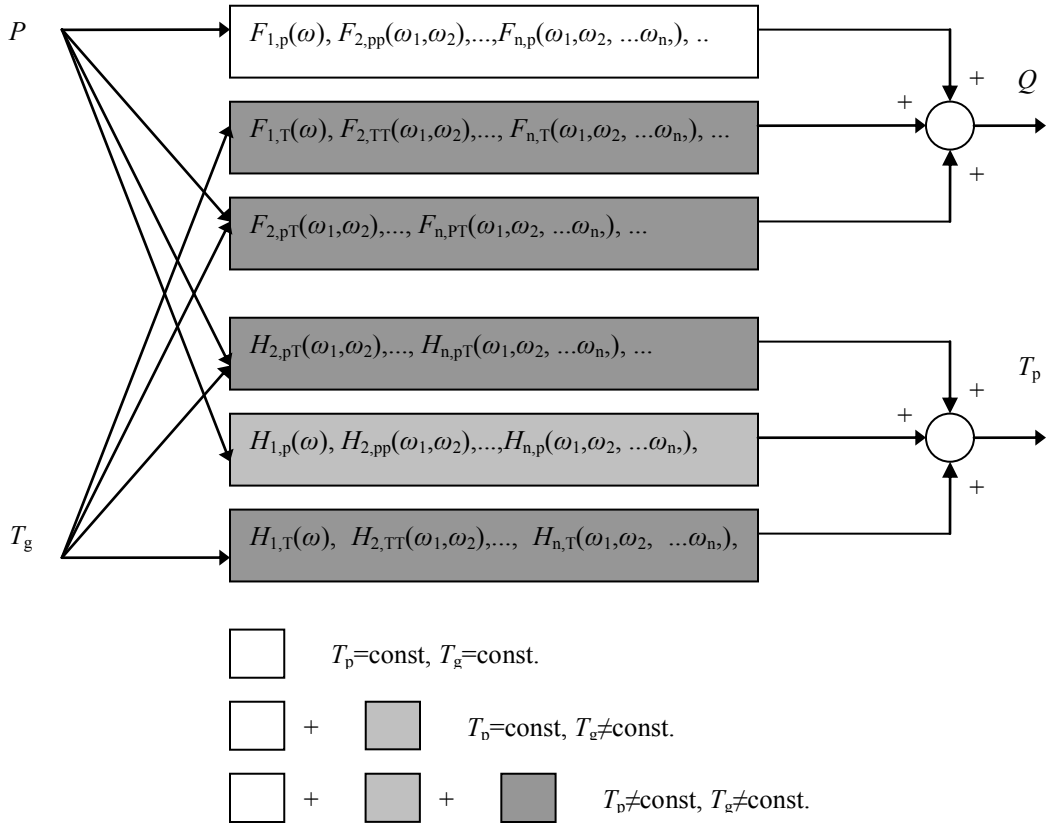

Fig.3.3.3 A general block diagram of an adsorbent particle and definitions of particle FRFs (Petkovska, 2001)

However, if we recognize the adsorbent particles as a subsystem of the adsorber, then P and T_g are inputs and Q and T_p outputs for this subsystem. For the general nonisothermal case, six sets of FRFs are needed to define the particle model, as it is represented in block diagram in Fig. 3.3.3.

Four sets of FRFs ($\boldsymbol{F}_p$, $\boldsymbol{F}_T$, $\boldsymbol{H}_p$, and $\boldsymbol{H}_T$) relate each output to each input, and two sets of cross-functions ($\boldsymbol{F}_{pT}$ and $\boldsymbol{H}_{pT}$), relate each output to both inputs. These FRFs are the particle FRFs. The adsorber FRFs (Fig. 3.3.2) represent the model of the adsorber and the particle FRFs (Fig. 3.3.3) represent the model of the kinetic mechanism in the frequency domain for a general nonlinear nonisothermal case.

For the special nonisothermal case (T_g=const., $T_p \neq$const.) the complete model is reduced to three series of adsorber FRFs ($\boldsymbol{G}$, $\boldsymbol{J}$ and $\boldsymbol{W}$ functions) and two series of particle FRFs ($\boldsymbol{F}_p$ and $\boldsymbol{H}_p$), while for isothermal case (T_p=const, T_g=const.) it reduces to two series of adsorber ($\boldsymbol{G}$ and $\boldsymbol{J}$) and one series of particle FRFs ($\boldsymbol{F}_p$).

According to the definitions given above, it can be concluded that the particle FRFs are those which are relevant for kinetic mechanism identification.

3.3.2 Procedure for application of the NFR method

The procedure for application of the NFR method on the example of a batch adsorber presented in Fig. 3.3.1., according to (Petkovska, 2001), consists of the following steps:

Step 1. Experimental FR measurements. The volume is modulated in a sinusoidal way and, after a quasi-steady state is reached, all directly measurable adsorber outputs are measured and recorded. The experiments are performed for a number of different frequencies and for several different values of the input amplitude.

Step 2. Harmonic analysis of the output signals. The recorded output signals are analyzed using Fast Fourier Transform. As a result, the amplitudes and phases of the first, second, third, …, harmonics of the measured outputs are obtained.

Step 3. Estimation of the adsorber FRFs. The adsorber FRFs corresponding to the measured outputs are estimated based on the values of individual harmonics obtained in Step 2, using the procedure given by Lee (1997)(Section 3.2.2). In the case that some of the adsorber outputs can not be measured directly (usually that is the case with the loading Q, and sometimes with the particle temperature T_p) the FRFs corresponding to the unmeasured

outputs are calculated using the adsorber model equations (Petkovska, 2001). An example, concerning the calculation of FRFs to unmeasured adsorbed quantity Q, will be given in Section 3.3.3.

Step 4. Calculation of the particle FRFs. The particle FRFs ("F" and "H" functions) have to be calculated from the adsorber ones, obtained in step 3. The key equations which relate the adsorber and particle FRFs are obtained by expressing Q and $T_{p,}$ once as the responses to the volume change (according to the block diagram in Figure 3.3.2) and the other time as the responses to P and/or T_g changes (according to the block diagram in Figure 3.3.3)(Petkovska, 2001). The relations between the particle and adsorber FRFs concerning special nonisothermal case (T_g=const., T_p≠const.) will be derived in Section 3.3.4.

Step 5. Identification of the kinetic model. The particle FRFs calculated in Step 4 are compared with theoretically derived sets of particle FRFs corresponding to different mechanisms. Recognizing the significant patterns of the FRFs, the most probable model or models are chosen. This step assumes that a library of theoretical sets of particle FRFs corresponding to different kinetic mechanisms has been previously formed. The procedure for derivation of theoretical particle FRFs as well as the review of the existing library of theoretical FRFs is given in the Section 3.3.5.

Step 6. Parameter estimation. Using the model chosen in Step 5 and the particle FRFs estimated from the experimental FR measurements, obtained in Step 4, the model parameters are estimated. The methodology of parameter estimation for several simpler kinetic mechanisms is given in (Petkovska, 2006).

3.3.3 Calculation of the adsorber FRF corresponding to unmeasurable loading (Q)

The procedure for calculation of the adsorber FRFs corresponding to unmeasurable outputs for general nonisothermal case can be found in Petkovska (2001). Since the assumption of constant gas temperature is commonly used in the FR studies regarding nonisothermal gas adsorption (Giesy et al., 2012; Bourdin et al., 1996; Sun et al., 1994; Sun et Bourdin, 1993), the special nonisothermal case T_p≠const. and T_g=const will be considered here. According to the block diagram in Fig. 3.3.2, for the case T_p≠const. and T_g=const., three series of adsorber FRFs $\boldsymbol{G}$, $\boldsymbol{W}$ and $\boldsymbol{J}$ functions, represent the model of adsorber. If we consider P and T_p as the

measurable outputs and Q as unmeasurable output (which is most often the case), than the functions $\boldsymbol{G}$ and $\boldsymbol{W}$ can be calculated directly from measured outputs P and T_p, respectively, by using the procedure given by Lee (1997), while the $\boldsymbol{J}$ functions (which correspond to the unmeasurable output Q) are calculated by using the adsorber model equation and the $\boldsymbol{G}$ and $\boldsymbol{W}$ functions obtained from the measurements. The procedure is presented below.

The mass balance of the batch adsorber (Fig. 3.3.1), when T_g=const. , is following:

$$\frac{1}{R_g T}\frac{d(PV)}{dt}+\frac{1}{V_p}\frac{dQ}{dt}=0 \tag{3.3.1}$$

If we define the dimensionles variables (volume, pressure and loading), as the deviation variables divided by the corresponding steady-state values:

$$v=\frac{V-V_s}{V_s}\ ;\qquad p=\frac{P-P_s}{P_s}\ ;\qquad q=\frac{Q-Q_s}{Q_s}\ ; \tag{3.3.2}$$

than the eq. (3.3.1) can be written as follows:

$$\frac{d}{dt}\left((1+p)(1+v)\right)+\beta\frac{dq}{dt}=0 \tag{3.3.1a}$$

where $\beta=\dfrac{m_p Q_s R_g T}{\rho_p V_s P_s}$ is the partition coefficient.

In order to obtain the first-order function $J_1(\omega)$, the volume is expresed as single harmonic function $v=Ae^{j\omega t}$ and the adsorber outputs, according to the block diagram in Fig. 3.3.2, are:

$$p=G_1(\omega)Ae^{j\omega t} \tag{3.3.3}$$

$$q=J_1(\omega)Ae^{j\omega t} \tag{3.3.4}$$

$$\theta_p=W_1(\omega)Ae^{j\omega t} \tag{3.3.5}$$

By substitution of the input $v=Ae^{j\omega t}$ and equations (3.3.3) and (3.3.4) into the balance equation (3.3.2), and by equalizing the terms with $Ae^{j\omega t}$ we obtain:

$$J_1(\omega)=-\frac{G_1(\omega)+1}{\beta} \tag{3.3.6}$$

For the second-order FRF $J_2(\omega,\omega)$, the input is dfined as two harmonic function $v=A_1e^{j\omega_1 t}+A_2e^{j\omega_2 t}$, and the outputs as follows:

$$\begin{aligned}p=&G_1(\omega_1)A_1e^{j\omega_1 t}+G_1(\omega_2)A_2e^{j\omega_2 t}+\\&G_2(\omega_1,\omega_1)A_1^2e^{2j\omega_1 t}+G_2(\omega_2,\omega_2)A_2^2e^{2j\omega_2 t}+2G_2(\omega_1,\omega_2)A_1A_2e^{j(\omega_1+\omega_2)t}+\ldots\end{aligned} \tag{3.3.7}$$

$$q = J_1(\omega_1)A_1e^{j\omega_1 t} + J_1(\omega_2)A_2e^{j\omega_2 t} + J_2(\omega_1,\omega_1)A_1^2e^{2j\omega_1 t} + J_2(\omega_2,\omega_2)A_2^2e^{2j\omega_2 t} + 2J_2(\omega_1,\omega_2)A_1A_2e^{j(\omega_1+\omega_2)t} + \ldots \quad (3.3.8)$$

$$\theta_p = W_1(\omega_1)A_1e^{j\omega_1 t} + W_1(\omega_2)A_2e^{j\omega_2 t} + W_2(\omega_1,\omega_1)A_1^2e^{2j\omega_1 t} + W_2(\omega_2,\omega_2)A_2^2e^{2j\omega_2 t} + 2W_2(\omega_1,\omega_2)A_1A_2e^{j(\omega_1+\omega_2)t} + \ldots \quad (3.3.9)$$

By substitution of the input $v = A_1e^{j\omega_1 t} + A_2e^{j\omega_2 t}$ as well as eqs. (3.3.7) and (3.3.8) into the mass balance equation (3.3.2), and by equalizing the terms with $A_1A_2e^{j(\omega_1+\omega_2)t}$ we obtain:

$$J_2(\omega_1,\omega_2) = -\frac{2G_2(\omega_1,\omega_2) + G_1(\omega_1) + G_1(\omega_2)}{2\beta} \quad (3.3.10)$$

3.3.4 Relations between the adsorber and the particle FRFs for special nonisothermal case (T_g=const. and T_p≠const.)

According to the block diagram in Fig. 3.3.3 for the special nonisothermal case (T_g=const. T_p≠const.), two series of particle FRFs represent the kinetic model ***F*** and ***H*** functions. In order to obtain the first-order FRFs $F_1(\omega)$ and $H_1(\omega)$, the outputs q and θ_p are expressed, once acording to the adsorber model (eqs. 3.3.4 and 3.3.5) and the other time according to the particle model:

$$q = G_1(\omega)F_1(\omega)Ae^{j\omega t} \quad (3.3.11)$$

$$\theta_p = G_1(\omega)H_1(\omega)Ae^{j\omega t} \quad (3.3.12)$$

By equating the right hand sides of eqs. (3.3.4) and (3.3.11) it follows:

$$J_1(\omega) = G_1(\omega)F_1(\omega) \quad (3.3.13)$$

which, by taking into account eq. (3.3.6) becomes:

$$F_1(\omega) = -\frac{G_1(\omega) + 1}{\beta G_1(\omega)} \quad (3.3.14)$$

Similarly, by equating the right hand sides of eqs. (3.3.5) and (3.3.12) one obtains:

$$W_1(\omega) = G_1(\omega)H_1(\omega) \quad (3.3.15)$$

Since $G_1(\omega)$ and $W_1(\omega)$ can be directly estimated from measurements, the function $H_1(\omega)$ can be calculated as follows:

$$H_1(\omega) = \frac{W_1(\omega)}{G_1(\omega)} \quad (3.3.16)$$

For the second order particle FRFs $F_2(\omega,\omega)$ and $H_2(\omega,\omega)$, q and θ_p are expressed once acording to the adsorber model (eqs.3.3.8 and 3.3.9) and then according to the particle model:

$$\begin{aligned} q = {} & G_1(\omega_1)F_1(\omega_1)A_1e^{j\omega_1 t} + G_1(\omega_2)F_1(\omega_2)A_2e^{j\omega_2 t} + \\ & A_1^2G_2(\omega_1,\omega_2)F_1(2\omega_1)e^{2j\omega_1 t} + 2A_1A_2G_2(\omega_1,\omega_2)F_1(\omega_1+\omega_2)e^{j(\omega_1+\omega_2)t} + \\ & A_2^2G_2(\omega_1,\omega_2)F_1(2\omega_2)e^{2j\omega_2 t} + A_1^2G_1(\omega_1)^2F_2(\omega_1,\omega_1)e^{2j\omega_1 t} + \\ & A_2^2G_1(\omega_2)^2F_2(\omega_2,\omega_2)e^{2j\omega_2 t} + 2A_1A_2G_1(\omega_1)G_1(\omega_2)F_2(\omega_1,\omega_2)e^{j(\omega_1+\omega_2)t} + \ldots \end{aligned} \tag{3.3.17}$$

$$\begin{aligned} \theta_p = {} & G_1(\omega_1)H_1(\omega_1)A_1e^{j\omega_1 t} + G_1(\omega_2)H_1(\omega_2)A_2e^{j\omega_2 t} + \\ & A_1^2G_2(\omega_1,\omega_2)H_1(2\omega_1)e^{2j\omega_1 t} + 2A_1A_2G_2(\omega_1,\omega_2)H_1(\omega_1+\omega_2)e^{j(\omega_1+\omega_2)} + \\ & A_2^2G_2(\omega_1,\omega_2)H_1(2\omega_2)e^{2j\omega_2 t} + A_1^2G_1(\omega_1)^2H_2(\omega_1,\omega_1)e^{2j\omega_1 t} + \\ & A_2^2G_1(\omega_2)^2H_2(\omega_2,\omega_2)e^{2j\omega_2 t} + 2A_1A_2G_1(\omega_1)G_1(\omega_2)H_2(\omega_1,\omega_2)e^{j(\omega_1+\omega_2)t} + \ldots \end{aligned} \tag{3.3.18}$$

By equating the right hand sides of eqs. (3.3.8) and (3.3.17) it follows:

$$F_2(\omega_1,\omega_2) = \frac{J_2(\omega_1,\omega_2) - G_2(\omega_1,\omega_2)F_1(\omega_1+\omega_2)}{G_1(\omega_1)G_1(\omega_2)} \tag{3.3.19}$$

which, by taking into account eq. (3.3.10) becomes:

$$F_2(\omega_1,\omega_2) = -\frac{1}{\beta}\frac{G_2(\omega_1,\omega_2) + \left[G_1(\omega_1) + G_1(\omega_2)\right]/2 + G_2(\omega_1,\omega_2)\beta F_1(\omega_1+\omega_2)}{G_1(\omega_1)G_1(\omega_2)} \tag{3.3.20}$$

For the case $\omega_1 = \omega_2 = \omega$, this function becomes:

$$F_2(\omega,\omega) = -\frac{1}{\beta}\frac{G_2(\omega,\omega) + G_1(\omega) + G_2(\omega,\omega)\beta F_1(2\omega)}{G_1(\omega)^2} \tag{3.3.21}$$

while for the case $\omega_1 = -\omega_2 = \omega$, this function becomes:

$$F_2(\omega,-\omega) = -\frac{1}{\beta}\frac{G_2(\omega,-\omega) + \left[G_1(\omega) + G_1(-\omega)\right]/2 + G_2(\omega,-\omega)\beta F_1(0)}{G_1(\omega)G_1(-\omega)} \tag{3.3.22}$$

Analogously, by equating the right hand sides of eqs. (3.3.9) and (3.3.18) it follows:

$$H_2(\omega_1,\omega_2) = \frac{W_2(\omega_1,\omega_2) - G_2(\omega_1,\omega_2)F_1(\omega_1+\omega_2)}{G_1(\omega_1)G_1(\omega_2)} \tag{3.3.23}$$

which for the case $\omega_1 = \omega_2 = \omega$ becomes:

$$H_2(\omega,\omega) = \frac{W_2(\omega,\omega) - G_2(\omega,\omega)F_1(2\omega)}{G_1(\omega)^2} \tag{3.3.24}$$

and for the case $\omega_1 = -\omega_2 = \omega$:

$$H_2(\omega,-\omega)=\frac{W_2(\omega,-\omega)-G_2(\omega,-\omega)F_1(0)}{G_1(\omega)G_1(-\omega)} \tag{3.3.25}$$

3.3.5 Theoretical derivation of FRFs for adsorption kinetic models

General procedure for theoretical derivation of FRFs is given in Section 3.2.3. In order to derive of the theoretical higher-order FRFs for the adsorbing particle (***F*** and ***H*** functions), it is necessary firstly to define the mass and heat balance equations which describe the certain kinetic model, which are generally PDEs (as it has been described in Section 2.4.2). The adsorption equilibrium is described with the adsorption isotherm, which has to be developed into Taylor series around a steady-state. According to the block diagram of the adsorbing particle (Fig. 3.3.3) the inputs may be pressure and/or gas temperature and the outputs: mean sorbate concentration in the particle and/or mean particle temperature. After definition of the input(s) and output(s), the harmonic probing method (described in Section 3.2.3) is applied. As a result, the ODEs in which the ***F*** and ***H*** functions are dependant variables of frequency are obtained. Those ODEs can be solved analytically or numerically. The existing library of theoretical FRFs contains FRFs up to the second-order for the following kinetic models: isthermal Langmuir kinetic, isothermal film resistance control, isothremal micropore diffusion, isothermal pore-surface diffusion (Petkovska and Do, 2000), non-isothermal micropore diffusion, two independamnt diffusional processes, diffusion-rearrangement process (Petkovska and Petkovska, 2003) and non-isothermal micropore diffusion with variable diffusivity (Petkovska, 2000). In this work the theoretical FRFs up to the second order for the nonisothermal macropore diffusion model will be derived and presented in Chapter 5.

3.4 Other applications of the NFR method in chemical engineering

Theoretical study of Petkovska and co-workers regarding application of the concept of higher-order FRFs has given impetus for application of that concept in similar fields of chemical engineering. Ilić and co-workers have applied the concept of higher-order FRFs in order to determine experimentally the single solute and competitive adsorption isotherms of

liquid-solid systems (Ilić et al., 2007a; Ilić et al., 2007b; Ilić et al., 2007c; Ilić et al., 2008; Ilić et al., 2009). They have measured the NFRs of a liquid chromatographic column and estimated the FRFs up to the third-order and used them further for calculation of first-, second- and third-order derivatives of the adsorption isotherm. Petkovska with a group of autors from the Max Planck Institute in Magdeburg made an effort to apply the NFR analysis for investigation of kinetics of electrochemical reactions. Bensmann et al. (2010) have derived theoretical FRFs for four different models for description of the kinetics of electrochemical methanol oxidation and showed that the shape of the second-order FRF can be used as a criterion for discrimination between different kinetic mechanisms. Vidaković-Koch et al. (2011) and Panić et al. (2011) have validated experimentally the NFR approach for investigation of the kinetics of electrochemical reactions on the example of ferrocyanide electrooxidation. Kadyk et al. (2012) have applied the concept of higher-order FRFs in order to diagnose different phenomena (such as flooding, dehydratation or CO poisoning) which may occur in the polymer electrolyte membrane (PEM) fuel cells. It was found that second-order FRF can be successfully used for diagnosis of the mentioned phenomena. The NFR approach has also been applied for theoretical analysis of the potential improvements of isothermal and non-isothermal CSTR performance by forced periodic operation (Nikolić et al. 2014a, 2014b, 2015). The FRFs up to the second-order corresponding to the cases of modulation of different input variables (inlet concentration, inlet flowrate, inlet temperature) have been derived and analyzed. The sign of the second-order asymetrical FRF has been proven as a criterion for estimation of the possible improvments in the reactor performances.

4. STUDY ON THE APPLICABILITY OF THE NFR METHOD FOR INVESTIGATING GAS ADSORPTION

Before constructing the experimental set-up for NFR measurements, an applicability study based on numerical simulations has been performed and presented in this chapter. It was necessary to evaluate the possibility of estimation of the experimental second-order FRF in order to design the NFR experiments. For that purpose, a mathematical model of a batch adsorber with film resistance kinetics has been implemented in MATLAB and the dynamic responses of the adsorber have been simulated. The simulations were performed using the adsorption isotherm for CO_2/zeolite 5A from the literature.

Based on the simulated responses for different input amplitudes, the nonlinearity of the system has firstly been analyzed and quantified. Based on the simulated NFRs, the possibility of estimation of the second-order FRF on the particle scale has been evaluated. By analyzing the influence of the following parameters: mass of the adsorbent, amplitude of volume modulation, frequency range and sampling rate, on the accuracy of estimation of the second-order FRF, criteria which define the optimal values of those parameters have been ascertained. Furthermore, a routine for determining the optimal values of the parameters for a concrete gas/solid system, based on the step responses, has been established. Finally, the procedure for application of the NFR method, described in Section 3.3.2, has been checked by using the simulated FRs as quasi-experimental data.

4.1. Model equations

The mathematical model of an isothermal ideally mixed adsorber with adsorption of a pure gas can be written as follows:

$$\frac{d}{dt}((1+p)(1+v))+\beta\frac{dq}{dt}=0 \qquad (4.1.1)$$

The dimensionless volume $v=(V-V_s)/V_s$, dimensionless pressure $p=(P-P_s)/P_s$ and dimensionless solid-phase concentration $q=(Q-Q_s)/Q_s$, are defined as the deviation variables divided by corresponding steady-state values (subscript s). The partition coefficient β is defined as follows:

$$\beta = \frac{m_p Q_s R_g T_g}{\rho_p V_s P_s} \tag{4.1.2}$$

where m_p is the mass of the adsorbent and ρ_p its density, R_g is the universal gas constant and T_g is the gas temperature. For simplicity, the film resistance model will be employed to describe the kinetic of adsorption:

$$\frac{dq}{dt} = k_m(p - p(q)) \tag{4.1.3}$$

where k_m is the modified mass transfer coefficient defined as:

$$k_m = k_a \frac{P_s}{Q_s} \tag{4.1.4}$$

where k_a (s^{-1}) is the mass transfer coefficient. The function $p(q)$ is the inverse of the adsorption isotherm relation $q(p)$ and may be represented as a Taylor series expansion:

$$p(q) = a_q q + b_q q^2 + \ldots \tag{4.1.5}$$

The coefficients a_q and b_q are proportional to the first and second derivatives of the function $p(q)$ at the given steady-state as follows:

$$a_q = \left.\frac{dp}{dq}\right|_s = \left.\frac{dP}{dQ}\right|_s \frac{Q_s}{P_s}, \quad b_q = \frac{1}{2}\left.\frac{d^2 p}{dq^2}\right|_s = \frac{1}{2}\frac{d^2 P}{dQ^2}\frac{Q_s^2}{P_s} \tag{4.1.6}$$

Adsorption isotherm used in the numerical simulations describes adsorption of CO_2 on zeolite 5A at 25°C (Brzić and Petkovska, 2015), which has a Toth form:

$$Q = mP(b + P^r)^{-1/r} \tag{4.1.7}$$

where parameters m, b and r have the following values: m=2354.3, b=2.6432 and r =0.4104. The units of those parameters are consistent pressure (P) in mbar and adsorbed quantity (Q) in mol/m^3.

4.2 Simulated step and FRs of the batch adsorber

In order to recognize and quantify the nonlinearity of the batch adsorption system (defined with the model given in the previous Section), the step responses and FRs, simulated for different steady-states, input amplitudes and frequencies, have been analyzed. The volume of the adsorber was the modulated input and the pressure was the output (response). The parameters used for simulations have been summarized in Table 4.2.1. The amplitudes of the

volume modulations have been varied up to 20 % of the steady-state volume, in order that the nonlinearity can be manifested and quantified based on the characteristics of the responses.

Table 4.2.1 Parameters used for step response and FR simulations

Volume of the adsorber in the steady-state (cm^3)	570
Temperature (K)	298
Density of the adsorbent (zeolite 5A) (kg/m^3)	640
Steady-state pressure (mbar)	20 50 100
Mass of the adsorbent* (g)	1.1 2.45 4.70
Mass transfer coefficient (s^{-1})	0.1, 1
Input amplitude (fraction) (-)	0.003 – 0.2
Frequency (rad/s)	10^{-6} - 1

*optimal mass corresponding to each steady-state (Section 4.3.1)

Step responses

The step change of the volume from the steady-state value V_s, can be defined as follows:

$$V = \begin{cases} V_s & t < 0 \\ V_s - AV_s & t \geq 0 \end{cases} \qquad (4.2.1)$$

where A is the amplitude (expressed as a fraction of V_s). An example of the volume step change for A= 0.05, together with the corresponding pressure response, is presented in Fig. 4.2.1.

It can be seen from Fig. 4.2.1b that the pressure response shows first an instant increase due to gas compression, and than gradual decrease due to adsorption. The obtained response has been approximated by a response of a series of a proportional element and a first-order system:

$$P - P_s = \Delta P_1 - \Delta P_2\left(1 - \exp\left(-t/\tau\right)\right) \qquad (4.2.2)$$

The first term on the right-hand side represents the pressure change due to compression:

$$\Delta P_1 = P_{s1}^{'} - P_s = K_1 \cdot \Delta V \qquad (4.2.3)$$

where K_1 ($mol/(m^3)^2$) is the static gain due to compression and $\Delta V = V_{s1} - V_s$. The second term on the right-hand side in eq. (4.2.2), represents the pressure change due to adsorption:

$$\Delta P_2 = P_{s1}^{'} - P_{s1} = K_2 \cdot \Delta V \qquad (4.2.4)$$

where K_2 (mol/(m^3)^2)is the static gain due to adsorption and τ (s) is an apparent time constant. The parameters K_1, K_2 and τ, estimated by fitting the simulated step responses for different amplitudes to eq. (4.2.2), are presented in Table 4.2.2.

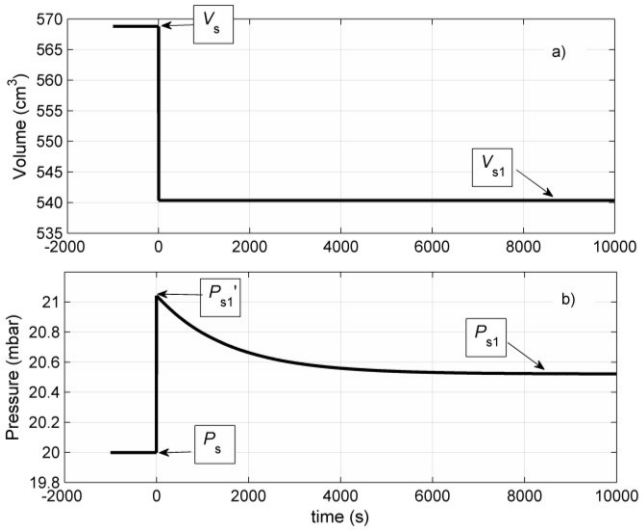

Fig. 4.2.1 a) Step change of the volume b) Pressure response (P_s=20 mbar, k_a=0.1s^{-1} and A= 0.05)

Table 4.2.2 Parameters of the step responses for different input amplitudes

A (-)	K_1 (mol/(m^3)^2)	K_2 (mol/(m^3)^2)	τ (s)	δK_1 (%)	δK_2 (%)
0.003	1406.5	692	1590	0	0
0.004	1406.5	692.2	1590	0	0.03
0.005	1406.5	692.7	1590	0	0.10
0.006	1406.5	694.7	1589	0	0.39
0.01	1424.1	698.8	1585	1.25	0.98
0.02	1432.8	709	1574	1.87	2.46
0.03	1453.4	719.6	1563	3.33	3.99
0.04	1468	730	1552	4.37	5.49
0.05	1480.3	740.9	1541	5.25	7.07
0.06	1497.3	752.2	1530	6.45	8.70
0.07	1514.5	763.5	1518	7.68	10.33
0.08	1529.5	775.3	1507	8.75	12.04
0.09	1547.1	787.2	1496	10.00	13.76
0.1	1564.7	799.6	1484	11.25	15.55

It can be seen that the model parameters are constant only for very small input amplitudes up to 0.005, where the system can be regarded as linear. For input amplitudes larger than 0.005 the model parameters vary with the input amplitude, which indicates the system nonlinearity.

The relative deviations of the static gains K_1 and K_2 from the values corresponding to the linear case $K_{1,0}$=1406.5 mol/(m^3)^2 and $K_{2,0}$ = 692.2 mol/(m^3)^2:

$$\delta K_i = \frac{K_i - K_{i,0}}{K_{i,0}} \cdot 100, \quad i = 1, 2 \tag{4.2.5}$$

can be used as a measure of the system nonlinearity. Those values are also given in Table 4.2.2.

Frequency responses

The FRs have been simulated for the cosinusoidal volume change around V_s:

$$V = V_s - AV_s \cdot \cos(\omega t) \tag{4.2.6}$$

An example of the simulated pressure response (expressed as a pressure deviation, ΔP=P-P_s), together with the corresponding volume change for A=0.05, is presented in Fig. 4.2.2.

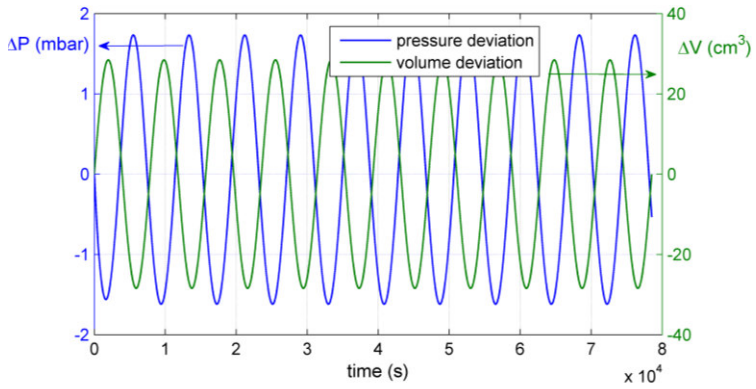

Fig.4.2.2 Pressure response to the sinusoidal volume change (P_s= 20 mbar, A= 0.05, k_a = 0.1 s^{-1}, ω = 0.0008 rad/s)

In the frequency domain, the volume and pressure time signals are represented by the corresponding frequency spectra, obtained by Fourier transform. The frequency spectrum is characterized the amplitude and phase of the time signal vs. frequency (or usually vs. dimensionless frequency = frequency/basic frequency). The frequency spectrum of the volume signal from Fig. 4.2.2 is presented in Fig. 4.2.3. Being a pure cosinusoidal function, the volume signal corresponds to a single harmonic (of amplitude 28.44 cm^3 and phase -1.57 rad). The frequency spectrum of the pressure response from Fig. 4.2.2 is presented in Fig. 4.2.4.

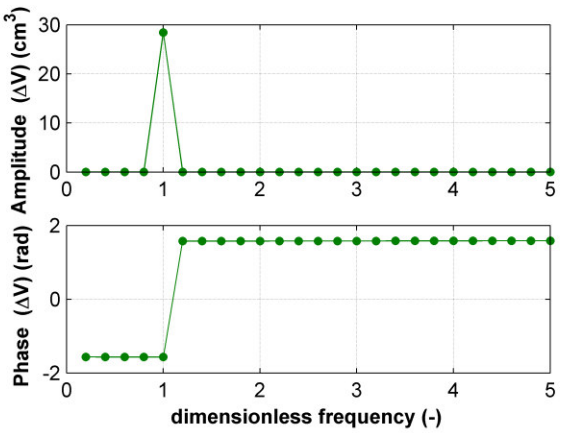

Fig 4.2.3 Frequency spectrum of the volume change from Fig. 4.2.2

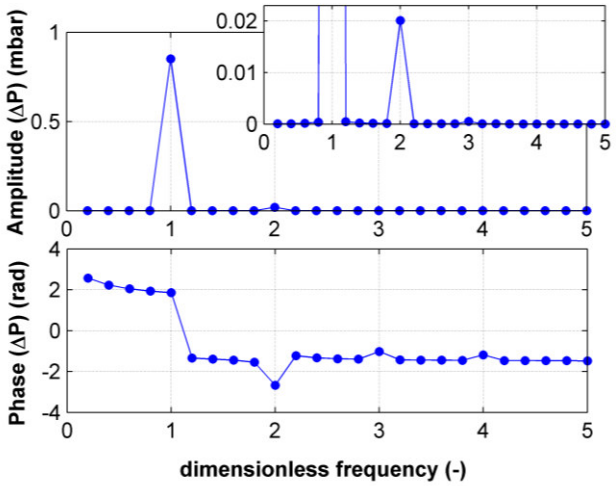

Fig. 4.2.4 Frequency spectrum of the pressure response from Fig. 4.2.2

It can be clearly seen from amplified magnitude of ΔP (Fig. 4.2.4) that, besides the component at the basic frequency (ω), higher harmonics are also present (at 2ω, 3ω,…), which means that the response of the nonlinear system is a complex periodic function which consists of the series of cosine waves (harmonics):

$$\begin{aligned}&\Delta P = \Delta P_I + \Delta P_{II} + \Delta P_{III} + \ldots = \\ &B_I \cos(\omega t + \varphi_I) + B_{II} \cos(2\omega t + \varphi_{II}) + B_{III} \cos(3\omega t + \varphi_{III}) + \ldots\end{aligned} \tag{4.2.7}$$

or in the frequency domain:

$$Y = Y_I + Y_{II} + Y_{III} + \ldots = B_I \exp(j\varphi_I) + B_{II} \exp(j\varphi_{II}) + B_{III} \exp(j\varphi_{III}) + \ldots \tag{4.2.8}$$

The first harmonic has the amplitude B_{I}=1.6751 mbar and phase φ_{I}=1.8973 rad (from Fig. 4.2.4), and it is defined, according to the concept of higher-order FRFs, by eq.(3.27). The second harmonic has the amplitude B_{II}=0.0333 mbar and phase φ_{II}=-2.5403 rad and it

corresponds to eq.(3.28). It is obvious that the magnitudes of the output harmonics decrease with increase of their order, which is characteristic for weakly nonlinear systems. In order to recognize the influence of the input amplitude on the output harmonics, the amplitudes of the first four harmonics of the output, for different input amplitudes, are given in Table 4.2.3.

Table 4.2.3 Amplitudes of the output harmonics for different input amplitudes (P_s=50 mbar, ω_0=0.0008 rad/s)

Input amplitude	Amplitude of the output harmonics (mbar)				$(Y_{II}/ Y_I)\cdot 100$ (%)
	Y_I	Y_{II}	Y_{III}	Y_{IV}	
0.01	0.3348	0.0013	$2.86\cdot10^{-5}$	$1.69\cdot10^{-5}$	0.39
0.02	0.6696	0.0053	$8.77\cdot10^{-5}$	$3.33\cdot10^{-5}$	0.79
0.05	1.6751	0.0333	$8.09\cdot10^{-4}$	$7.07\cdot10^{-5}$	1.98
0.1	3.3582	0.1336	$5.90\cdot10^{-3}$	$1.71\cdot10^{-4}$	3.98

It can be seen from Table 4.2.3 that the output harmonics increase with increase of the input amplitude. If we compare the magnitudes of the harmonics for input amplitudes 0.01 and 0.1, it can be concluded that, when the input amplitude increases 10 times, the first-harmonic increases linearly, while the second harmonic increases 10^2 times, the third harmonic increases $2\cdot10^2$ times, and the fourth harmonic about 10 times. This clearly shows how higher harmonics reflect the nonlinearities. The ratio of the second and the first harmonic (Y_{II}/Y_I) for a certain input amplitude can be regarded as a measure of nonlinearity, and those values (in percents) are also given in Table 4.2.3. Since the second harmonic is directly used for calculations of the second-order adsorber FRF (eq. 3.28), its magnitude is important from the point of view of measurability. While the first harmonic is of the order of magnitude of 1 mbar, the second harmonic has significantly lower values (up to 4 % of the first one) and these are in the range between 10^{-3} and 10^{-1} mbar. The magnitude of the second harmonic (as well as all others) depends, besides on the input amplitude, also on the steady state and frequency. In Figure 4.2.5 the amplitude of the second harmonic vs. frequency for three different steady-states and for the input amplitude 0.05 is presented. The amplitude of the second harmonic is a monotonously increasing *S*-shaped function of frequency. Figure 4.2.5 also shows that the second harmonic and its total change with the frequency become larger for higher steady-state pressures.

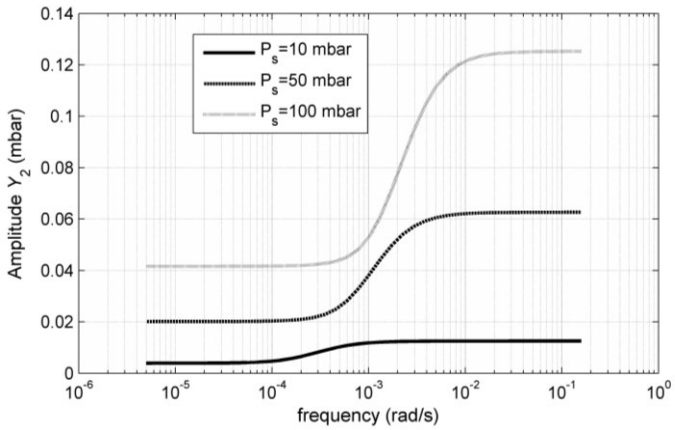

Fig. 4.2.5 Amplitude of the second harmonic of the pressure response ΔP vs. frequency for different steady-states (A=0.05, k_a=0.1 s^{-1})

It can be seen from Table 4.2.3 that the third harmonic rises very fast in the given range of input amplitudes and has the values from 10^{-5} – 10^{-3} mbar, while the fourth harmonic is of the order of magnitude of 10^{-5} mbar and shows only slight increase. The magnitude of the third harmonic reflects the contribution of the nonlinearities of the third order in the first harmonic (eq. 3.27), while the magnitude of the fourth harmonic reflects the contribution of the nonlinearities of the fourth order in the second harmonic (eq. 3.28), which is important for determination of the first- and second-order FRFs and this will be discussed in Section 4.3.2.

4.3 Optimal parameters for NFR experiments

As already mentioned, the key parameters which affect the accuracy of estimation of the second-order FRF from the batch NFR experiments are: mass of the adsorbent, amplitude of volume modulation, frequency range and sampling rate. Mass of the adsorbent influence the partition of the adsorbate between gas and solid phase and consequently the amplitude of the pressure response. Amplitude of the volume modulation directly influences the appearance and magnitude of the output harmonics, as it was shown in Section 4.2. The range of the frequencies for which NFRs should be measured, is related to the kinetic constant(s) of the adsorption process. For slower kinetics the lower frequencies are needed and for the faster kinetics the higher frequencies. Sampling rate determines the number of data points per period of timewave, which is important for accurate Fourier transform of the measured responses. In this Section we aim to establish the criteria which define optimal values of the mentioned parameters, by using the simulated FRs. We aim also to ascertain the procedure

for estimation of optimal parameters, based on the step response experiments which are easy to be performed.

4.3.1 Determining the optimal mass of the adsorbent

The intensity of the pressure signal, as a response of a batch adsorber to the volume change, for a given steady state and input amplitude, depends on the mass of the adsorbent. In order to recognize the significance of the mass of the adsorbent for successful FR experiments, FRs for the steady-state pressure 20 mbar and input modulation with amplitude 0.05 and frequency 0.0008 rad/s, for three different masses (0.4, 1.1 and 2 g) were simulated and presented in Fig. 4.3.1, together with the blank experiment (adsorbate at the same temperature and pressure without adsorbent) for the same input amplitude.

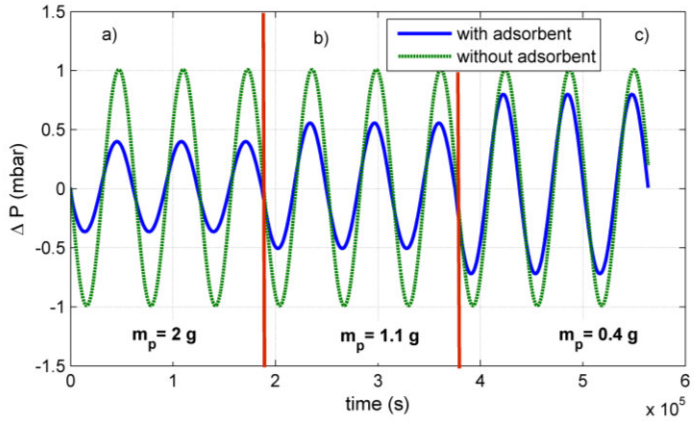

Fig. 4.3.1 Pressure response for different masses of adsorbent a) 2g, b) 1.1g and c) 0.4g together with the response without adsorbent (P_s= 20 mbar, A= 0.05 k_a = 0.1 s^{-1}, ω = 0.0008 rad/s)

As it can be seen from Fig. 4.3.1a, with 2g of adsorbent, the output signal has very small amplitude which may be experimentally undetectable (especially for higher frequencies). With 0.4g of adsorbent (Fig. 4.3.1c), the amplitude of the output signal is almost equal to the amplitude of the blank experiment, thus such FR contains no information about adsorption. The conclusion can be drawn that the best compromise between reliable measurability and sufficient distinction from blank experiment is achieved when the amplitude of the output signal is half of the amplitude of the blank experiment for the same input amplitude. This fact is used as a criterion for choice of the optimal mass of the adsorbent. A simple procedure for

determination of the optimal mass of the adsorbent, based on a preliminary step response experiment, is presented below.

Estimation of the optimal mass of the adsorbent from the step response

The step responses, corresponding to FRs shown in Fig. 4.3.1. (steady-state pressure 20 mbar, input amplitude A =0.05, three masses of adsorbent: 0.4, 1.1 and 2g) are presented in Fig. 4.3.2.

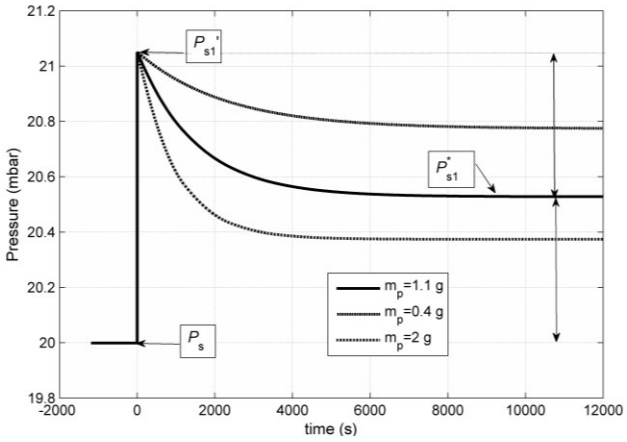

Fig. 4.3.2 Pressure responses to the step change of the volume (A=0.05) with different masses of adsorbent

The criterion that the output amplitude of the FR is about a half of the amplitude of the blank experiment, corresponds to the following one in terms of the step response:

$$P_{s1}^* \approx \frac{P_{s1}' - P_s}{2} \qquad (4.3.1)$$

where P_{s1}^* is the new steady-state pressure obtained with the optimal mass of the adsorbent (Fig. 4.3.2). Based on this fact, the following procedure for estimation of the optimal mass of the adsorbent for any unknown adsorption system is proposed:

1. Performing the step experiment from a desired steady-state (P_s) with an arbitrary mass of the sample (m_p) and any feasible amplitude (A)
2. From the obtained response curve, the value P_{s1}' and P_{s1} are estimated (see Fig. 4.2.1b)
3. Calculation of the value P_{s1}^* according to equation (4.3.1)
4. The optimal mass of the sample is determined from a simple proportion:

$$m_p^* = m_p \frac{P_{s1}}{P_{s1}^*} \tag{4.3.2}$$

It should be emphasized that the optimal mass of the adsorbent depends on the slope of the adsorption isotherm in the given steady-state, thus an optimal mass can be associated with each steady-state. The optimal masses of the adsorbent (zeolite 5A) for the tested steady-states (20, 50, 100 mbar), estimated from the simulated step responses and the previously described procedure, are given in Table 4.2.1. For higher steady-state pressures, where the slope of the adsorption isotherm is lower, the larger mass of the adsorbent is required.

4.3.2 Determining the optimal input amplitude

As it has already been explained in Section 3.2.2, the first-order FRF $G_1(\omega)$ is determined from the first harmonic of the NFR. $G_1(\omega)$ is directly proportional to the first harmonic when the third-order FRF (and higher odd-order FRFs) can be neglected (eq. 3.27). Taking into account that the third harmonic increases significantly with the input amplitude (Table 4.2.3), it follows that the input amplitude should be kept very small (0.01-0.02) in order to obtain quasi-linear FR (which contains only the first harmonic) and calculate accurate first-order FRF.

Regarding the optimal input amplitude for estimation of the second-order FRF $G_2(\omega,\omega)$ the choice is not as straightforward as for the first-order FRF. The second-order FRF is estimated from the second harmonic of the NFR (eq. 3.28). Since the values of the second harmonic are low (only several percent of the first one, Table 4.2.3), the first requirement is that the input amplitude has to be enough large to provide measurable second harmonic. Furthermore, the second-order FRF is directly proportional to the second harmonic only when the contribution of the fourth-order FRF (and higher odd-order FRFs) can be neglected (eq. 3.28).

For the FR pressure measurements, a highly accurate Baratron capacitance manometers (MKS Instruments) are mainly used (Grenier et al. 1999; Song and Rees, 1997; Turner, 2001). Taking into account the level of noise typical for this type of measuring instruments (MKS Product Catalogue), the minimal magnitude of the signal, expressed as pressure deviation, which can be measured reliably, is estimated to $P_s \cdot 10^{-3}$ mbar. That means that the second harmonic of the FR should have a minimal amplitude of $P_s \cdot 10^{-3}$ mbar. In Fig. 4.3.3a the amplitude of the second harmonic of simulated pressure responses, Y_{II}, for different input

amplitudes in the range from 0.01 to 0.2, for three different steady-states, have been presented. It can be seen that the second harmonic of $P_s \cdot 10^{-3}$ mbar is obtained for input amplitude of about 0.08.

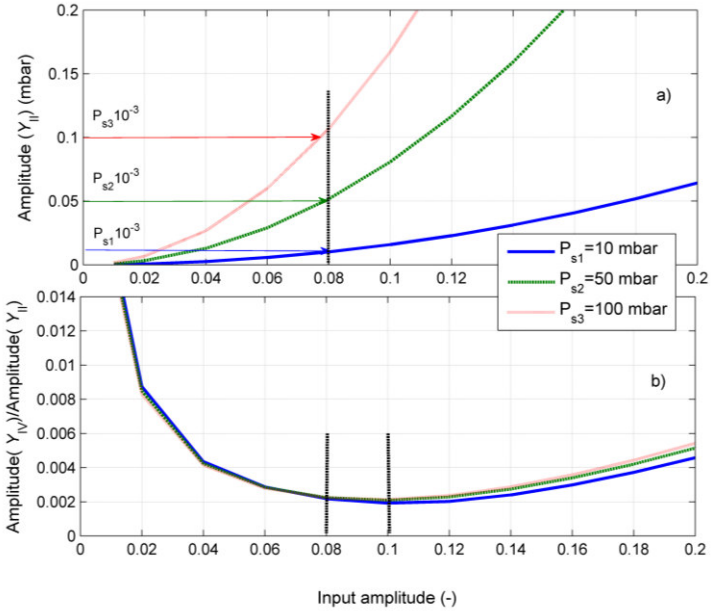

Fig.4.3.3 a)Amplitude of Y_{II} and b) Ratio of Y_{IV}/ Y_{II} vs. input amplitude (ω=2·10^{-5} rad/s)

In order to estimate the contribution of the fourth-order FRF in the second harmonic, the ratio of the amplitudes of the fourth and second harmonic (Y_{IV}/Y_{II}) vs. input amplitude, has been presented in Fig. 4.3.3b. For input amplitudes up to 0.08, Y_{II} increases faster than Y_{IV} (for all three steady-states) and the ratio Y_{IV}/Y_{II} decreases, while for input amplitudes larger than 0.1 Y_{IV} increases faster than Y_{II} and the ratio Y_{IV}/Y_{II} increases. In the range from 0.08 to 0.1 the ratio Y_{IV}/Y_{II} has the minimal values (of about 2·10^{-3}), which means that in that range the contribution of the fourth-order FRF is the lowest. It turns out that the optimal input amplitudes for estimation of the second-order FRF are from 0.08 to 0.1.

Estimation of the appropriate input amplitude from the step responses

Similarly as for the optimal mass of the adsorbent, the simple procedure for estimation of the optimal input amplitude, based on the step experiments has been developed and presented below.

The degree of nonlinearity, expressed in terms of FRs, $(Y_{II}/Y_I)\cdot 100$ and in terms of step responses, δK_2 vs. input amplitude, for the same parameters as in Fig.4.3.3, is presented in Fig. 4.3.4.

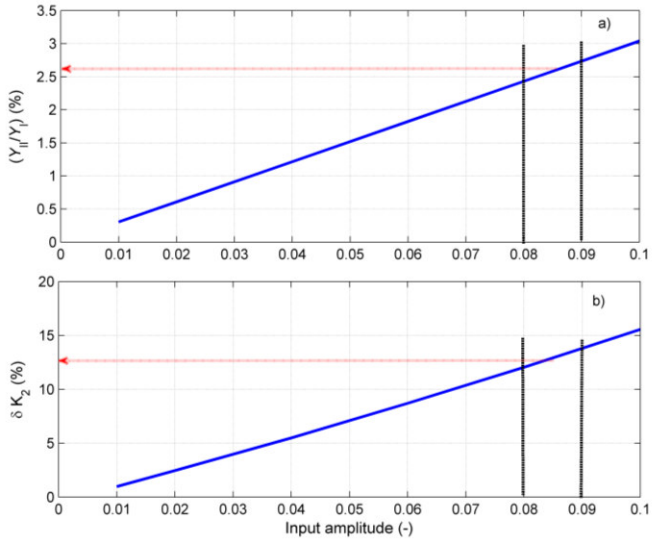

Fig.4.3.4 a) $(Y_{II}/Y_I)\cdot 100$ vs. input amplitude b) δK_2 vs. input amplitude

It can be seen that the optimal input amplitudes for estimation of $G_2(\omega,\omega)$, 0.08-0.1, correspond to the degree of nonlinearity (Y_{II}/Y_I) of 2,5 -3 % and δK_2 of 12-15 %.
Based on this fact, the preliminary step responses can be used for estimation of the required input amplitude for the NFR experiments. It is necessary to perform several step experiments for different input amplitudes in the range from 0.02 - 0.2. Input amplitudes for which δK_2 is 12-15 % can be used for estimation of the second-order FRF.

4.3.3 Determining the optimal frequency range

The required range of frequencies for the NFR experiments is determined in such a way that the low and the high asymptotic behaviour of the first- and second-order FRFs is reached. In order to ascertain the required frequency range, $G_1(\omega)$ and $G_2(\omega,\omega)$ have been calculated based on the simulated NFRs. $G_1(\omega)$ is calculated using eq.(3.29) and the FRs for input amplitude 0.02, while $G_2(\omega,\omega)$ is calculated using eq.(3.30) and the FRs for input amplitude 0.08. Three different cases, corresponding to different system parameters, presented in Table 4.3.1, have been considered.

Table 4.3.1 Parameters for simulations of the NFRs

Parameter	Case1	Case2	Case3
P_s (mbar)	20	50	50
k_a (s^{-1})	0.1	0.1	1
τ (A=0.08) (s)	2605	821.7	82.1

Figs. 4.3.6a and b illustrate the amplitudes of the first- and second-order adsorber FRFs, both in dimensionless form. The asymptotic behaviour is assumed to be reached when the amplitude changes less than 0.2 % for $\Delta\omega=5\cdot10^{-6}$ rad/s.

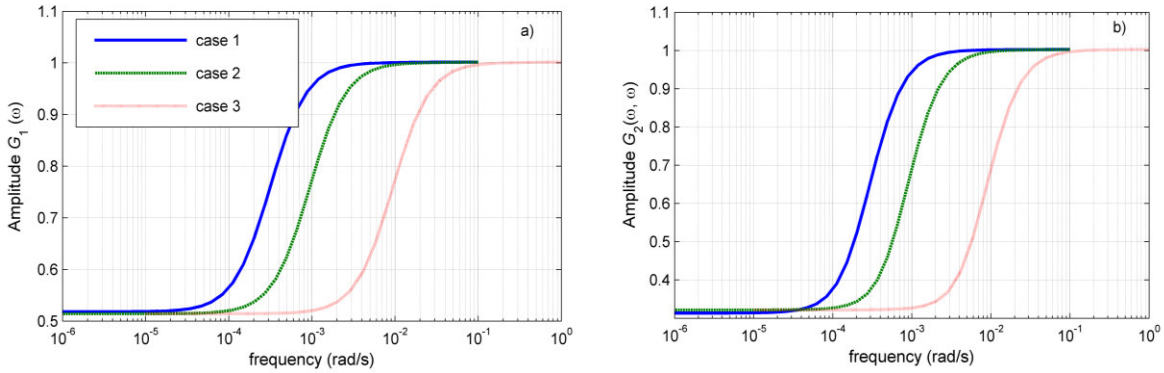

Fig. 4.3.6 a)Amplitude of $G_1(\omega)$ vs. frequency b)Amplitude of $G_2(\omega,\omega)$ vs. frequency

It can be noticed from Figs. 4.3.6a and b that the required frequency range for $G_1(\omega)$ and $G_2(\omega,\omega)$ is approximately the same for each case. For example, for case 1, the low critical frequency is 10^{-5} rad/s and the high critical frequency 10^{-2} rad/s, both for $G_1(\omega)$ and $G_2(\omega,\omega)$. It can be further noticed that both the steady-state pressure and the mass transfer coefficient influence the critical frequencies. By comparing cases 1 and 2, it can be concluded that for higher steady-state pressures higher values of the low and high critical frequencies are obtained. For the mass transfer coefficients with one order of magnitude difference (cases 2 and 3), the critical frequencies differ also about one order of magnitude.

However, if we express $G_1(\omega)$ and $G_2(\omega,\omega)$ as functions of dimensionless frequency defined as:

$$\omega^* = \omega \cdot \tau \qquad (4.3.3)$$

where τ is the apparent time constant determined from the step response for A_{opt} (Table 4.3.1), they become invariant of P_s and k_a regarding the frequency range, as it is illustrated in Figs. 4.3.7a and b.

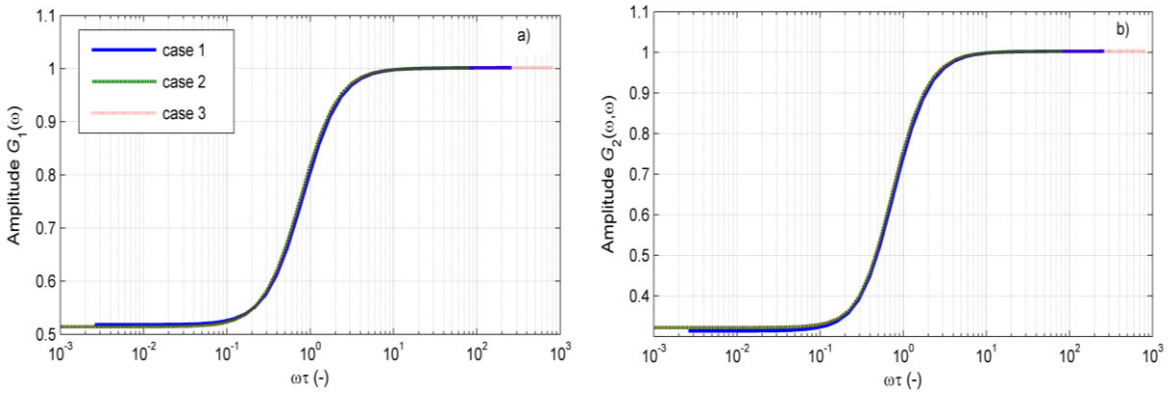

Fig. 4.3.7 a)Amplitude of $G_1(\omega)$ vs. dimensionless frequency b)Amplitude of $G_2(\omega,\omega)$ vs. dimensionless frequency

The amplitudes of $G_1(\omega)$ completely overlap (Fig. 4.3.7a), while the amplitudes of $G_2(\omega,\omega)$ have slightly different low-limiting values for different steady-states (Fig. 4.3.7b). However, the dimensionless critical frequencies are the same for all three cases, and they can be used to define a universal dimensionless frequency range. The low and the high critical dimensionless frequencies are $\omega^*_{min} = 0.01$ and $\omega^*_{max} = 10$, respectively (Figs. 4.3.7a and b).

Estimation of the frequency range from the step response

In order to estimate the required frequency range for a particular system, the apparent time constant (τ) should be determined from the step response experiment for A_{opt} from the desired steady-state with the corresponding optimal mass of the sample, by fitting the response curve to eq. 4.2.2. The required frequency range is than calculated as follows:

$$\omega_{min} = \frac{\omega_{min}^*}{\tau} = \frac{0.01}{\tau} \qquad (4.3.4)$$

$$\omega_{max} = \frac{\omega_{max}^*}{\tau} = \frac{10}{\tau} \qquad (4.3.5)$$

4.3.4 Determining the optimal sampling rate

In the NFR analysis, the measured FRs in the time domain are transferred into a frequency domain usually by means of discrete Fourier transform (DFT). We use the fast Fourier transform (FFT) algorithm that computes approximately DFT (Birgham, 1988). In order to get the accurate values of the output harmonics by using the FFT, the sampling interval (t_s) and the number of the analyzed data points (N) have to be properly chosen (Birgham, 1988). Moreover, the entire length of the sample ($t_s \cdot N$) has to be equal to an integer multiple of the period of the waveform (Birgham, 1988):

$$t_s \cdot N = N_T \cdot T \tag{4.3.6}$$

where T is the period of waveform ($T=2\pi/\omega$) and N_T is the number of periods. In this section we aim to quantify the sampling interval and number of data points necessary for accurate calculation of the second harmonic in the output. For that purpose, FFT of five periods (N_T=5) of the simulated output signal (pressure deviation, P-P_s) with different sampling intervals (t_s), for three different periods of waveform (T=10000, 1000 and 100s), have been performed. The obtained values of the amplitude of the second harmonic are presented in Table 4.3.2.

Table 4.3.2. Second harmonic of the output (P-P_s) for different sampling intervals (N_T=5)

	T=10000s		T=1000s		T=100s	
t_s (s)	N	Y_{II} (mbar)	N	Y_{II} (mbar)	N	Y_{II} (mbar)
1000	50	0.0438				
500	100	0.0349				
250	200	0.0314				
100	500	0.0298	50	0.0789		
50	1000	0.0293	100	0.0668		
25	2000	0.0291	200	0.0631		
10	5000	0.0289	500	0.0618	50	0.0789
5	10000	0.0289	1000	0.0615	100	0.0670
1	50000	0.0289	5000	0.0613	500	0.0629
0.5			10000	0.0613	1000	0.0628
0.25			20000	0.0613	2000	0.0627
0.1			50000	0.0613	5000	0.0626
0.05					10000	0.0626
0.025					20000	0.0626
0.01					50000	0.0626

When the sampling interval decreases (and consequently the number of data points N increases), the second harmonics first changes and then reaches a constant value (which is considered as the accurate one).

The minimal number of data points for which the second harmonic becomes constant is found to be 5000 i.e. 1000 points per period (gray fields in Table 4.3.2). The sampling interval which satisfies the condition of 1000 points per period, can be calculated simply for any period of waveform as follows:

$$t_s = \frac{T}{1000} \tag{4.3.7}$$

4.3.5 Guideline for design of the NFR experiments

In order to design successful NFR experiments in a batch system for an unknown adsorption gas/solid system, it is necessary to perform several preliminary step response experiments and to determine the optimal parameters (m_p^*, A_{opt}, ω_{min}, ω_{max}, $t_{s,min}$, $t_{s,max}$) according to the procedures described in the previous sections and shematically represented in Fig. 4.3.8.
At first a desired steady-state (P_s, T_s) is chosen. The volume in the steady-state (V_s) is the constant of the experimental system. A single step response experiment from (P_s, T_s) with an arbitrary mass of the sample (m_p) and any feasible amplitude (A) is performed and the parameters of the response curve (P_{s1}' and P_{s1}) are used for calculation of the optimal mass of the sample (m_p^*) using eqs. (4.3.1) and (4.3.2). Further, several step response experiments with optimal mass (m_p^*) for input amplitudes in the range 0.02 - 0.2 are performed and the parameters K_2 and τ are determined for each response. The optimal amplitude for estimation of the second-order FRF (A_{opt}) is the one for which δK_2 is about 12-15%. With the time constant (τ) corresponding to A_{opt}, the required range of frequencies (ω_{min}, ω_{max}) is calculated using eqs. (4.3.4) and (4.3.5). By comparing this range with the range of feasible frequencies of the FR device, a conclusion can be drawn weather the desired system can be examined by that device. When the optimal parameters are determined, a reasonable number of points (20-30) in the range (ω_{min}, ω_{max}) is chosen and for each frequency (i.e.period) the corresponding sampling interval, t_s, is calculated according to eq. (4.3.7).

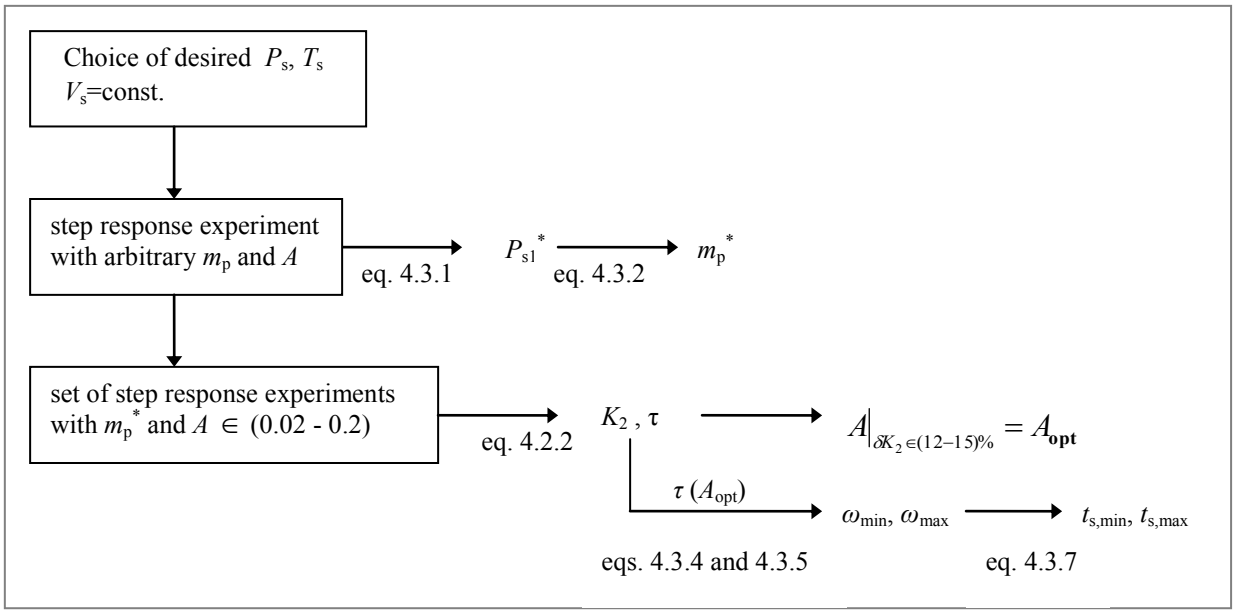

Fig.4.3.8 Shematic representation of the procedure for estimation of the optimal parameters for the NFR experiments

Two series of FR experiments are necessary to be performed for each desired steady-state. The first series with input amplitude A=0.01-0.02 in the range of frequencies (ω_{min}, ω_{max}) in order to estimate $G_1(\omega)$ and the second series with A_{opt} in the same range of frequencies in order to estimate $G_2(\omega,\omega)$.

4.4 The NFR procedure applied on the quasi-experimental data obtained by numerical experiments

In order to check weather the procedure for application of NFR method (described in Section 3.3.2) enables estimation of accurate first- and second- order particle FRFs and consequently the equilibrium and kinetic data, the simulated FRs have been used as the quasi-experimental data. The accuracy of the particle FRFs, obtained from the simulated FRs, have been evaluated by comparison with the theoretical FRFs for the film resistance control. The FRs have been simulated for the steady-state pressures 10 mbar, 50 mbar and 100 mbar. The optimal masses for those steady-states are given in Table 4.4.1 and mass transfer coefficient was k_a=0.1 s^{-1}. The procedure is demonstrated step by step below.

Step 1 Obtaining of the FRs

For each of the chosen steady state pressures two series of pressure responses, $p(t)$, for A=0.02 and A=0.08, have been simulated.

Step 2 Harmonic analysis of the simulated FRs

The simulated pressure responses have been transferred into the corresponding frequency spectra, $Y(\omega)$, by means of FFT. The segment of five periods (N=5000) of each response has been used. The first and the second harmonics, Y_{I} and Y_{II} , have been determined from the obtained spectra.

Step 3 Adsorber FRFs

In this step the adsorber FRFs, $G_1(\omega)$ and $G_2(\omega,\omega)$, have been calculated by using equations (3.29) and (3.30), respectively. $G_1(\omega)$ was calculated by using Y_{I} for A=0.02 and $G_2(\omega,\omega)$ by using Y_{II} for A=0.08. The quasi-experimental first- and second-order adsorber FRFs were presented in Figs. 4.4.1. and 4.4.2, in standard Bode-plot representation (amplitude vs. frequency in log-log and phase vs. frequency in semi-log diagrams).

The amplitudes of both $G_1(\omega)$ and $G_2(\omega,\omega)$ exhibit the S-shaped form (Figs. 4.4.1a and 4.4.2a) and asymptotically approach unity for high-frequencies. The phases of $G_1(\omega)$ and $G_2(\omega,\omega)$ exhibit maximums. The phase of $G_1(\omega)$ asymptotically approaches $-\pi$ for low and high frequencies, while the phase of $G_2(\omega,\omega)$ approaches zero for both limiting cases.

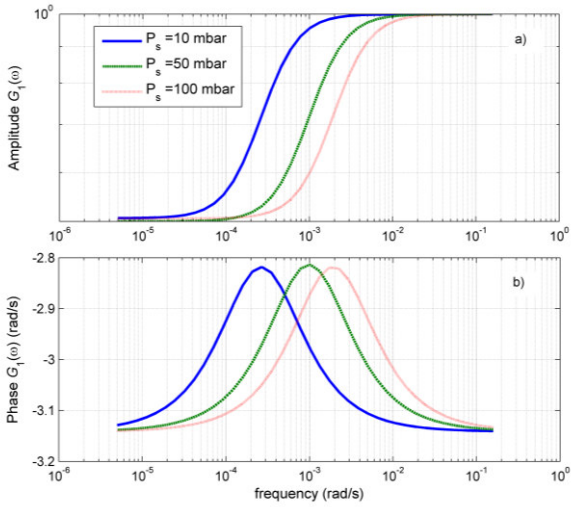

Fig.4.4.1 First-order adsorber FRF for three different steady-states

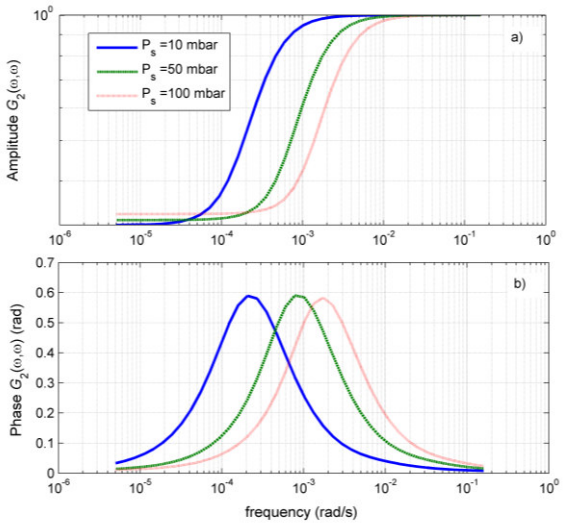

Fig.4.4.2 Second-order adsorber FRF for three different steady-states

Step 4 Particle FRFs

Using the quasi-experimental first- and second-order adsorber FRFs $G_1(\omega)$ and $G_2(\omega,\omega)$, the corresponding particle FRFs $F_1(\omega)$ and $F_2(\omega,\omega)$ are calculated, using equations (3.3.13) and

(3.3.20). They are presented in Figs. (4.4.3) and (4.4.4), respectively. In order to check the accuracy of the estimated FRFs, they are compared with the corresponding theoretical ones (presented with lines in Figs. 4.4.3. and 4.4.4). The theoretical FRFs for film resistance control model (defined by eq. (4.1.4)) have been derived by Petkovska and Do (2000) and have following forms:

$$F_1(\omega) = \frac{1/a_q}{\tau_F \omega j + 1} \tag{4.4.1}$$

$$F_2(\omega,\omega) = -\frac{b_q}{a_q^3}\left(\frac{1}{2\tau_F \omega j + 1}\right)\left(\frac{1}{\tau_F \omega j + 1}\right)^2 \tag{4.4.2}$$

where τ_F is the time constant of the process:

$$\tau_F = 1/(a_q k_m) \tag{4.4.3}$$

and a_q and b_q are the derivatives of the inverse isotherm relation defined by eq. (4.1.7). Fig. 4.4.3 shows that the quasi-experimental $F_1(\omega)$ functions agree very well with the theoretical ones for all three investigated steady-states, with negligible discrepancies of the phase of $F_1(\omega)$ for 100 mbar at high frequencies.

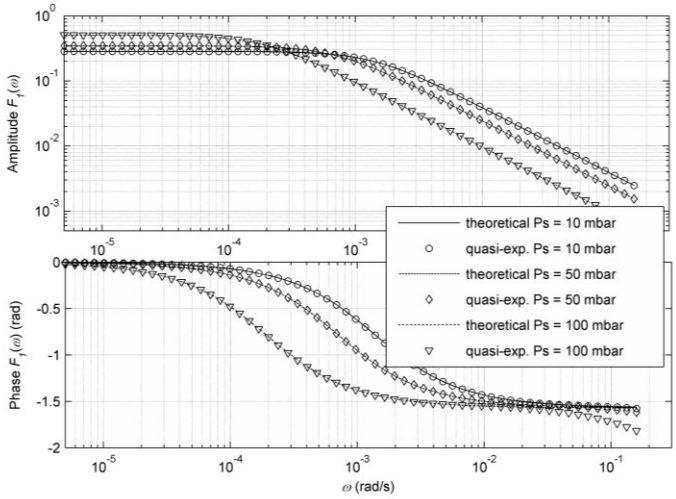

Fig. 4.4.3 First-order particle FRF $F_1(\omega)$

However, the quasi-experimental $F_2(\omega,\omega)$ agree well with theoretical ones in the range of low and medium frequencies for all three steady-states. For high frequencies, where $F_2(\omega,\omega)$ has very small values (amplitude lower than 10^{-3}, see theoretical lines in Fig. 4.4.4), it can not be estimated from the quasi-experimental data. At high frequencies the adsorbed quantity

becomes very small, which causes the numerical errors associated with calculations with small numbers. The limiting frequency up to which $F_2(\omega,\omega)$ can be estimated increases with the increase of the steady-state pressure and it is about $3/\tau_F$.

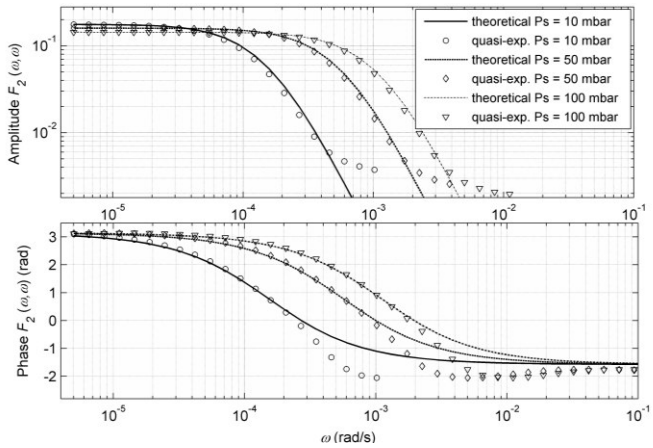

Fig. 4.4.4 Second-order particle FRF $F_2(\omega,\omega)$

Step 5 Estimation of the equilibrium and kinetic parameters

The equilibrium parameters are obtained from the low-frequency asymptotes of the particle FRFs (Petkovska, 2006). For the film resistance control model, the following low-frequency limiting values are obtained from eqs. (4.4.1) and (4.4.2):

$$\lim_{\omega\to 0} F_1(\omega) = \frac{1}{a_q} \tag{4.4.4}$$

$$\lim_{\omega\to 0} F_2(\omega,\omega) = -\frac{b_q}{a_q^3} \tag{4.4.5}$$

The process kinetic constant for simple kinetic models can be estimated from the extremum of the imaginary part of the first-order particle FRF $F_1(\omega)$ (Petkovska, 2006). For the film resistance control model, the time constant, τ_F is obtained as a reciprocal of the frequency for which the negative the imaginary part of $F_1(\omega)$ has a maximum (ω_{crit}):

$$\tau_F = \frac{1}{\omega_{crit}} \tag{4.4.6}$$

The low-frequency asymptotic values of the quasi-experimental $F_1(\omega)$ and $F_2(\omega,\omega)$ for P_s=10 mbar, 50 mbar and 100 mbar (Figs. 4.4.3 and 4.4.4) are presented in Table 4.4.1.

Table 4.4.1 The low-frequency asymptotic values of the quasi-experimental $F_1(\omega)$ and $F_2(\omega,\omega)$ and ω_{crit}

	P_s=10 mbar	P_s=50 mbar	P_s=100 mbar
$\lim_{\omega\to 0} F_1(\omega)$	0.5065	0.3463	0.2849
$\lim_{\omega\to 0} F_2(\omega,\omega)$	-0.1756	-0.1593	-0.1434
ω_{crit} (rad/s)	$1.9\cdot10^{-4}$	$7\cdot10^{-4}$	$1.4\cdot10^{-3}$

The imaginary parts of the quasi-experimental $F_1(\omega)$ functions, corresponding to the three steady-state pressures are shown in Figure 4.4.5, and the frequencies for which these curves have their maximums (ω_{crit}) are also given in Table 4.4.2.

Table 4.4.2 Estimated equilibrium and kinetic parameters from numerical FR experiments – comparison with the original parameters used for simulation

	a_q (-)	b_q (-)	k_m (s^{-1})
	Ps = 10 mbar		
Exact (used for simulations)	1.9777	-1.3649	$9.7047\cdot10^{-4}$
Quasi-experimental	1.9743	-1.3513	$9.6239\cdot10^{-4}$
Relative error (%)	0.17	1.00	0.83
Quasi-experimental with noise	1.9740	-1.2976	$9.6254\cdot10^{-4}$
Relative error (%)	0.18	4.93	0.82
	Ps = 50 mbar		
Exact (used for simulations)	2.8967	-3.8782	$2.4471\cdot10^{-4}$
Quasi-experimental	2.8877	-3.8358	$2.4244\cdot10^{-4}$
Relative error (%)	0.31	1.09	0.92
Quasi-experimental with noise	2.8869	-3.9190	$2.4226\cdot10^{-4}$
Relative error (%)	0.34	1.06	1.00
	Ps = 100 mbar		
Exact (used for simulations)	3.5232	-6.2747	$3.9338\cdot10^{-4}$
Quasi-experimental	3.5100	-6.2011	$3.9885\cdot10^{-4}$
Relative error (%)	0.37	1.17	1.39
Quasi-experimental with noise	3.5137	-6.1947	$3.9843\cdot10^{-4}$
Relative error (%)	0.27	1.27	1.28

Based on the values of the low-frequency asymptotes, first and second derivatives of the inverse adsorption isotherm (a_q and b_q), have been calculated using eqs. (4.4.4) and (4.4.5). The time constants (τ_F) have been calculated as the reciprocal values of ω_{crit} and the modified mass transfer coefficients (k_m) from eq. (4.4.3).

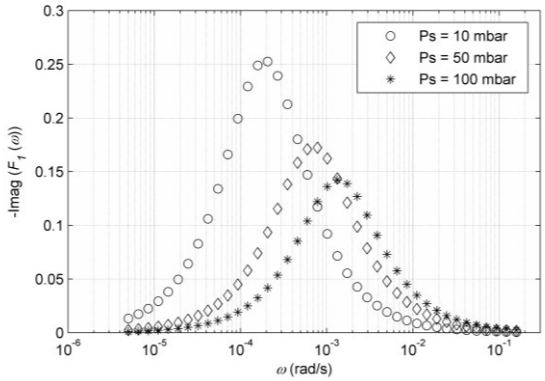

Fig. 4.4.5 Negative imaginary part of $F_1(\omega)$

The estimated parameters a_q b_q and k_m are given in Table 4.4.2, together with the original (exact) values used for simulations. It can be seen that very good agreement has been achieved, with maximal error of about 1 %.

4.4.1 Influence of noise on the accuracy of the estimated FRFs

Since noise is unavoidable in experimental work, its influence on the accuracy of the estimated first- and second-order FRFs has been checked. A random noise with variance of $0.001P_s$ has been added to the simulated pressure responses for input amplitudes 0.02 and 0.08 for each of the three investigated steady-state pressures (10 mbar, 50 mbar and 100 mbar), and they have been used for estimation of the particle first- and second-order FRFs, using the same procedure as in the case without noise. The extent of noise used for this analysis is somewhat larger than expected in the real experiments. As illustration, $F_1(\omega)$ and $F_2(\omega,\omega)$ estimated from the pressure responses with noise, for the steady-state pressure 50 mbar, are presented in Figs. 4.4.6 and 4.4.7, respectively, together with the corresponding ones estimated from the FRs without noise and the theoretical ones. It can be seen from Figs. 4.4.6 and 4.4.7 that $F_1(\omega)$ is unaffected by the noise, while $F_2(\omega,\omega)$ is more sensitive to the noise, which is reflected in a certain scattering of the data.

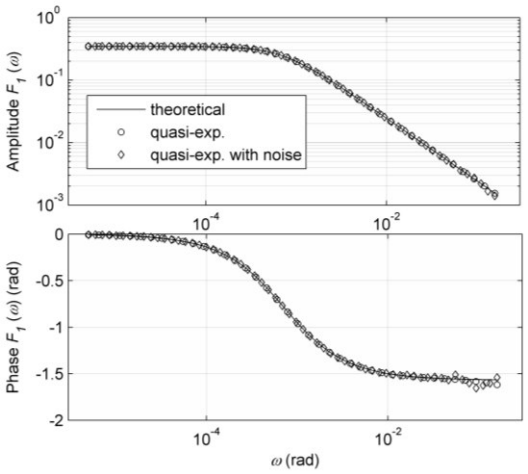

Fig. 4.4.6 First-order particle FRF $F_1(\omega)$

The equilibrium parameters (a_q and b_q) as well as the mass transfer coefficient (k_m), determined from quasi-experimental $F_1(\omega)$ and $F_2(\omega,\omega)$ estimated from the FRs with noise, are added in Table 4.4.2. Comparison of those parameters with the corresponding ones estimated from the FR without noise shows that no significant errors are caused by the noise. Exceptionally, the error of estimation of the parameter b_q for P_s=10 mbar is slightly larger (4.93 %). It is due to the fact that the second harmonic for P_s=10 mbar is very low (see Fig. 4.2.5) and consequently it is more affected by the noise.

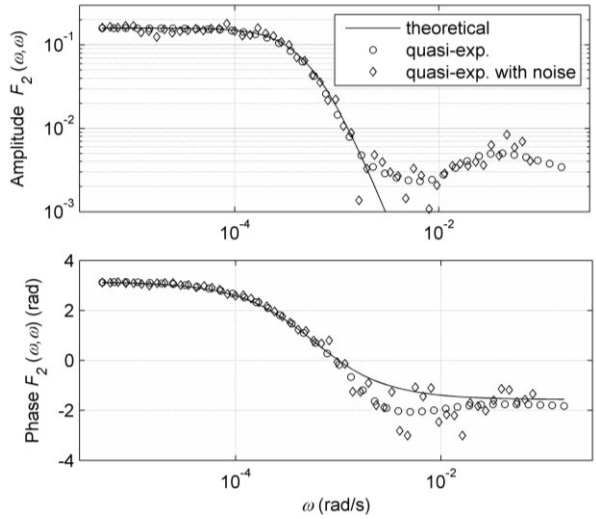

Fig. 4.4.7 Second-order particle FRF $F_2(\omega,\omega)$

Summary

The results of the theoretical study presented in this chapter indicate that construction of the apparatus for experimental investigations of gas-solid adsorption by the NFR method would be reasonable and justified. The second harmonic of the pressure response, which is used for calculation of the second-order adsorber FRF, is of the order of magnitude of 10^{-2} mbar, which is measurable with available instruments. In order to obtain an accurate experimental second-order FRF on the particle scale, the NFR experiments should be performed with optimal values of the parameters (mass of the adsorbent, input amplitude, frequency range and sampling rate). The optimal values of the parameters for a certain gas/solid system can be determined from simple preliminary step response experiments, by following the procedure described in Section 4.3.5.

The results presented in this chapter have been published in the following articles:

D. Brzić, M. Petkovska, Some practical aspects of nonlinear frequency response method for investigation of adsorption equilibrium and kinetics, *Chem. Eng. Sci* 82 (2012), 62–72

D. Brzić, M. Petkovska, A study of applicability of nonlinear frequency response method for investigation of gas adsorption based on numerical experiments, *Ind. Eng.Chem.Res.* 52, (2013), 16341-16351

5. PARTICLE FRFs FOR NON-ISOTHERMAL MACROPORE DIFFUSION MODEL

The procedure for application of the NFR method includes identifying the most probable kinetic mechanism by comparison of the experimentally obtained first- and second-order particle FRFs with the corresponding theoretical ones for different possible kinetic models. The review of the adsorption kinetic models for which the theoretical FRFs up to the second order have been published, presented in Section 3.3.5, shows that the existing library of theoretical FRFs is rather limited. The theoretical FRFs of the second-order for nonisothermal macropore diffusion (NMD) model did not exist in the literature up to now. Since the NMD mechanism is one of the suggested mechanisms for adsorption of CO_2 on commercial zeolite 5A particles (which will be investigated in experimantal part of this work) in the literature, the theoretical particle FRFs up to the second-order for this model and spherical geometry have been derived and presented in this chapter. The FRFs for isothermal macropore diffusion (IMD) have firstly been derived, since they are needed as the first assumptions in numerical solution of FRFs for NMD. The procedure for deriving the theoretical particle FRFs, described in Section 3.2.3, was applied for this case. The obtained FRFs have been simulated and analyzed regarding the influence of the steady-state pressure, particle size and temperature. A methodology for direct estimation of the kinetic constants (diffusion coefficient and heat transfer coefficient), based on the first- and second-order FRFs, has been established.

5.1 Mathematical models of isothermal and nonisothermal macropore diffusion

As the first step in derivation of theoretical FRFs, the mathematical models of isothermal and nonisothermal macropore diffusion into single porous spherical adsorbent particle surrounded by uniform gas phase, are postulated. For isothermal macropore diffusion, the mass balance for the particle is given by the following equation:

$$(1-\varepsilon_p)\frac{\partial q_i}{\partial t}+\varepsilon_p'\frac{\partial c_i}{\partial t}=\varepsilon_p'\frac{1}{r^\sigma}\frac{\partial}{\partial r}\left(D_p r^\sigma \frac{\partial c_i}{\partial r}\right) \tag{5.1.1}$$

with boundary conditions:

$$r = 0: \quad \frac{\partial c_i}{\partial r} = \frac{\partial q_i}{\partial r} = 0 \tag{5.1.2}$$

$$r = R: \quad c_i = p \tag{5.1.3}$$

where q_i represents the sorbate concentration in the solid phase, c_i the sorbate concentration in the pore, p is the pressure of gas surrounding the particle, ε_p is porosity of the particle, ε'_p modified porosity (Table 5.1.1) and D_p is diffusion coefficient. The shape factor is σ=2 for spherical geometry, t is time, r is spatial coordinate of the adsorbent particle and R its radius. The boundary conditions are based on the assumptions of concentration profiles symmetry (eq. (5.1.2)) and negligible film resistance (eq. (5.1.3)). Local equilibrium between the gas in the pores and adsorbed phase is assumed:

$$q_i = f(c_i) \tag{5.1.4}$$

and the adsorption isotherm is given in the Taylor series form:

$$q_i(c_i) = a_p c_i + b_p c_i^{\,2} + \ldots \tag{5.1.5}$$

where a_p and b_p are proportional to the first- and second-order concentration coefficients of the adsorption isotherm, respectively (Table 5.1.1). In eqs. (5.1.1) – (5.1.5) all concentrations were defined as dimensionless deviations from their steady-state values. Their definitions are given in Table 5.1.1.

Solution of the eqs. (5.1.1) and (5.1.5) with boundary conditions eqs. (5.1.2) and (5.1.3) gives the functions $q_i(r)$ and $c_i(r)$. The overall sorbate concentration at the position r, $q(r)$, is defined as:

$$q(r) = \frac{\varepsilon'_p}{\varepsilon'_p + (1-\varepsilon_p)} c_i(r) + \frac{(1-\varepsilon_p)}{\varepsilon'_p + (1-\varepsilon_p)} q_i(r) \tag{5.1.6}$$

and the mean concentration in the adsorbent particle $\langle q \rangle$:

$$\langle q \rangle = \frac{\sigma+1}{R^{\sigma+1}} \int_0^R r^\sigma q(r) dr \tag{5.1.7}$$

For the nonisothermal macropore diffusion, besides the mass balance (eq. (5.1.1)) and its boundary conditions (eqs. (5.1.2) and (5.1.3)), a heat balance equation is defined, under the assumptions of gas film transfer control and uniform particle temperature:

$$\frac{d\theta_p}{dt} = \xi \frac{d\langle q_i \rangle}{dt} - \varsigma(\theta_p - \theta_g) \tag{5.1.8}$$

where θ_p is particle temperature, θ_g gas temperature (dimensionless variables, Table 5.1.1) and $<q_i>$ the mean sorbate concentration in the solid phase. The parameter ξ represents the modified heat of adsorption and ζ the modified heat transfer coefficient (Table 5.1.1). The assumption of local equilibrium within the pores can now be written as:

$$q_i = f\left(c_i, \theta_p\right) \tag{5.1.9}$$

and the adsorption isotherm is again given in the Taylor series form, taking into account both concentration and temperature dependency:

$$q_i\left(c_i, \theta_p\right) = a_p c_i + b_p c_i^{\,2} + a_T \theta_p + b_T \theta_p^2 + b_{pT} c_i \theta_p + \ldots \tag{5.1.10}$$

where a_T is the first-order temperature coefficient, b_T is the second-order temperature coefficient and b_{pT} is the second-order mixed coefficient of the adsorption isotherm (Table 5.1.1).

Table 5.1.1 Definitions of dimensionless variables and model parameters

$q_i(r) = \dfrac{Q_i(r) - Q_{is}}{Q_{is}}$	$c_i(r) = \dfrac{C_i(r) - C_{is}}{C_{is}}$	$\theta_p = \dfrac{T_p - T_s}{T_s}$	$\theta_g = \dfrac{T_g - T_s}{T_s}$
$\varepsilon_p' = \varepsilon_p \dfrac{C_{is}}{Q_{is}}$	$\xi = \dfrac{(-\Delta H) Q_{is}}{\rho_p c_{ps} T_s}$	$\varsigma = \dfrac{3h}{R(1-\varepsilon_p)\rho_p c_{ps}}$	
$a_p = \dfrac{\partial q_i}{\partial c_i}$	$a_T = \dfrac{\partial q_i}{\partial \theta_p}$	$b_p = \dfrac{1}{2}\dfrac{\partial^2 q_i}{\partial c_i^{\,2}}$	$b_T = \dfrac{1}{2}\dfrac{\partial^2 q_i}{\partial \theta_p^{\,2}}$	$b_{pT} = \dfrac{1}{2}\dfrac{\partial^2 q_i}{\partial c_i \partial \theta_p}$

5.2 Definitions of the FRFs

According to the block diagram for adsorbing particle, given in Fig. 3.3.3, for the case of nonisothermal diffusion, under assumption of constant gas temperature (T_g=const., $T_p \neq$const.), two sets of FRFs are needed to define the process on the particle scale: *F*- the functions which relate the mean concentration in the particle $<q>$ to the pressure of the gas surrounding the particle, and *H*- the functions which relate the particle temperature θ_p to the pressure. Because of the complexity of the system, some auxiliary FRFs will be used during the derivation of *F*- and *H*-functions and they will be defined as follows: I^*- the functions

relating the local sorbate concentration in the pore $c_i(r)$ to the pressure and F^*- the functions relating the overall concentration at the position r, $q(r)$ to the pressure.

5.3 Derivation of the first- and second-order FRFs

5.3.1 Isothermal macropore diffusion

First-order FRF. If pressure as the input is defined as $p = Ae^{j\omega t}$ and the local sorbate concentration $c_i(r)$ as the output is represented in the form of Volterra series according to eq. (3.2.14):

$$c_i = I_1^*(\omega)Ae^{j\omega t} + I_2^*(\omega,\omega)Ae^{2j\omega t} + \ldots \tag{5.3.1}$$

and substituted into the model eqs. (5.1.1), (5.1.2), (5.1.3) and (5.1.5), after collecting the terms containing $Ae^{j\omega t}$ and equalizing them to zero, the following equation is obtained:

$$\frac{d^2 I_{1,iso}^*(\omega,r)}{dr^2} + \frac{2}{r}\frac{dI_{1,iso}^*(\omega,r)}{dr} - e\frac{j\omega}{D_p} I_{1,iso}^*(\omega,r) = 0 \tag{5.3.2}$$

with boundary conditions:

r=0 $$\frac{dI_{1,iso}^*(\omega,r)}{dr} = 0 \tag{5.3.3}$$

r=R $$I_{1,iso}^*(\omega,r) = 1 \tag{5.3.4}$$

The parameter e in eq. (5.3.2) is defined as follows:

$$e = \frac{(1-\varepsilon_p)a_p + \varepsilon_p'}{\varepsilon_p'} \tag{5.3.5}$$

Equation (5.3.2) is a second-order homogeneous ODE and has the following analytical solution:

$$I_{1,iso}^*(\omega,r) = \frac{R}{r}\frac{\sinh\left(r\sqrt{ej\omega/D_p}\right)}{\sinh\left(R\sqrt{ej\omega/D_p}\right)} \tag{5.3.6}$$

Using eq. (5.1.6) the function $F_1^*(\omega, r)$ is obtained:

$$F_1^*(\omega,r)=a_{p,eff}I_1^*(\omega,r) \tag{5.3.7}$$

where $a_{p,eff}$ is the effective first-order concentration coefficient of the adsorption isotherm, defined in Table 5.3.1. Finally, the first-order FRF with respect to the mean concentration in the particle <*q*> is obtained using eq. (5.1.7):

$$F_{1,iso}(\omega)=a_{p,eff}\frac{3}{R^2}\frac{R\sqrt{ej\omega/D_p}\cdot ctgh\left(R\sqrt{ej\omega/D_p}\right)-1}{ej\omega/D_p} \tag{5.3.8}$$

Second-order FRF. For the derivation of the second-order FRF the pressure is expressed as $p=A_1e^{j\omega_1 t}+A_2e^{j\omega_2 t}$, and the local sorbate concentration $c_i(r)$ again in the form of Volterra series according to eq. (3.2.14):

$$\begin{aligned}c_i &= I_1(\omega_1)A_1e^{j\omega_1 t}+I_1(\omega_2)A_2e^{j\omega_2 t}+\\ &I_2(\omega_1,\omega_1)A_1^2e^{2j\omega_1 t}+2I_2(\omega_1,\omega_2)A_1A_2e^{j(\omega_1+\omega_2)t}+I_2(\omega_2,\omega_2)A_2^2e^{2j\omega_2 t}+....\end{aligned} \tag{5.3.9}$$

and substituted into the model into the model eqs. (5.1.1), (5.1.2), (5.1.3) and (5.1.5). After collecting the terms containing $A_1A_2e^{j(\omega_1+\omega_2)t}$ and equalizing them to zero, the following equation is obtained:

$$\frac{d^2I_{2,iso}^*(\omega,\omega,r)}{dr^2}+\frac{2}{r}\frac{dI_{2,iso}^*(\omega,\omega,r)}{dr}-e\frac{2j\omega}{D_p}I_{2,iso}^*(\omega,\omega,r)=fb_p\frac{2j\omega}{D_p}I_{1,iso}^{*^2}(\omega,r) \tag{5.3.10}$$

with boundary conditions:

r=0 $$\frac{dI_{2,iso}^*(\omega,\omega,r)}{dr}=0 \tag{5.3.11}$$

r=R $$I_{2,iso}^*(\omega,\omega,r)=0 \tag{5.3.12}$$

Parameter f in eq. (5.3.10) is defined as follows:

$$f=\frac{(1-\varepsilon_p)}{\varepsilon_p'} \tag{5.3.13}$$

By incorporating eq. (5.3. 6) for $I_{1,iso}^*(\omega,r)$ into eq. (5.3.10), the final equation defining the $I_{2,iso}^*(\omega,\omega,r)$ function is obtained. This non-homogeneous ODE cannot be solved analytically, so it was solved numerically, by using the *bvp4c* solver in MATLAB. By using eq. (5.1.6), the function $F_{2,iso}^*(\omega,\omega,r)$ is obtained:

$$F^*_{2,iso}(\omega,\omega,r) = a_{p,eff} I^*_{2,iso}(\omega,\omega,r) + b_{p,eff} I^{*^2}_{1,iso}(\omega,r) \tag{5.3.14}$$

where $b_{p,eff}$ is the effective second-order concentration coefficient of the adsorption isotherm (Table 5.3.1). Finally, the second-order FRF with respect to the mean concentration in the particle <q> is obtained by using eq. (5.1.7):

$$F_{2,iso}(\omega,\omega) = \frac{3}{R^3}\int_0^R r^2 F^*_{2,iso}(\omega,\omega,r)dr \tag{5.3.15}$$

5.3.2. Nonisothermal macropore diffusion

First-order FRFs. The pressure is again the input defined as $p = Ae^{j\omega t}$, the local sorbate concentration $c_i(r)$ is already defined by eq. (5.3.1) and the particle temperature θ_p is defined in an analogous way:

$$\theta_p = H_1(\omega)Ae^{j\omega t} + H_2(\omega,\omega)Ae^{2j\omega t} + \ldots \tag{5.3.16}$$

and substituted into the model eqs. (5.1.1), (5.1.2), (5.1.3) and (5.1.10). After collecting the terms containing $Ae^{j\omega t}$ and equalizing them to zero, the following equation is obtained:

$$\frac{d^2 I^*_1(\omega,r)}{dr^2} + \frac{2}{r}\frac{dI^*_1(\omega,r)}{dr} - e\frac{j\omega}{D_p} I^*_1(\omega,r) = fa_T \frac{j\omega}{D_p} H_1(\omega) \tag{5.3.17}$$

with boundary conditions:

r=0 $$\frac{dI^*_1(\omega,r)}{dr} = 0 \tag{5.3.18}$$

r=R $$I^*_1(\omega,r) = 1 \tag{5.3.19}$$

Equation (5.3.17) is a non-homogeneous second-order ODE and contains on the right-hand side the temperature FRF $H_1(\omega)$. The heat balance (eq. (5.1.8)) becomes:

$$H_1(\omega) = I_1(\omega)L(\omega) \tag{5.3.20}$$

where $I_1(\omega)$ is the function $I^*_1(\omega,r)$ averaged along the pore:

$$I_1(\omega) = \frac{3}{R^3}\int_0^R r^2 I^*_1(\omega,r)dr \tag{5.3.21}$$

and the function $L(\omega)$ is defined as:

$$L(\omega)=\frac{a_p\xi j\omega}{(1-a_T\xi)j\omega+\zeta} \tag{5.3.22}$$

Since the function $H_1(\omega)$ is independent on the spatial coordinate r, eq. (5.3.17) can be solved analytically and has the following solution:

$$I_1^*(\omega,r)=\frac{R}{r}\frac{\sinh\left(r\sqrt{ej\omega/D_p}\right)}{\sinh\left(R\sqrt{ej\omega/D_p}\right)}\left(1+\frac{f}{e}a_T H_1(\omega)\right)-\frac{f}{e}a_T H_1(\omega) \tag{5.3.23}$$

or in the terms of $I_{1,iso}^*(\omega,r)$:

$$I_1^*(\omega,r)=I_{1,iso}^*(\omega,r)\left(1+\frac{f}{e}a_T H_1(\omega)\right)-\frac{f}{e}a_T H_1(\omega) \tag{5.3.23a}$$

Equation (5.3.23a) clearly shows that for constant particle temperature, when $H_1(\omega)$=0, the function $I_1^*(\omega,r)$ is equal to the one obtained for isothermal case.

After averaging the function $I_1^*(\omega,r)$(eq. 5.3.23a) along the pore, according to eq.(5.3.21), the following equation, relating the $I_1(\omega)$ functions for the isothermal and non-isothermal case, is obtained:

$$I_1(\omega)=I_{1,iso}(\omega)+\frac{f}{e}a_T H_1(\omega)\left(I_{1,iso}(\omega)-1\right) \tag{5.3.24}$$

After substituting eq. (5.3.20) into eq. (5.3.24), the final equation for $I_1(\omega)$ for the non-isothermal case is obtained:

$$I_1(\omega)=I_{1,iso}(\omega)+\frac{1}{1-\frac{f}{e}a_T L(\omega)\left(I_{1,iso}(\omega)-1\right)} \tag{5.3.25}$$

and the corresponding $H_1(\omega)$ (eq. (5.3.20)) becomes:

$$H_1(\omega)=\frac{I_{1,iso}(\omega)L(\omega)}{1-\frac{f}{e}a_T L(\omega)\left(I_{1,iso}(\omega)-1\right)} \tag{5.3.26}$$

Using eq. (5.1.6) the function $F_1^*(\omega, r)$ is obtained:

$$F_1^*(\omega,r)=a_{p,eff}I_1^*(\omega,r)+a_{T,eff}H_1(\omega) \tag{5.3.27}$$

where $a_{T,eff}$ is the effective first-order temperature coefficient of the adsorption isotherm (Table 5.3.1). Using eq. (5.1.7) the first-order FRF with respect to the mean concentration in the particle $\langle q\rangle$ is obtained:

$$F_1(\omega) = a_{p,eff} I_1(\omega) + a_{T,eff} H_1(\omega) \tag{5.3.28}$$

Second-order FRFs. For the derivation of the second-order FRF the pressure is again expressed as $p = A_1 e^{j\omega_1 t} + A_2 e^{j\omega_2 t}$, the local sorbate concentration $c_i(r)$ is already defined by eq. (5.3.9) and the particle temperature θ_p is defined in an analogous way:

$$\begin{aligned}\theta_p = {} & H_1(\omega_1) A_1 e^{j\omega_1 t} + H_1(\omega_2) A_2 e^{j\omega_2 t} + \\ & H_2(\omega_1,\omega_1) A_1^2 e^{2j\omega_1 t} + 2H_2(\omega_1,\omega_2) A_1 A_2 e^{j(\omega_1+\omega_2)t} + H_2(\omega_2,\omega_2) A_2^2 e^{2j\omega_2 t} + \ldots.\end{aligned} \tag{5.3.29}$$

and substituted into the model eqs. (5.1.1), (5.1.2), (5.1.3) and (5.1.10). After collecting the terms containing $A_1 A_2 e^{j(\omega_1+\omega_2)t}$ and equalizing them to zero, the following equation are obtained:

$$\begin{aligned}&\frac{d^2 I_2^*(\omega,\omega,r)}{dr^2} + \frac{2}{r}\frac{dI_2^*(\omega,\omega,r)}{dr} - e\frac{2j\omega}{D_p} I_2^*(\omega,\omega,r) = \\ &f\frac{2j\omega}{D_p}\left[b_p I_1^{*^2}(\omega,r) + a_T H_2(\omega,\omega) + b_T H_1^2(\omega) + b_{pT} H_1(\omega) I_1^*(\omega,r)\right]\end{aligned} \tag{5.3.30}$$

with boundary conditions:

r=0 $$\frac{dI_2^*(\omega,\omega,r)}{dr} = 0 \tag{5.3.31}$$

r=R $$I_2^*(\omega,\omega,r) = 0 \tag{5.3.32}$$

The heat balance (eq. (5.1.8)) becomes:

$$H_2(\omega,\omega) = \left[a_p I_2(\omega,\omega) + b_p I_1^2(\omega) + b_T H_1^2(\omega) + b_{pT} I_1(\omega) H_1(\omega)\right]\frac{L(2\omega)}{a_p} \tag{5.3.33}$$

Equations (5.3.30) and (5.3.33) have to be solved numerically, by an iterative procedure leading to the solutions for $I_2^*(\omega,\omega,r)$ and $H_2(\omega,\omega)$. In this iterative procedure, $I_{2,iso}(\omega,\omega)$ ($I_{2,iso}(\omega,\omega) = \frac{3}{R^3}\int_0^R r^2 I_{2,iso}^*(\omega,\omega,r)dr$) was used as the first assumption for $I_2(\omega,\omega)$ in eq. (5.3.33). Using eq. (5.1.6) the function $F_2^*(\omega,\omega,r)$ is obtained:

$$\begin{aligned}F_2^*(\omega,\omega,r) = {} & a_{p,eff} I_2^*(\omega,\omega,r) + b_{p,eff} I_1^{*^2}(\omega,r) + a_{T,eff} H_2(\omega,\omega) + b_{T,eff} H_1^2(\omega) + \\ & b_{pT,eff} I_1^*(\omega,r) H_1(\omega)\end{aligned} \tag{5.3.34}$$

where $b_{T,eff}$ is the second-order temperature coefficient and $b_{pT,eff}$ is the effective second-order mixed coefficient of the adsorption isotherm (Table 5.3.1). The second-order FRF with respect to the mean concentration in the particle <q> is obtained using eq. (5.1.7):

$$F_2(\omega,\omega)=\frac{3}{R^3}\int_0^R r^2 F_2^*(\omega,\omega,r)dr \qquad (5.3.35)$$

Table 5.3.1 Definitions of the effective isotherm coefficients

Coefficient	Expression
$a_{p,eff}$	$\frac{\varepsilon_p^{'}+(1-\varepsilon_p)a_p}{\varepsilon_p^{'}+(1-\varepsilon_p)}$
$b_{p,eff}$	$\frac{(1-\varepsilon_p)b_p}{\varepsilon_p^{'}+(1-\varepsilon_p)}$
$a_{T,eff}$	$\frac{(1-\varepsilon_p)a_T}{\varepsilon_p^{'}+(1-\varepsilon_p)}$
$b_{T,eff}$	$\frac{(1-\varepsilon_p)b_T}{\varepsilon_p^{'}+(1-\varepsilon_p)}$
$b_{pT,eff}$	$\frac{(1-\varepsilon_p)b_{pT}}{\varepsilon_p^{'}+(1-\varepsilon_p)}$

5.4 Simulation and analysis of the FRFs

5.4.1 Plan and parameters for simulations

In order to analyze the characteristics of the first- and second-order FRFs for the IMD and NMD models, derived in the previous section, they were simulated using MATLAB software. For the simulations, the literature equilibrium data for CO_2/zeolite 5A, (Tlili et al., 2009), were used:

$$Q=\frac{Q_m KP}{1+KP},\quad K=K_0\exp(\frac{-\Delta H}{RT}) \qquad (5.4.1)$$

where P(bar) is the pressure, Q(mol/kg) is the adsorbed quantity and Q_m is the maximum adsorbed quantity, given in Table 5.4.1 for three different temperatures. The heat of adsorption is $(-\Delta H)$=13.9 kJ and the pre-exponential factor $K_0=6.53\cdot10^{-2}$ bar^{-1}.

Table 5.4.1 Parameters of the adsorption isotherm (Tlili et al.,2009)

T (K)	Q_m (mol/kg)	K(bar^{-1})
298	3.15	18.92
373	2.25	4.77
423	1.35	3.57

The isotherm concentration and temperature coefficients (a_p, a_T, b_p, b_T and b_{pT}) were obtained by expanding the eq. (5.4.1) into a Taylor series and they are given in Table 5.4.1.

Table 5.4.1 Adsorption isotherm coefficients

	P_s= 0.025 bar T_s= 298 K	P_s= 0.05 bar T_s= 298 K	P_s= 0.15 bar T_s= 298 K	P_s= 0.025 bar T_s= 373 K	P_s= 0.025 bar T_s= 423 K
a_p	0.6917	0.5287	0.2721	0.8739	0.9217
b_p	-0.2133	-0.2492	-0.1981	-0.1102	-0.0722
a_T	-3.8801	-2.9657	-1.5266	-3.9166	-3.6425
b_T	8.0522	3.4428	-0.4247	10.4797	9.7129
b_{pT}	-0.7437	-0.0851	0.3479	-1.4644	-1.5361

Physical and transport parameters for the simulations are taken from the literature for the system CO_2/zeolite 5A and they are given in Table 5.4.2. The simulations were performed through seven runs with different combination of parameters defined in Table 5.4.3. The steady-state pressure was varied in the runs 1, 2 and 3, the adsorbent particle size was varied in the runs 1, 4 and 5 and the steady-state temperature was varied in the runs 1, 6 and 7. The parameters were varied in the ranges which correspond roughly to those reported by Onyestyak et al. (1996) and Giesy et al. (2012) , who have investigated the CO_2/zeolite systems.

Table 5.4.2 Parameters for simulations of the theoretical particle FRFs

parameter	value	unit	reference
D_p	$5 \cdot 10^{-7}$	m^2/s	Onyestyak et al.(1996)
h	3	W/m^2K	Bourdin et al.(1996)
ρ_p	1200	kg/m^3	Yang et al.(1997)
c_{ps}	921	J/kgK	Yang et al.(1997)
$(-\Delta H)$	40	kJ/mol	Garces et al.(2013)
ε_p	0.35	-	Yang et al.(1997)

Table 5.4.3 Plan of numerical simulations

	P_s (bar)	T_s (K)	R (m)	t_D (s)	t_h (s)	$t_D/\ t_h$ (-)	δ (-)
Run 1	0.025	298	$2 \cdot 10^{-4}$	118,87	15.96	7.45	2.75
Run 2	0.05	298	$2 \cdot 10^{-4}$	69.43	15.96	4.35	3.22
Run 3	0.15	298	$2 \cdot 10^{-4}$	18.45	15.96	1.15	2.55
Run 4	0.025	298	$4 \cdot 10^{-5}$	4.75	3.19	1.50	2.75
Run 5	0.025	298	$8 \cdot 10^{-5}$	19.0	6.38	3.00	2.75
Run 6	0.025	373	$2 \cdot 10^{-4}$	43.88	15.96	2.75	0.63
Run 7	0.025	423	$2 \cdot 10^{-4}$	17.29	15.96	1.1	0.19

For the nonisothermal macropore diffision model, two time constants are defined:

- the diffusional time constant:

$$t_D = \frac{R^2 e}{D_p} \tag{5.4.2}$$

where parameter e is defined by eq. (5.3.5).

- the heat-transfer time constant:

$$t_h = \frac{1}{\zeta} = \frac{R\rho_p(1-\varepsilon_p)c_{ps}}{3h} \tag{5.4.3}$$

In Table 5.4.3, the diffusional time constant (t_D) and the heat-transfer time constant (t_h), (as well as their ratio) corresponding to each parameter combination are given. Furthermore, the nonisothermality coefficient of the adsorption system (δ), calculated according to Sun et al.(1993) as:

$$\delta = \frac{1-\varepsilon_p}{\varepsilon_p}\frac{(-\Delta H)a_p P_s}{c_{ps}T_s}\left(\frac{(-\Delta H)}{R_g T_s}-1\right) \tag{5.4.4}$$

is also given in Table 5.4.3. The larger value of δ indicates more pronounced nonisothermal behavior of the system.

The simulated first- and second-order FRFs for the conditions defined in Table 5.4.3, will be presented and analyzed in the following sections. Since the FRFs are complex functions of frequency, there are in principle two ways for their graphical presentation: amplitude and phase vs. frequency and real and imaginary part vs. frequency. In order to enable recognizing of all important patterns that can be attributed to the investigated models, we will use both presentations.

5.4.2. The first- and second-order FRFs for isothermal and nonisothermal macropore diffusion control

The calculated first-order FRFs for IMD ($F_{1,\mathrm{iso}}(\omega)$) and NMD ($F_1(\omega)$) corresponding to run 1 (Table 5.4.3) are presented in parallel, as amplitude and phase vs. frequency in Figs. 5.4.1a and 5.4.1b and as the real and negative imaginary part vs. frequency in Figs. 5.4.1c and 5.4.1d.

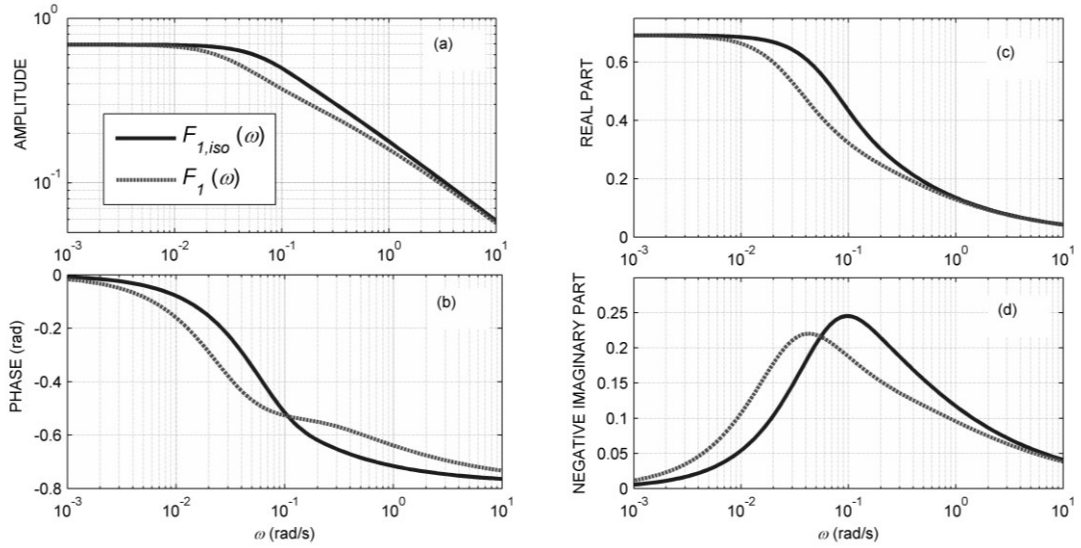

Fig. 5.4.1 First-order FRFs for IMD and NMD (run 1)

It can be noticed from Fig. 5.4.1, that at low and high frequencies the limiting values of the first-order FRF for the IMD and NMD models have identical characteristics. Namely, the amplitudes of both functions ($F_{1,iso}(\omega)$ and $F_1(\omega)$) have the same horizontal asymptote for $\omega \to 0$ and an asymptote with the slope -0.5 for $\omega \to \infty$ (Fig. 5.4.1a), while their phases have the asymptotic value zero for $\omega \to 0$ and $-\pi/4$ for $\omega \to \infty$ (Fig. 5.4.1b). This can be explained with the fact that very low frequencies correspond to very long periods, which are long enough for complete thermal relaxation. On the other hand, very high frequencies correspond to the periods which are several orders of magnitude smaller than the heat transfer characteristic time (t_h). In the middle frequency range, the amplitude and the real part of $F_1(\omega)$ have lower values than those of $F_{1,iso}(\omega)$, which is the consequence of the lower adsorbed quantity at higher temperature (Figs. 5.4.1a and 5.4.1c). The phase of $F_{1,iso}(\omega)$ has one inflection point while the phase of $F_1(\omega)$ exhibits two inflection points (Fig. 5.4.1b). Both functions, $F_{1,iso}(\omega)$ and $F_1(\omega)$, exhibit one maximum of the negative imaginary part (Fig. 5.4.1d), whereby the maximum of $F_1(\omega)$ is shifted towards lower frequency and has slightly lower magnitude. It can be concluded from Fig. 5.4.1, that two rate constants which characterize the NMD mechanism (heat transfer and diffusion) can not be distinguished one form another in the frequency window of the first-order FRF. A single maximum of -Im ($F_1(\omega)$) may be erroneously considered as a process with single time constant.

In Fig. 5.4.2 the calculated second-order FRFs for IMD ($F_{2,iso}(\omega,\omega)$) and NMD ($F_2(\omega,\omega)$) corresponding to run 1 (Table 5.4.3) are presented.

Similarly as for the first-order FRFs, it can be seen from Fig. 5.4.2 that the characteristics of $F_2(\omega,\omega)$ for limiting values of frequencies are the same as for $F_{2,iso}(\omega,\omega)$. The amplitudes of both functions have the same horizontal asymptote for $\omega \to 0$ and the asymptote with a slope -0.5 for $\omega \to \infty$ (Fig. 5.4.2a), while their phases have the asymptote $-\pi$ for $\omega \to 0$ and $-5\pi/4$ for $\omega \to \infty$ (Fig. 5.4.2b). In the middle frequency range, significant difference in the shape of the second-order FRF for IMD and NMD is observed. The amplitude of $F_{2,iso}(\omega,\omega)$ changes the slope once (Fig. 3a) and the phase has a minimum (Fig. 5.4.2b). The real part of $F_{2,iso}(\omega,\omega)$ has a sigmoidal shape (Fig. 5.4.2c) and the negative imaginary part has one very pronounced minimum (Fig. 5.4.2d).

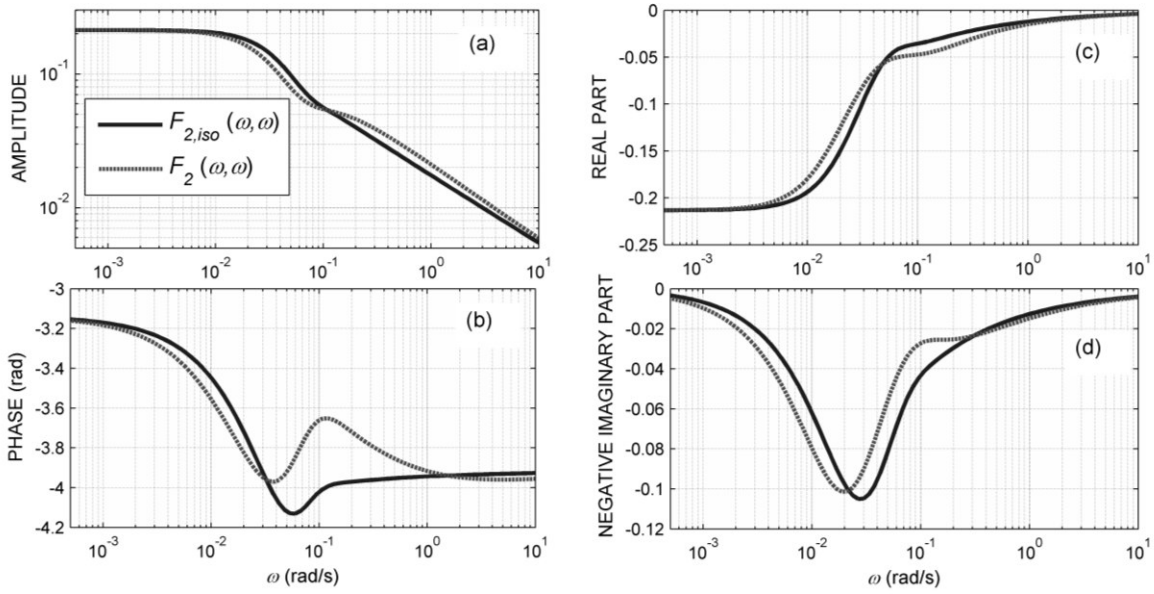

Fig. 5.4.2 Second-order FRFs for IMD and NMD (run 1)

However, the second-order FRF for NMD has the following bimodal features: the amplitude of $F_2(\omega,\omega)$ changes the slope twice (Fig. 5.4.2a) and the phase has a distinct minimum followed by a distinct maximum (Fig. 5.4.2b). The real part of $F_2(\omega,\omega)$ has two changes of slope (Fig. 5.4.2c) and -Im ($F_2(\omega,\omega)$) has a pronounced minimum followed by a very small maximum (Fig. 5.4.2d). As it can be seen from Fig. 5.4.2, the NMD second-order FRF exhibits a bimodal pattern, indicating thus that the heat transfer and diffusional time constant can be separated in the frequency window of $F_2(\omega,\omega)$.

5.4.3 Influence of the steady-state pressure on the first- and second-order FRFs for NMD

The calculated first-order FRF for NMD ($F_1(\omega)$) for three different steady-state pressures (runs 1, 2 and 3) and temperature 298 K are presented in Figs. 5.4.3a and 5.4.3b as amplitude and phase vs. frequency and in Figs. 5.4.3c and 5.4.3d as the real and negative imaginary part vs. frequency.

Figure 5.4.3 shows that the shape of $F_1(\omega)$ is qualitatively affected by the steady-state pressure. For the steady-state pressure of 0.05 bar, the function $F_1(\omega)$ has the same shape as

for 0.025 bar, which is (as described in the previous section) characterized by a single maximum of the negative imaginary part.

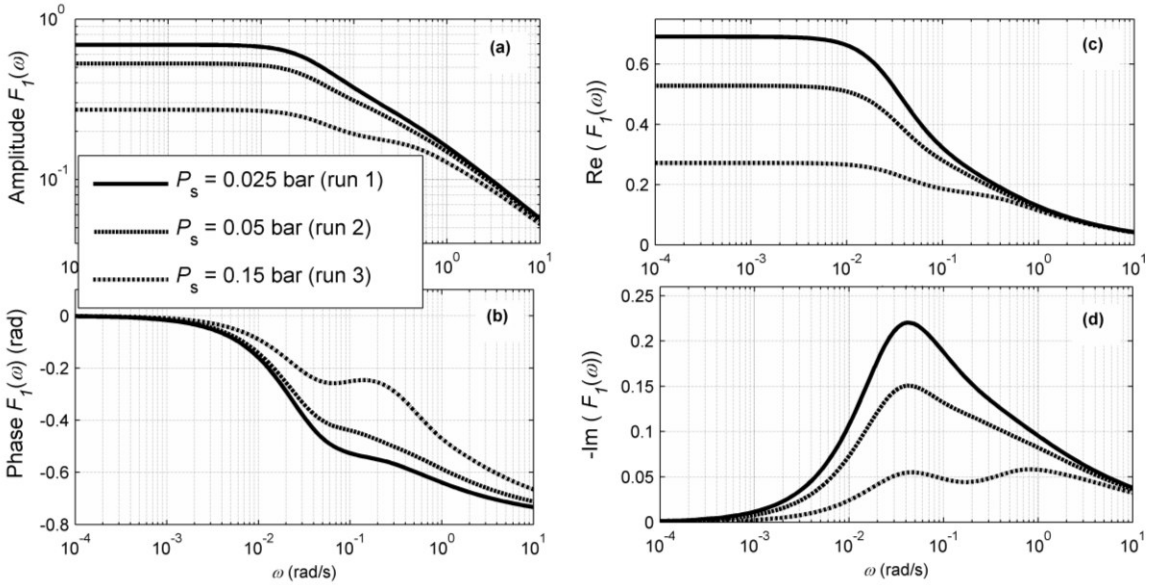

Fig. 5.4.3 First-order FRF for NMD for different steady-state pressures (runs 1, 2 and 3)

However, for steady-state pressure of 0.15 bar, a clear bimodal pattern of $F_1(\omega)$ can be observed. The amplitude (Fig. 5.4.3a) and the real part (Fig. 5.4.3c) change the slope twice, the phase (Fig. 5.4.3b) exhibits a plateau between two inflection points and the negative imaginary part has two maxima (Fig. 5.4.3d). As it can be seen from Table 5.4.3, different steady-state pressures correspond to different ratios t_D/t_h (runs 1,2 and 3). The steady-state pressure influences the diffusional time constant (t_D) through the coefficients a_p and ε'_p (see Eqs. (5.4.2) and (5.3.5)), while the heat transfer time constant (t_h) remains unchanged (Eq. (5.4.3)). As a consequence, the ratio t_D/t_h changes, and it is higher for the lower steady-state pressures (Table 5.4.3). The nonisothermality coefficient δ has approximately the same values for the tested steady-state pressures (Table 5.4.3). It can be concluded from Fig. 5.4.3, that for the ratio $t_D/t_h \approx 1$ (run 3, 0.15 bar) the bimodal behavior of $F_1(\omega)$ is clearly observed. However, for the ratio $t_D/t_h \approx 4$ (run 2, 0.05 bar), the bimodal behavior disappears and only one peak of -Im($F_1(\omega)$) can be observed, as well as for $t_D/t_h \approx 7.5$ (run 1, 0.025 bar). The fact that -Im($F_1(\omega)$) can exhibit either one or two maxima, shows that $F_1(\omega)$ is not sufficient for identification and characterization of NMD mechanism.

The simulated second-order FRFs, $F_2(\omega,\omega)$, corresponding to runs 1, 2 and 3 are presented in Figs. 5.4.4a and 5.4.4b as amplitude and phase vs. frequency and in Figs. 5.4.4c and 5.4.4d as real part and negative imaginary part vs. frequency.

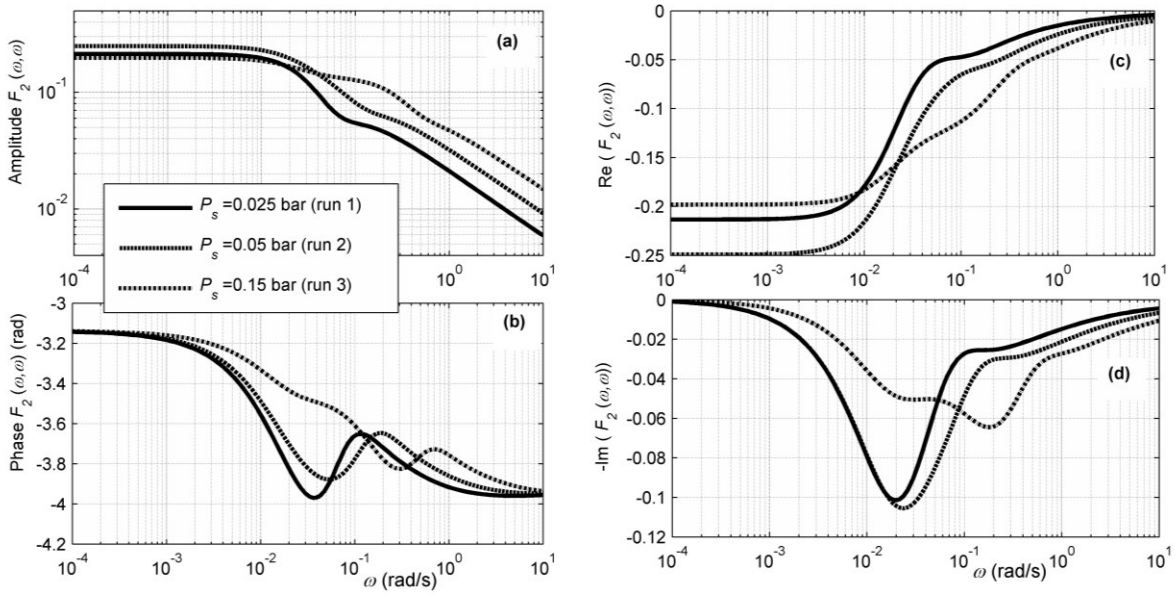

Fig. 5.4.4 Second-order FRF for NMD for different steady-state pressures (runs 1, 2 and 3)

The first important observation from Fig. 5.4.4 is, that unlike $F_1(\omega)$, the characteristic bimodal pattern of $F_2(\omega,\omega)$ (two changes of the slope of the amplitude and real part, and a minimum followed by a maximum of the phase and negative imaginary part), is observable for all three steady-state pressures. Exceptionally, for the steady-state pressure 0.15 bar, in the range of frequencies between 10^{-2} and 10^{-1} rad/s, the amplitude and the real part of $F_2(\omega,\omega)$ exhibit one additional change in the slope, the phase has an inflection point and the negative imaginary part has a horizontal plateau. This behavior may be associated with the negative sign of the second-order temperature coefficient of the adsorption isotherm at 0.15 bar (b_T=-0.4247, Table 5.4.1). It can be concluded from Fig. 5.4.4, that the characteristic bimodal features of $F_2(\omega,\omega)$ are qualitatively independent of the ratio t_D/t_h in the tested range. This fact means that $F_2(\omega,\omega)$ can be used for reliable identification of the NMD mechanism.

5.4.4 Influence of the particle size on the first- and second-order FRFs for NMD

The simulated $F_1(\omega)$ functions for three different particle sizes (runs 1, 4 and 5) and temperature 298 K are presented in Figs. 5.4.5a (real part) and 5.4.5b (imaginary part). The corresponding $F_2(\omega,\omega)$ functions are presented in Figs. 5.4.5c (real part) and 5.4.5d (imaginary part). (The amplitudes and phases of $F_1(\omega)$ and $F_2(\omega,\omega)$ for those runs are not presented, because they contain the same information as the real and imaginary part, regarding the influence of the particle size).

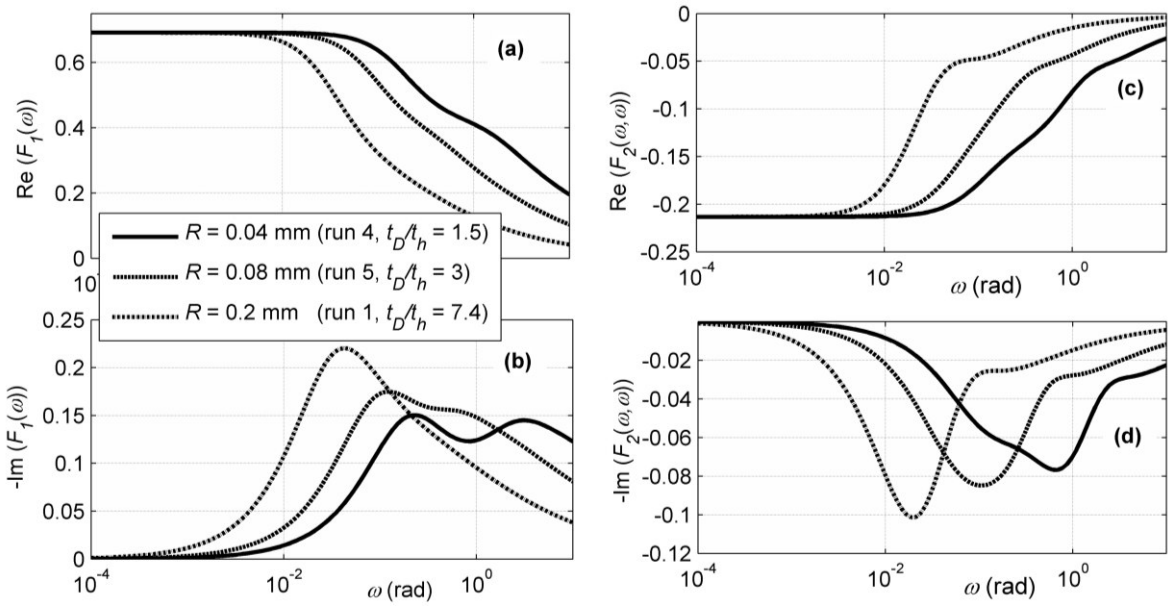

Fig. 5.4.5 First- and second-order FRFs for NMD for different particle sizes (runs 1, 4 and 5)

It can be seen from Fig. 5.4.5 that, similarly as for the change of the steady-state pressure, the shape of the first-order FRF changes with the change in the particle size, while the shape of the second-order FRF remains qualitatively the same. The particle size influences both t_D and t_h (Eqs. (5.4.2) and (5.4.3), respectively). Since t_D is proportional to R^2 and t_h is proportional to R, the ratio t_D/t_h increases with increase of the particle radius. The nonisothermality coefficient is unaffected by the particle radius (Eq. (5.4.4)). For the smallest particle radius (R=4·10^{-5} m, run 4, Table 5.4.3), which corresponds to the ratio t_D/t_h of 1.5, the function $F_1(\omega)$ shows bimodal behavior (two inflections point of the real part and two maxima of negative imaginary part). With increase of the particle radius, and consequently t_D/t_h (runs 5 and 1), the bimodal behavior of $F_1(\omega)$ gradually disappears (Figs. 5.4.5a and 5.4.5b). As

already mentioned, the function $F_2(\omega,\omega)$ exhibits the characteristic bimodal pattern (two changes of the slope of the real part and a minimum followed by a small maximum of the negative imaginary part) for all three particle sizes (and consequently for all three ratios t_D/t_h). It is interesting to notice from Fig. 5.4.5 that, with increase of the ratio t_D/t_h, the bimodal features of $F_1(\omega)$ disappear, while the bimodal features of $F_2(\omega,\omega)$ become more pronounced.

5.4.5 Influence of the steady-state temperature on the first- and second-order FRFs for NMD

The simulated functions $F_1(\omega)$ for three different steady-state temperatures (runs 1,6 and 7) are presented (as lines) in Figs. 5.4.6a (real part) and 5.4.6b (imaginary part), while the corresponding functions $F_2(\omega,\omega)$ are presented in Figs. 5.4.6c (real part) and 5.4.6d (imaginary part). The functions for the isothermal case, $F_{1,\mathrm{iso}}(\omega)$ and $F_{2,\mathrm{iso}}(\omega,\omega)$, for the same temperatures, are given in parallel for comparison (symbols in Fig. 5.4.6).

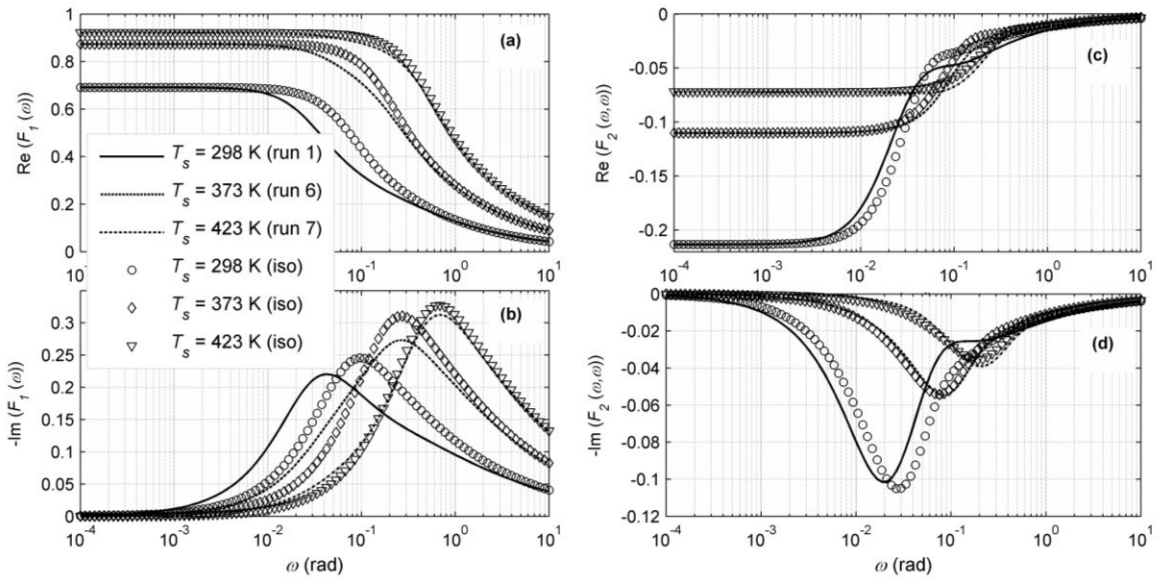

Fig. 5.4.6 First- and second-order FRFs for IMD (symbols) and NMD (lines) for different steady-state temperatures (runs 1, 6 and 7)

It can be seen from Figs. 5.4.6a and 5.4.6b that the function $F_1(\omega)$ has the same shape for all tested temperatures, characterized with one maximum of -Im($F_1(\omega)$). The comparison of the function $F_1(\omega)$ with the corresponding one for isothermal case shows that the maximum of -

Im($F_1(\omega)$) is shifted towards lower frequencies at 289 K, the magnitude of the maximum of -Im($F_1(\omega)$) is slightly lower at 373 K, while the overlapping of these two functions is observed at 423 K (Figs. 5.4.6a and 5.4.6b). This can be explained with the fact that with the increase of the steady-state temperature, the nonisothermality of the system (expressed through the coefficient δ, Eq. (5.4.4)) decreases. As a consequence, the rise of the particle temperature becomes smaller at high temperatures and the system is practically isothermal. For the steady-state temperature 423 K, the nonisothermality coefficient is δ=0.19 (Table 5.4.3), which means that the nonisothermality of the system is negligible (δ=0 for isothermal system) and therefore the functions $F_1(\omega)$ and $F_{1,iso}(\omega)$ overlap.

The second-order FRF (Figs 5.4.6c and 5.4.6d) has different shapes for different steady-state temperatures (Figs. 5.4.6c and 5.4.6d). At 298 K, the bimodal behavior with a pronounced minimum and a small maximum of -Im($F_2(\omega,\omega)$) is present. However, at 323 K and 423 K the second-order FRFs overlap the ones for the isothermal case and have only one minimum of -Im($F_2(\omega,\omega)$). It can be concluded from Fig. 5.4.6 that the shape of the second-order FRF gives information weather the adsorption system can be treated as isothermal, which is not possible from the first-order FRF.

In summary, the parameter variation analysis shows that the second-order FRF for NMD model has a bimodal pattern qualitatively independent from the ratio t_D/t_h. A minimum followed by a maximum of the phase of $F_2(\omega,\omega)$ (or a pronounced minimum followed by a small maximum of -Im($F_2(\omega,\omega)$)) is the characteristic feature which can be used for recognition of the NMD model.

5.4.6 Temperature FRFs

In Figs. 5.4.7 and 5.4.8 the first- and the second-order temperature FRFs ($H_1(\omega)$ and $H_2(\omega,\omega)$) for different combination of parameters (runs 1, 2, 5 and 7) are presented, respectively, as real and imaginary part vs. frequency. Comparison of Runs 1 and 2 shows the influence of the steady-state pressure, of runs 1 and 5 the influence of the particle size, and of runs 1 and 7 represent the influence of the steady-state temperature.

Figure 5.4.7 shows that there is no qualitative change in the shape of $H_1(\omega)$ due to the variation of the mentioned parameters (and consequently different ratios t_D/t_h). The real part

(Fig. 5.4.7a) is characterized with one maximum, while the imaginary part (Fig. 5.4.7b) has a maximum at lower frequencies and a minimum at higher frequencies.

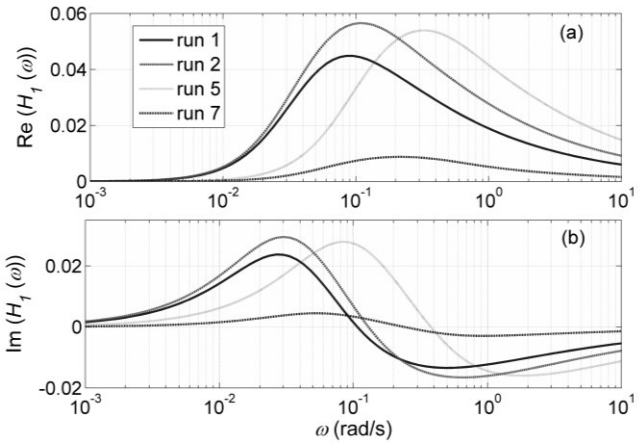

Fig. 5.4.7 First-order temperature FRF for different parameter combinations

According to the study of Bourdin et al. (1996), who have treated NMD model in the linear range, the low frequency region of $H_1(\omega)$ is affected by the heat transfer limitations, which result in the increase of the real part and the maximum of the imaginary part. The higher frequency range of $H_1(\omega)$ is affected by the mass transfer limitations resulting in the decrease of the real part and the minimum of the imaginary part. The magnitude of the maximum of the real part is mainly affected by the nonisothermality coefficient (δ), i.e. the particle temperature rise. As it can be seen from Fig. 5.4.7a, the highest value of the maximum of Re($H_1(\omega)$) is for Run 2, for which the coefficient δ has the largest value (3.22 , Table 5.4.3). The positions of the extrema of the imaginary part of $H_1(\omega)$ depend on the heat transfer time constant (maximum) and diffusional time constant (minimum). For run 5, for which t_h has lower value than for runs 1 and 2 (Table 5.4.3), the imaginary part exhibits a maximum at higher frequency. Similarly, since t_D is lower for run 5 than for runs 1 and 2, the minimum of the imaginary part lies at higher frequencies (Fig. 5.4.7b). Although the heat and diffusional time constants are more obviously distinguished in the frequency window of $H_1(\omega)$ than in that of $F_1(\omega)$, they can still not be directly estimated from $H_1(\omega)$. It should also be noticed from Fig. 5.4.7 that in the case of the temperature of 423 K (run 7), where the nonisothermality is very low, the temperature FRF $H_1(\omega)$ has very low values close to zero.

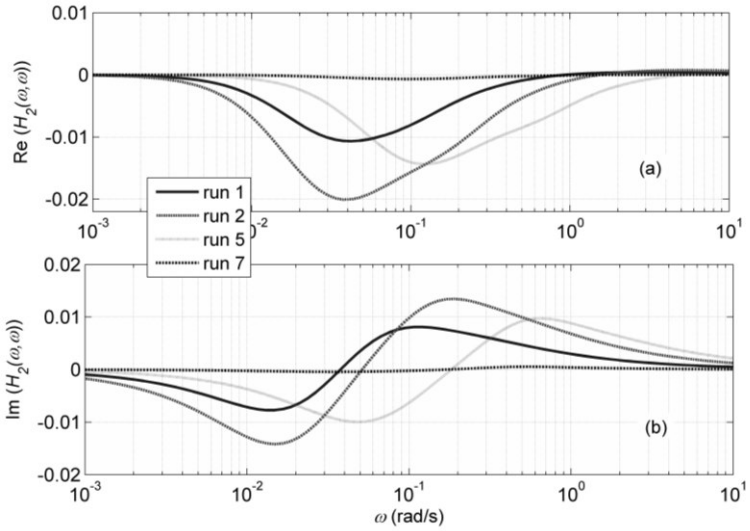

Fig. 5.4.8 Second-order temperature FRF for different parameter combinations

Regarding the shape of the function $H_2(\omega,\omega)$, it can be seen from Fig. 5.4.8, that $H_2(\omega,\omega)$ has a reversed pattern then that of $H_1(\omega)$. The real part of $H_2(\omega,\omega)$ (Fig. 5.4.8a) is negative and has a single minimum, while the imaginary part (Fig. 5.4.8b) has a minimum at lower frequencies and a maximum at higher frequencies. Figure 5.4.8 also shows that the shape of $H_2(\omega,\omega)$ is not qualitatively changed by variation of the steady-state pressure, particle size and temperature. For the temperature 423 K (run 7), as expected for an almost isothermal system (δ=0.19), the function $H_2(\omega,\omega)\approx 0$. It can be also concluded from Fig. 5.4.8, that $H_2(\omega,\omega)$ is affected by the values of δ, t_h and t_D in the same way as $H_1(\omega)$. The absolute value of the magnitude of the minimum of the real part is larger when δ is larger (Fig. 5.4.8a). For higher t_h, the minimum of the imaginary part is obtained at lower frequency, and for higher $t_{D,}$ the maximum of the imaginary part is obtained at lower frequency (Fig. 5.4.8b).

5. 5 A methodology for estimation of the model parameters

The theoretical first- and second-order FRFs for NMD, derived in Section 5.3, contain sufficient information for reliable estimation of the diffusional and heat-transfer time constants, effective first- and second-order concentration coefficients of the adsorption isotherm, as well as the heat of adsorption, as it will be presented bellow.

5.5.1 Estimation of the kinetic parameters

In the case of isothermal macropore diffusion, it was already shown (Sun et al., 1993; Petkovska, 2006) that the diffusional time constant t_D (as a single kinetic parameter) can be estimated from the frequency at which the negative imaginary part of $F_1(\omega)$ has a maximum (ω_{crit}), using the relation $\omega_{crit} t_D = 11.56$ for the spherical shape of the particles.

In the case of nonisothermal macropore diffusion, as it was shown in Section 5.4. (Figs. 5.4.3d and 5.4.5b), the diffusional time constant (t_D) and the heat transfer time constant (t_h) can not be separated in the frequency window of $F_1(\omega)$. However, if the new function is defined, as the ratio of $H_1(\omega)$ (eq. (5.3.20)) and $F_1(\omega)$ (eq. (5.3.28)):

$$\frac{H_1(\omega)}{F_1(\omega)} = \frac{L(\omega)}{a_{p,eff} + a_{T,eff} L(\omega)} \tag{5.5.1}$$

it becomes invariant of t_D. If this ratio is plotted as a function of $\omega \cdot t_h$ (Fig. 5.5.1), it becomes invariant of t_h, as well. In Fig. 5.5.1 only the functions for runs 1, 4 and 5, corresponding to different t_h are shown. For any set of parameters, the maximums of the curves $\mathrm{Im}(H_1(\omega)/F_1(\omega))$ correspond to $\omega \cdot t_h = 1$, thus giving the possibility to estimate t_h from the frequency at which the experimentally determined function $\mathrm{Im}(H_1(\omega)/F_1(\omega))$ has a maximum.

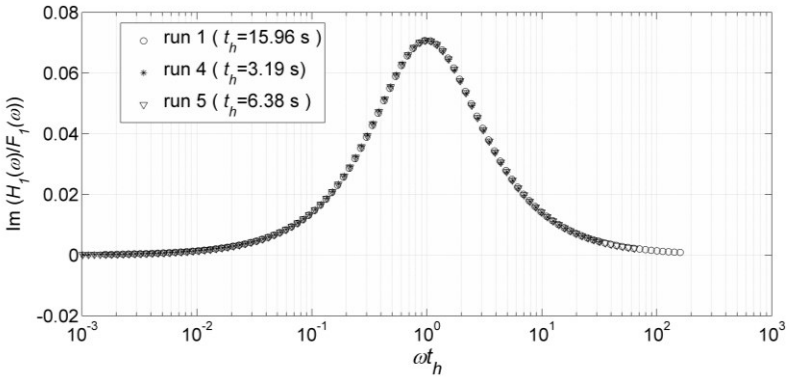

Fig. 5.5.1 Imaginary part of $H_1(\omega)/F_1(\omega)$ vs. $\omega \cdot t_h$

As already mentioned in Section 5.4, the function $F_2(\omega,\omega)$ clearly reflects the bimodal nature of the NMD mechanism, which is best noticeable in the phase frequency window, as a

minimum followed by a maximum (Fig. 5.4.4b). If the phase of $F_2(\omega,\omega)$ is plotted as a function of $\omega \cdot t_D$, for all seven runs from Table 5.4.3 (Fig. 5.5.2), it turns out that the maximums of all curves (except for run 7, which represents almost isothermal case and shows no maximum) correspond to $\omega \cdot t_D$=13.6, which means that t_D can be estimated from the frequency for which the phase of the experimental $F_2(\omega,\omega)$ has the maximum.

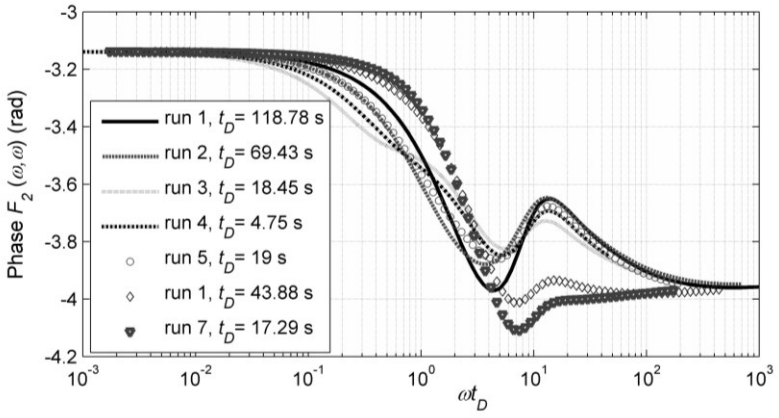

Fig. 5.5.2 Phase of $F_2(\omega,\omega)$ vs. $\omega \cdot t_D$

Figure 5.5.3 shows the imaginary part of $H_2(\omega,\omega)$ vs. $\omega \cdot t_D$ for runs 1-6 from Table 5.4.3 (for run 7 $H_2(\omega,\omega) \approx 0$, Fig. 5.4.8). It can be seen that the maximums of all curves correspond to $\omega \cdot t_D \approx 12.8$, which means that t_D can alternatively be estimated from the frequency for which the imaginary part of the experimental $H_2(\omega,\omega)$ has a maximum.

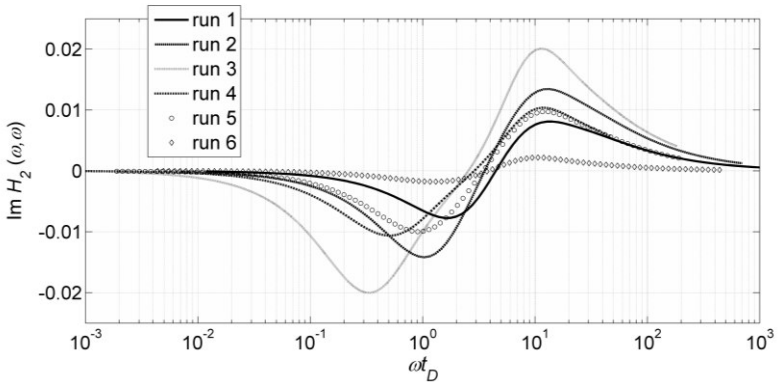

Fig. 5.5.3 Imaginary part of $H_2(\omega,\omega)$ vs. $\omega \cdot t_D$

5.5.2 Estimation of the equilibrium parameters

The equilibrium parameters can be estimated from the low-frequency asymptotes of the FRFs (Petkovska, 2006). For the cases of IMD and NMD, the low frequency asymptote of $F_{1,\mathrm{iso}}(\omega)$ as well as of $F_1(\omega)$ corresponds to the effective first-order concentration coefficient of the adsorption isotherm ($a_{p,eff}$):

$$\lim_{\omega\to 0} F_{1,iso}(\omega) = \lim_{\omega\to 0} F_1(\omega) = a_{p,eff} \tag{5.5.2}$$

while the low frequency asymptote of $F_{2,\mathrm{iso}}(\omega,\omega)$ as well as of $F_2(\omega,\omega)$ corresponds to the effective second-order concentration coefficient ($b_{p,eff}$):

$$\lim_{\omega\to 0} F_{2,iso}(\omega,\omega) = \lim_{\omega\to 0} F_2(\omega,\omega) = b_{p,eff} \tag{5.5.3}$$

5.5.3 Estimation of the heat of adsorption

It can be shown, that for the ratio $H_1(\omega)/F_1(\omega)$ defined by eq. (5.5.1), holds:

$$\lim_{\omega\to\infty}\left(\frac{H_1(\omega)}{F_1(\omega)}\right) = \xi \tag{5.5.4}$$

which means that modified heat of adsorption coefficient can be determined from the high-frequency asymptote of the experimental $H_1(\omega)/F_1(\omega)$ and the heat of adsorption ($-\Delta H$) can be calculated from the definition equation of the modified heat of adsorption, ξ (Table 5.1.1).

Summary

The nonisothermal macropore diffusion (NMD) model describes a complex kinetic mechanism with simultaneous diffusion and heat transfer, and consequently contains two time constants. In the frequency domain, this model is defined with two series of FRFs: the ***F-*** functions (which relate the mean concentration in the particle to the pressure) and the ***H***-functions (which relate particle temperature to the pressure). The analysis of the derived ***F-*** and ***H*** -functions up to the second order has shown that, for reliable recognition of the NMD model and estimation of individual time constants of diffusion and heat transfer,

experimental functions: $F_1(\omega)$, $H_1(\omega)$ and $F_2(\omega,\omega)$ are necessary. Moreover, knowing those three functions enables estimation of the first and second-order derivatives of the adsorption isotherm, as well as the heat of adsorption.

The results presented in this chapter have been published in the following article:

D. Brzić, M. Petkovska, Nonlinear frequency response analysis of nonisothermal adsorption controlled by macropore diffusion, *Chem. Eng. Sci* 118 (2014), 141–153

6. EXPERIMENTAL PART

In order to validate and exploit the NFR approach for studying adsorption of pure gases, a new apparatus has been designed and constructed. it is described in this chapter. The apparatus has a batch configuration with sinusoidal modulation of the volume, with an amplitude that can be varied. The responses to the volume modulation, pressure, gas temperature and particle temperature, have been measured with highly accurate and fast response measuring instruments. The procedure for planning the experiments, regarding the choice of optimal parameters, has already been described in Chapter 4. The measurement routine and data analysis have been demonstrated on the example of CO_2 adsorption on commercial zeolite 5A particles. A concept of blank FRFs has been introduced as a new way to incorporate the results of blank experiments for eliminating spurious effects. The first- and second-order FRFs which relate the adsorbed quantity to the pressure ($F_1(\omega)$ and $F_2(\omega,\omega)$) as well as the first-order FRF which relates the particle temperature to the pressure ($H_1(\omega)$) have been calculated based on the measured responses, while $H_2(\omega,\omega)$ was not possible to determine from the measured data. Based on the obtained experimental FRFs, identification of the kinetic mechanism and estimation of the kinetic and equilibrium parameters have been demonstrated. This represents the proof of validity and applicability of the NFR method.

6.1 Design of the NFR experimental set-up

Theoretical basis of the concept of higher-order FRFs (Chapter 3) as well as the results of the simulations of NFRs of a batch adsorber (Chapter 4), impose some requirements regarding the design of NFR experimental set-up:

(1) *Variable input amplitude*. This requirement arises from the fact that the first- and second-order FRFs are not determined from the same input amplitude, as it was described in Section 4.3.2. Also, the amplitude is adjusted in order to correspond to each investigated system and chosen steady-state point.

(2) *Accurate sine wave-form of the input*. Since the equations which are used for estimation of the FRFs from individual harmonics (eqs. 3.2.27 and 3.2.28) are derived by expanding

Volterra series for single sine-wave input, good approximation of the sine wave-form of the volume change is important issue to be realized in practice.

(3) *Temperature measurements*. Since the nonisothermality of the adsorption system is expected to be manifested under larger amplitude modulations, the gas and particle temperature measurements (along with the standard pressure measurements) are necessary for complete characterization of the system.

(4) *Recording the data with high sampling frequency*. Numerical analysis regarding the number of data points per period required for accurate Fourier transform of the complex time signal, performed in Section 4.3.4, has shown that the minimal sampling interval is a thousandth part of the period of the time-wave. With shortening the period, the required sampling frequency increases (i.e. for period of 10 seconds, sampling frequency of 100Hz is required).

The design of our set-up combines the properties of the batch FR devices reported in literature (described in Section 2.5) with specific requirements for the NFR approach, mentioned above. The sine-wave volume modulation is commonly performed by metal bellows coupled with a rotary motor and a suitable mechanism for converting circular into a linear motion (Yasuda, 1976; Reyes et al., 1997). This arrangement enables varying frequency by varying the rotation speed, while variable amplitude is not feasible. In our set-up, we also use a metal bellows to modulate the volume, while the sinusoidal form with variable amplitude is accomplished by using a servomotor with linear actuator. The sine wave-form of the stroke of the motor shaft ($s=s_0\sin(\omega t)$) over time is generated by entering the values of velocity ($\mathrm{d}s/\mathrm{d}t$) and acceleration ($\mathrm{d}^2s/\mathrm{d}t^2$) at certain times (Fig. 6.1.1).

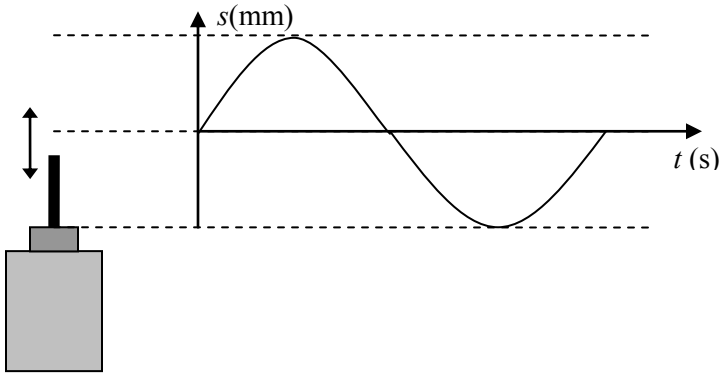

Fig. 6.6.1 Motor with linear actuator as a generator of the sinusoidal wave-form

Besides the option of easy variation of the input amplitude, using a linear actuator has additional advantages: (1) mechanical mechanisms for transferring circular into linear motion are avoided and (2) step changes of the volume with variable amplitude can be easily performed. The accuracy of the sine-wave approximation of the input is provided by applying feedback control of the motor axis position.

The pressure response is measured as a differential pressure between an adsorption and a reference cell (a cell without adsorbent at the same steady-state temperature and pressure). This concept, already used by Turner et al. (2001), enables large range of operating pressures to be covered with only one (costly) differential pressure transducer.

The infra red (IR) measurement of the particle temperature, introduced by Bourdin et al. (1998), is in our apparatus significantly simplified by using an IR detector of the newest generation which has small size and enables easy mounting.

The gas temperature measurement is employed for the first time in the FR technique. The thinnest available thermocouple (0.15 mm in diameter) was used for gas temperature measurements in order to achieve fast response.

A schematic representation of the experimental set-up is shown in Fig. 6.1.2 and specification of the equipment and measuring instruments is given below.

The adsorption cell (1) and the reference cell (5) are double-wall cylinders made of stainless steal. A heating circulator (up to180 °C) is used to heat up the cells by circulating oil through both shells. At the bottom of the adsorption cell, a stainless steal metal bellows (2) of 39/59 mm diameter (MEWASA FLEX) is connected. A servomotor (4) (RCS2-RA7BD, IAI Industrieroboter GmbH) with linear actuator is used to drive the bellows. For the starting position of the motor axis (the half of the effective stroke), the volume of the adsorption cell is 568.8 cm^3. The feedback control of the motor shaft position is accomplished by SCON-C controller (IAI Industrieroboter GmbH). Frequencies up to 1 Hz and amplitudes up to 10 % of the steady-state volume are feasible. The adsorption and the reference cell are placed together in an insulated box (6). A spiral heater on the inside wall of this box serves for additional heating of the system during cleaning of the adsorbent. By lowering the pressure in this box (using the pump P-2), uniform motion of the bellows is achieved as well as lower power consumption of the motor.

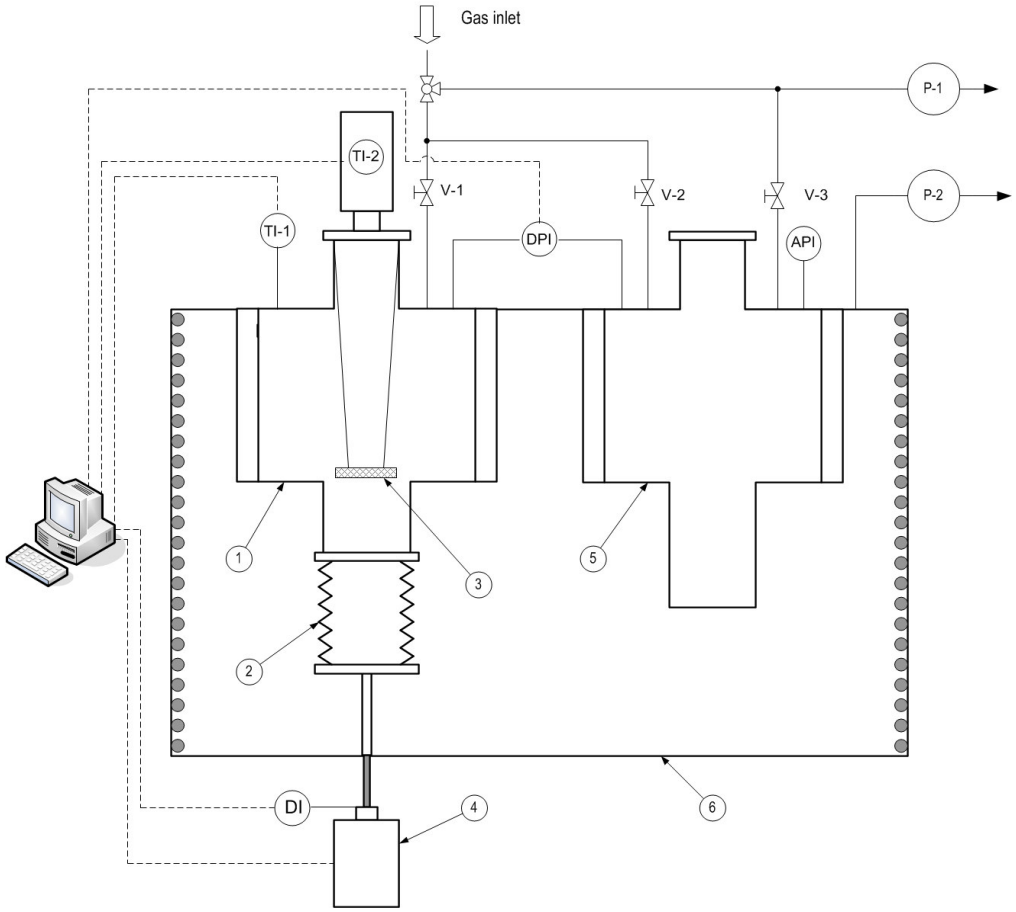

Fig. 6.1.2 Experimental apparatus for NFR experiments: adsorption cell (1), metal bellows (2), sample holder (3), servo–motor (4), reference cell (5) thermostat (6).

The position sensor (DI), Type T 150, Ahlborn, placed on the axis of the servomotor, measures the distance and thus indicates the volume of the system. Fast response Baratron differential pressure transducer (DPI), Model 120 AD, MKS Instruments, measures the pressure difference between the adsorption and the reference cell. The measurement range of the pressure transducer is 10^{-2}-10^{3} Pa with accuracy ±0.05 Pa. The steady-state pressure is measured by an absolute pressure sensor (API). The infrared detector (TI-2), (KT15IIP, Heitronics), with accuracy of ±0.15 K and with 300 ms response time, is mounted tightly at the top of the adsorption cell and used for particle temperature measurement. A K type thermocouple (TI-1) of 0.15 mm in diameter and 150 ms nominal response time is used for gas temperature measurements. Standard high-vacuum dosing valves, seals and fittings are

used. The National Instruments acquisition board suitable for high sampling rates and LabVIEW software are employed for data acquisition.

6.2 Materials and operating conditions

Commercial zeolite 5A beads (Sylobead MS 522, Grace Davison) of 1.6 -1.8 mm in diameter (ρ_p=640 kg/m^3, c_{ps}=921 J/kgK) were used as the adsorbent. These beads were crushed, sieved and the fraction of 0.2 - 0.224 mm was used for an additional series of NFR experiments. The porosities, pore areas and pore distributions for both samples were investigated by mercury porosimetry and the results are summarized in Table 6.2.1.

Table 6.2.1 Adsorbent samples properties

	Porosity (-)	Total pore area (m^2/g)	Pore diameter (μm)
original beads d_p=1.7mm	0.35	8.493	0.25 0.05*
crushed particles d_p=0.21mm	0.65	11.672	0.25 0.05*

* very small fraction of the pores

Pure CO_2 was used as the adsorbate gas. The adsorption isotherm for this system at 25°C was determined by gravimetric method, using a Rubotherm magnetic suspension balance (Fig. 6.2.1). These isotherm data were fitted with Toth equation:

$$Q = mP(b + P^r)^{-1/r} \qquad (6.2.1)$$

with the following parameters m=2352.2, b= 17.5813 and r= 0.41096. In equation (6.2.1) Q is in mol/m^3 and P in Pa.

The experiments were performed at 25°C and 20 mbar. Two series of FRs were measured for each particle diameter: one with input amplitude $0.03V_s$ and the other with input amplitude $0.08V_s$, both for a number of frequencies in the range 0.00125 - 6.28 rad/s. Blank responses

(at the same temperature and pressure without adsorbent) were measured for each tested amplitude and frequency.

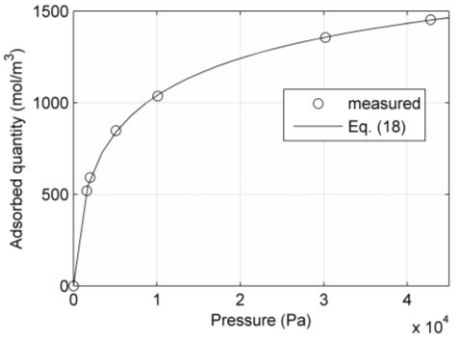

Fig. 6.2.1 Adsorption isotherm for CO_2/zeolite 5A at 25 °C (from gravimetric measurements)

6.3 Procedure for the NFR experiments

A measured sample of the zeolite particles was first activated for 12 hours in an oven at 400 °C. After cooling down, the sample was transferred into a holder. The coarse particles were arranged as a double layer and the small particles as a thin layer. The system was evacuated by using the pump P-1 in Fig. 6.1.2 (during that time the valves V-1 and V-3 were open and V-2 was closed) and heated up to ≈220°C for cleaning the sample. After 12 h, V-1 and V-3 were closed and the system was cooled down to 25°C. Pure CO_2 was first introduced into the reference cell (V-3 open, V-1 and V-2 closed) and than left to enter gradually into the adsorption cell (V-3 closed, V-1 and V-2 open). After equilibration at the desired pressure (indicated by API), V-1 and V-2 were closed. Prior to the experiments, leak tightness of the system was checked by measuring the differential pressure between the adsorption and reference cell under static conditions. The pressure increase below 10^{-4} Pa/s was considered as acceptable.

After assigning the desired values of amplitude and period of the time wave, the motor was started producing the volume modulation. The axis position, differential pressure, gas and particle temperature were continuously measured. After reaching the quasi-stationary state, minimum five periods of time-wave were recorded with a sampling rate $1000/T$ (where $T=2\pi/\omega$ is the period of the time wave, in seconds). The motor was turned off and the system

was left to equilibrate again. Next, a new period and/or amplitude were set and the experiment was repeated for two amplitudes and a number of frequencies. The whole procedure was repeated for other steady-state pressures.

6.4 Experimental NFRs of a batch adsorber

As illustration, In Fig. 6.4.1 we show samples of the measured volume (a), pressure (b), gas temperature (c) and particle temperature (d) in the quasi-stationary state (presented as deviations from the steady-state values), obtained for sinusoidal volume modulation with A=0.08 and ω=0.78 rad/s. The signals of the pressure and gas temperature obtained in the corresponding blank experiment are given in parallel. As expected, the pressure response in the adsorption experiment has lower amplitude than in the blank experiment (Fig. 6.4.1 b). The gas temperature response shows no difference in the adsorption and blank experiment (Fig. 6.4.1 c). It is interesting to notice that the periodic change of the gas temperature can be registered, although with a very small amplitude of ±0.1 K. The measurements in a broad range of frequencies showed that the periodic change of the gas temperature could be registered only for frequencies higher than 0.125 rad/s.

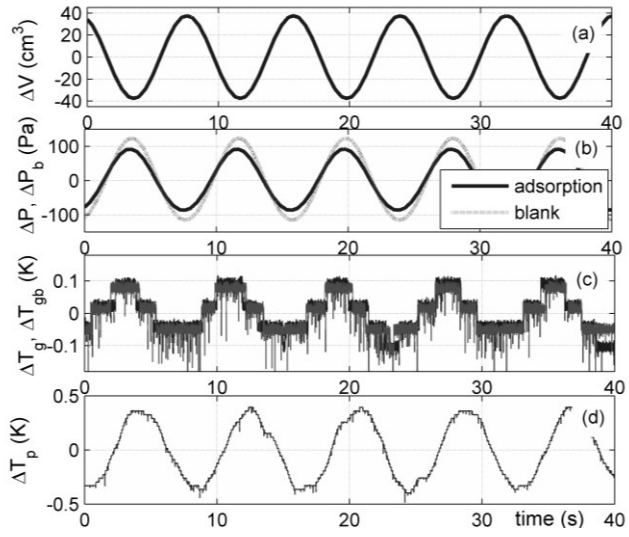

Fig. 6.4.1 Measured input (ΔV) and output signals (ΔP, ΔT_g, ΔT_p) (A = 0.08 ω= 0.78 rad/s)

In order to be analyzed in the frequency domain, the measured signals are transferred into the corresponding frequency spectra by applying the fast Fourier transform (function *fft* in

MATLAB). The data length of five periods were used for fast Fourier transform. Exceptionally, for the periods longer then 800 s, only three periods were measured and analyzed. The frequency spectra corresponding to the signals presented in Fig. 6.4.1 are presented in Figs. 6.4.2-6.4.4, as the amplitude and phase vs. dimensionless frequency (frequency normalized by the basic frequency).

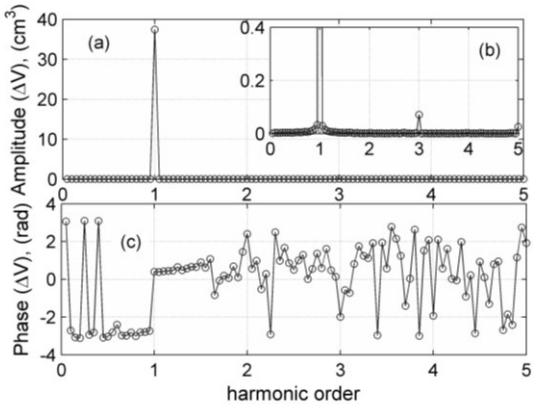

Fig. 6.4.2 Frequency spectrum of the volume signal from Fig. 6.4.1a

Fig. 6.4.2 represents the frequency spectrum of the volume signal and it serves to evaluate the accuracy of sine-wave approximation. The frequency spectrum of the ideal sine-wave is represented by a single harmonic (Fig 4.2.3, Chapter 4). Figs. 6.4.2a and 6.4.2b show that the measured volume signal contains the first harmonic $|X_1|$=39 cm^3 and the third harmonic $|X_3|$=0.07 cm^3 (0.18 % of the first one), which means that, for the given frequency, very good sine-wave approximation is achieved. However, for frequencies larger than 0.6 rad/s the second harmonic $|X_2| \approx$ 0.5cm^3 is also registered. If the second-harmonic in the input is present, than the second harmonic in the output contains also the contribution of the first-order FRF at 2ω, as follows:

$$Y_2 = \frac{1}{2} G_2(\omega,\omega) X_1^2 + G_1(2\omega) X_2 + \frac{1}{2} G_4(\omega,\omega,\omega,-\omega) X_1(\omega)^3 \overline{X}_1(\omega) + \ldots \qquad (6.4.1)$$

This fact should be considered when the second-order adsorber FRF is estimated , as it will be presented in following section.

Fig. 6.4.3 represents the frequency spectra of the measured pressure signals for the adsorption and the corresponding blank experiment. As expected, the pressure response in both cases contains the first, second and higher harmonics (Figs. 6.4.3 a and 6.4.3 b) with the

decreasing trend of amplitude ($|Y_1|$=89 Pa, $|Y_2|$ =2.5 Pa, $|Y_3|$ =0.25 Pa,...). The amplitudes of the first four harmonics of the pressure response vs. frequency for input amplitudes 0.03 and 0.08 are shown in Fig. 6.4.5.

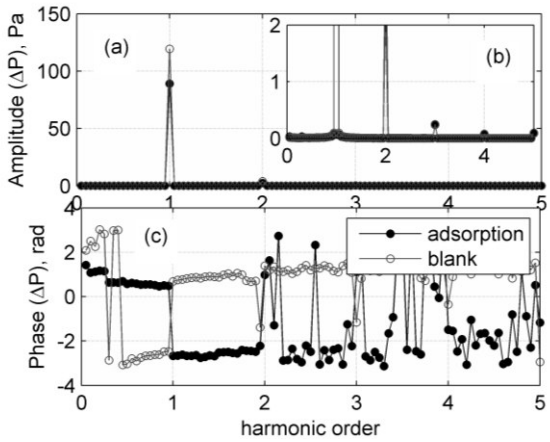

Fig. 6.4.3 Frequency spectra of the pressure signals from Fig. 6.4.1b

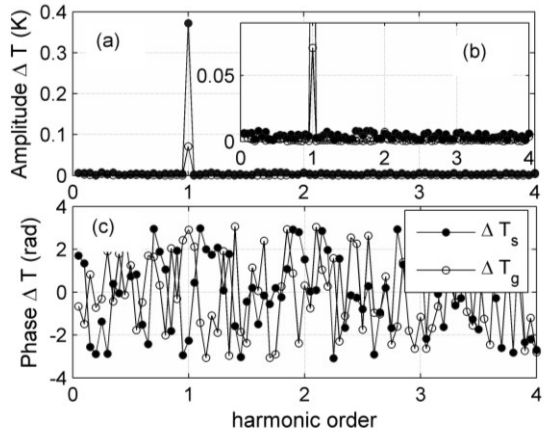

Fig. 6.4.4 Frequency spectra of the gas and particle temperature from Figs. 6.4.1c and 6.4.1d

The amplitude of the first harmonic (Fig. 6.4.5 a) increases linearly with the input amplitude and has the values of the order of magnitude 10^1 Pa for both input amplitudes. However, the amplitude of the second harmonic (Fig. 6.4.5 b) is more sensitive to the input amplitude, and increases by a factor of about 5, when the input amplitude is increased by a factor of 2.5. The amplitudes of the second harmonic for A=0.08 are of the order of magnitude 10^0 Pa, which can be reliably measured with available Baratron pressure sensors. The amplitudes of the third harmonic (Fig. 6.4.5 c) are of the order of magnitude 10^{-1} Pa, whereby the third

harmonic for A=0.08 shows scattering and increase for the frequencies higher than 0.6 rad/s. The amplitude of the fourth harmonic (Fig. 6.4.5 d) is $\approx 1 \cdot 10^{-2}$ Pa for A=0.03 and $\approx 5 \cdot 10^{-2}$ Pa for A=0.08.

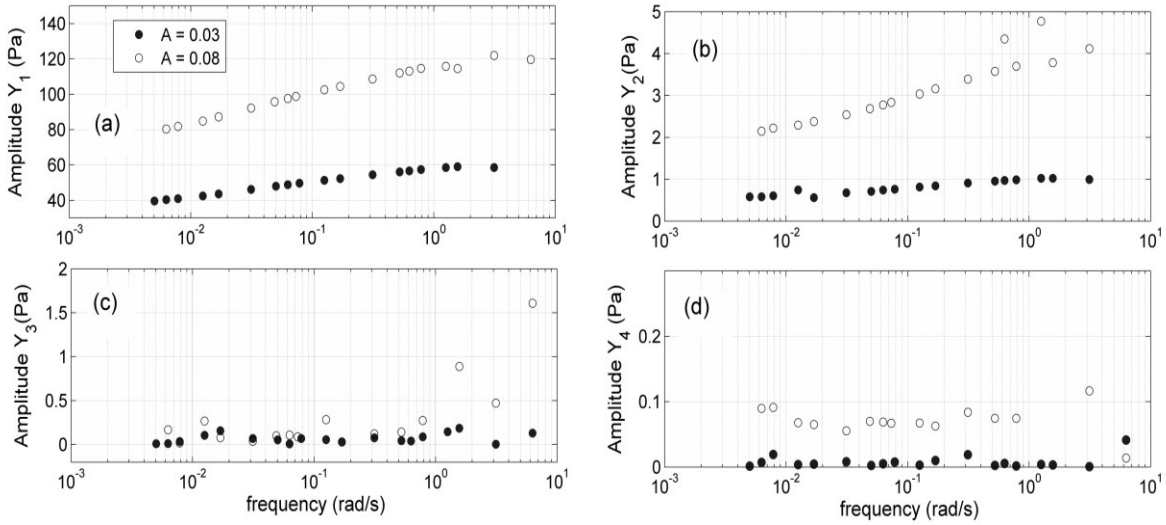

Fig. 6.4.5 Amplitudes of the first four harmonics of the pressure response vs. frequency for two different input amplitudes

From Fig. 6.4.5 it can be concluded:

1) the degree of nonlinearity, expressed as $(Y_2/Y_1)\cdot 100$, of the tested CO_2/zeolite 5A system, for input amplitude 0.08 is about 3%, which agree to the theoretical one obtained by simulations (Chapter 4).

2) The ratio (Y_3/Y_1) for input amplitude 0.03 is about $5 \cdot 10^{-2}$, which means that contribution of the third-order FRF in the first harmonic (eq. 3.2.7) can be neglected, and Y_1 can be used for calculation of the first-order adsorber FRF from the approximate equation:

$$Y_1 \approx G_1(\omega) X_1 \qquad (6.4.2)$$

3) The ratio (Y_4/Y_2) for input amplitude 0.08 is about 10^{-2}, which means that contribution of the fourth-order FRF in the second harmonic (eq. 6.4.1) can be neglected, and Y_2 can be used for calculation of the second-order adsorber FRF from the approximate equation:

$$Y_2 \approx \frac{1}{2} G_2(\omega,\omega) X_1^2 + G_1(2\omega) X_2 \qquad (6.4.3)$$

Fig. 6.4.4 represents the frequency spectra of the measured gas and particle temperatures. Since the measurements have shown the change of gas temperature of less than 0.1 K (in the

whole range of the tested frequencies), the gas can be considered as isothermal. In the frequency spectrum of the particle temperature only the first harmonic can be observed (Fig. 6.4.4a) ($|Z_1|$=0.39 K), while the second harmonic can not be distinguished from noise (Fig. 6.4.4a).

6.5 Estimation of the particle FRFs

Due to the negligible changes in the measured gas temperature, the tested adsorption system will be considered as the special nonisothermal case (T_g=const., $T_p \neq$const.)(Petkovska, 2001) and consequenly described with two series of particle FRFs: ***F***- and ***H***- functions (Fig. 3.3.3). Although in the theoretical considerations in previous chapters, the FRFs which relate dimensionless variables have been used, the experimental FRFs which relate dimensional variables (deviation variables) will be calculated here, since the equilibrium loading (Q_s) nedeed for the calculation of dimensionless ***F***- functions (eqs. 3.3.13 and 3.3.20), is generally not known.

The ***H***-functions can be calculated directly from the measured particle temperature and pressure, as follows:

$$Z_1 = H_1(\omega)Y_1 \tag{6.5.1}$$

$$Z_2 = \frac{1}{2}H_2(\omega,\omega)Y_1^2 + H_1(2\omega)Y_2 \tag{6.5.2}$$

where Y_1 and Y_2 are the first and the second harmonic of the pressure (P-P_s) and Z_1 and Z_2, are the first and the second harmonic of the particle temperature (T_p-T_{ps}).

The ***F***-functions have to be calculated from adsorber ***G***-functions (Petkovska, 2001). The relations which relate the dimensionless ***F***- and ***G***-functions for the batch asdorber under special nonisothermal conditions (T_g=const., $T_p \neq$const.), were derived in Chapter 3 (Section 3.3.4) (Eqs. 3.3.13 and 3.3.20). The corresponding equations in dimensional form can be written as follows:

$$F_1(\omega) = \frac{-P_s - G_1(\omega)V_s}{\beta^* G_1(\omega)} \tag{6.5.3}$$

$$F_2(\omega,\omega) = \frac{G_1(\omega) + G_2(\omega,\omega)V_s + \beta^* G_2(\omega,\omega)F_1(2\omega)}{-\beta^* G_1(\omega)^2} \tag{6.5.4}$$

In Eqs.(6.5.3 and 6.5.4) $G_1(\omega)$ and $G_2(\omega,\omega)$ are the first and the second order adsorber FRFs which relate pressure deviation (P-P_s) to the volume deviation (V-V_s). The partition coefficient is defined as $\beta^*=m_p R_g T_s/\rho_p$ (Pa·m^6/mol), and does not contain the equilibrium loading Q_s.

Equations 6.5.3 and 6.5.4 were derived assuming ideal gas behaviour and ideal mixing in the adsorber. However, in real experiments, phenomena like adsorption on the walls, deviation from the ideal gas behaviour, pressure change due to the gas heating by compression and delays of the measuring and acquisition systems can affect the measured pressure responses and cause errors in the calculation of the ***G***-functions and consequently in obtained ***F***-functions. A common way to account for those spurious effects is through blank experiments. Since the NFR analysis is performed in the frequency domain, we have developed a new concept, which describes how to incorporate the results of the blank experiments in the frequency domain. It is based on estimation of so called blank FRFs and is presented below.

Relations between the F- and G- functions which include blank FRFs

In the NFR measurements, blank experiments are performed at the same steady-state temperature and pressure as the adsorption experiments, just in absence of the adsorbent. The adsorber FRFs, calculated from eqs. ((6.4.2) and (6.4.3)) using blank pressure responses ($\Delta P_b=P_b-P_s$), are called blank FRFs (the $\boldsymbol{G_b}$-functions).

If we assume that all unknown spurious effects can be represented as a single term in the mass balance equation, which is identical for the adsorption and blank experiments, than the mass balance of the batch adsorber (for the case of constant gas temperature) can be written in the following way:

$$V_s\Delta P + \Delta V\Delta P + P_s\Delta V + \beta^*\Delta Q + \Phi = 0 \qquad (6.5.5)$$

where $\Delta Q=Q-Q_s$ is the perturbation of the adsorbed quantity (mol/m^3) and Φ represents all unknown effects. When written for the blank experiments, eq. (6.5.5) becomes:

$$V_s\Delta P_b + \Delta V\Delta P_b + P_s\Delta V + \Phi = 0 \qquad (6.5.6)$$

By combining eqs. (6.5.5) and (6.5.5) the adsorbed quantity can be expressed as a function of the volume change and the pressure difference in the blank and adsorption experiment:

$$\Delta Q = \frac{(V_s - \Delta V)}{\beta^*}(\Delta P_b - \Delta P) \tag{6.5.7}$$

According to the concept of higher order FRFs, the pressure and adsorbed quantity can be expressed in the form of Volterra series. By applying the method of harmonic probing, the following relations between the ***F-***functions, ***G-***functions and $\boldsymbol{G_b}$-functions are derived:

$$F_1(\omega) = \frac{[G_{1b}(\omega) - G_1(\omega)]V_s}{\beta^* G_1(\omega)} \tag{6.5.8}$$

$$F_2(\omega,\omega) = \frac{G_{1b}(\omega) - G_1(\omega) + G_{2b}(\omega,\omega)V_s - G_2(\omega,\omega)(V_s + \beta^* F_1(2\omega))}{\beta^* G_1(\omega)^2} \tag{6.5.9}$$

In this way, by defining the blank FRFs, the results of blank experiments are incorporated directly in the frequency domain. This approach is advantageous compared to the signal subtracting in the time domain, since it tolerates small discrepancies in conditions under which blank and adsorption experiments are preformed.

In the further text, the estimation of blank FRFs, adsorber FRFs and particle FRFs will be given step by step.

6.5.1 Blank FRFs

The first-order blank FRF *c* is estimated from eq. (6.4.2) using the first harmonic of the blank pressure response (Y_{1b}) for A=0.03:

$$G_{1b} = \frac{Y_{1b}}{X_1} \tag{6.5.10}$$

The second-order blank FRF $G_{2b}(\omega,\omega)$ is estimated from eq. (6.4.3) using the measured second harmonic of the blank pressure response (Y_{2b}) for A =0.08:

$$G_{2b}(\omega,\omega) = \frac{2\left[Y_{2b} - X_2 G_{1b}(2\omega)\right]}{X_1^2} \tag{6.5.11}$$

The experimental $G_{1b}(\omega)$ and $G_{2b}(\omega,\omega)$ are presented in Figs. 6.5.1 and 6.5.2 respectively, as amplitude and phase vs. frequency. The lines in Figs. 6.5.1 and 6.5.2 represent first and second-order adsorber FRFs derived from the model of ideal gas. It can be seen from Fig. 6.5.1 that the amplitude of $G_{1b}(\omega)$ is slightly lower than that for the ideal gas, which reflects the gas nonideality. However, the amplitude of $G_{2b}(\omega,\omega)$ is slightly higher than that for the ideal gas (Fig. 6.5.2), which is most probably the consequence of neglecting the contribution

of the fourth-order FRF in eq. (6.4.1). The phases of both $G_{1b}(\omega)$ and $G_{2b}(\omega,\omega)$ show significant lags for frequencies higher than 0.1 rad/s, which can be atributed to the delays in the pressure sensor or/and acquisition system.

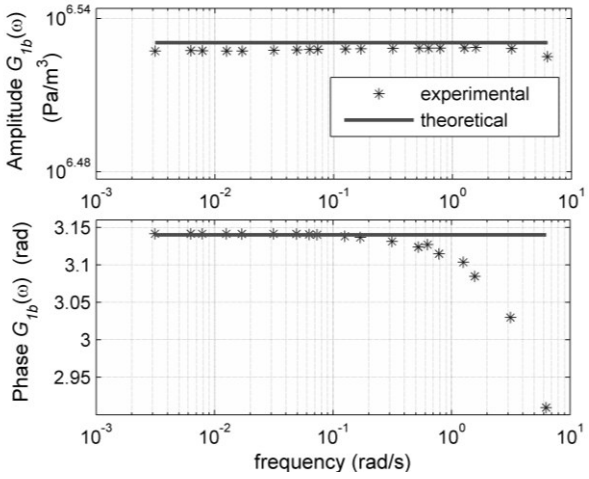

Fig. 6.5.1 First-order blank FRF $G_{1b}(\omega)$

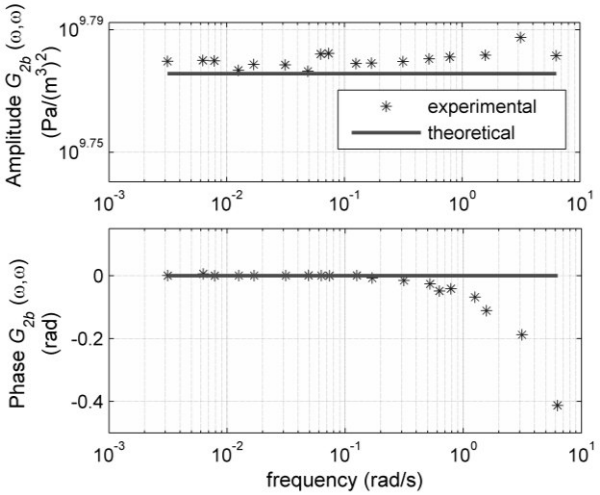

Fig. 6.5.2 Second-order blank FRF $G_{2b}(\omega, \omega)$

6.5.2 Adsorber FRFs

The first-order adsorber FRF $G_1(\omega)$ is estimated from eq. (6.4.2) using the first harmonic of the pressure response (Y_1) for A=0.03:

$$G_1(\omega) = \frac{Y_1}{X_1} \tag{6.5.12}$$

The second-order adsorber FRF $G_2(\omega,\omega)$ is estimated from eq. (6.4.3) using the measured second harmonic of the pressure response (Y_2) for A =0.08:

$$G_2(\omega,\omega) = \frac{2\left[Y_2 - X_2 G_1(2\omega)\right]}{X_1^2} \tag{6.5.13}$$

The adsorber FRFs, $G_1(\omega)$ and $G_2(\omega,\omega)$, for two different particle diameters, are presented in Figs. 6.5.3 and 6.5.4, as the amplitude and phase vs. frequency.

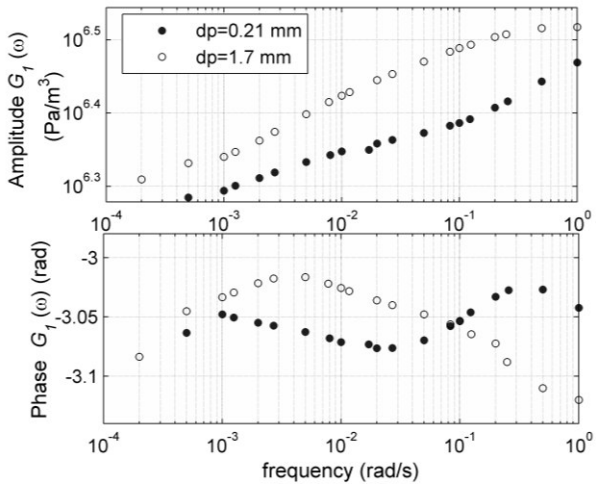

Fig. 6.5.3 First-order adsorber FRFs $G_1(\omega)$

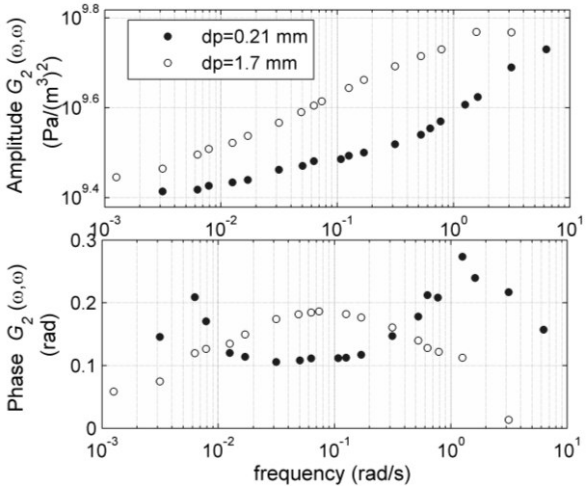

Fig. 6.5.4 Second-order adsorber FRFs $G_2(\omega,\omega)$

As it can be seen from Fig. 6.5.3, the first-order adsorber FRFs have different shapes for different particle diameters. The amplitude of $G_1(\omega)$ for the coarse particles (d_p=1.7 mm) has one inflection point and the phase has a single maximum, while for the fine particles (d_p=0.21 mm) the amplitude of $G_1(\omega)$ has two inflection points and the phase has two corresponding maxima. The phase of $G_1(\omega)$ tends to $-\pi$ for both low and high frequencies. The second-order adsorber FRFs (Fig.6.5.4) exhibit almost the same patterns as $G_1(\omega)$ depending on the particle size (one inflection point of the amplitude and a single maximum of the phase for the coarse particles and two inflection points of the amplitude and the two maxima of the phase for the fine particles). The phase of $G_2(\omega,\omega)$ tends to zero for both low and high frequencies. The obtained $G_1(\omega)$ and $G_2(\omega,\omega)$ are further used for calculation of particle FRFs.

6.5.3 Particle FRFs

Using $G_1(\omega)$ and $G_2(\omega,\omega)$ as well as $G_{1b}(\omega)$ and $G_{2b}(\omega,\omega)$, estimated in the previous sections, the particle FRFs $F_1(\omega)$ and $F_2(\omega,\omega)$ have been calculated from eqs. (6.5.8) and (6.5.9), and presented in Figs. 6.5.5 and 6.5.6, respectively. The amplitude of $F_1(\omega)$ (Fig. 6.5.5) has one inflection for the coarse and two inflections for the fine particles. The phase of $F_1(\omega)$ has two inflections for both particle diameters, whereby in the case of fine particles a plateau can also be observed. The phase of $F_1(\omega)$ tends to zero for low frequencies and to $-\pi/4$ for high frequencies. The amplitude of $F_2(\omega,\omega)$ (Fig. 6.5.6) for the coarse particles has two inflections which correspond to a minimum and a maximum of the phase. For the fine particles only one inflection of the amplitude of $F_2(\omega,\omega)$ can be clearly observed and the phase of $F_2(\omega,\omega)$ has a small minimum. It can be seen from Fig. 6.5.6 that for the frequencies higher than 0.6 rad/s the data for $F_2(\omega,\omega)$ are scattered and thus unreliable.

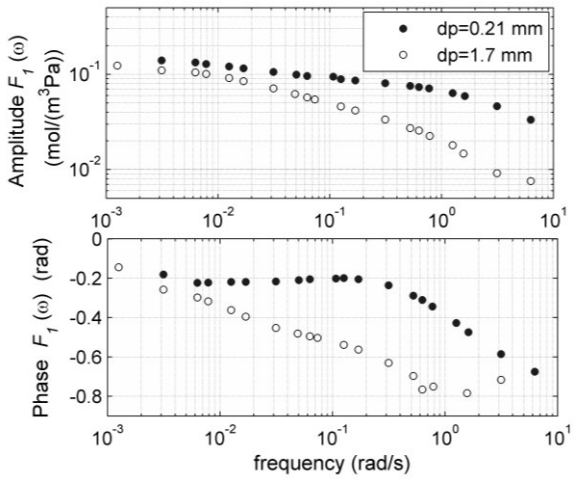

Fig. 6.5.5 Particle first-order FRFs $F_1(\omega)$

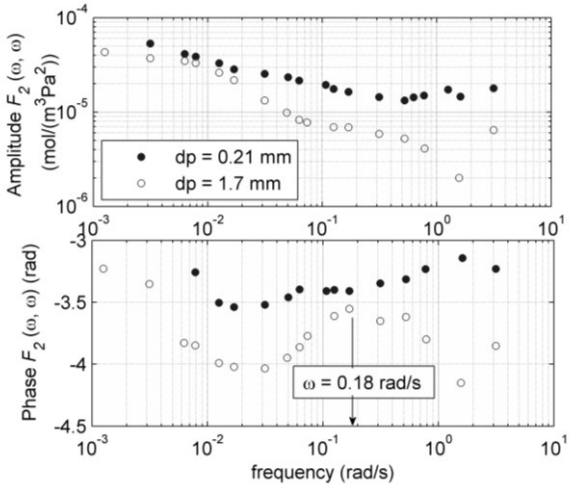

Fig. 6.5.6 Particle second-order FRFs $F_2(\omega,\omega)$

The temperature FRF, $H_1(\omega)$, is calculated from Eq. (6.5.1), using the first harmonics of the measured particle temperature (Z_1) and pressure (Y_1), and presented in Fig. 6.5.7. The amplitude of $H_1(\omega)$ has one maximum for the coarse particles and two maxima for the fine particles. The phase of $H_1(\omega)$ has two inflections for both particle diameters and changes in the sign at a frequency about 0.1 rad/s. The second-order temperature FRF $H_2(\omega,\omega)$ could not be estimated because second harmonic in the particle temperature response was not measurable (Fig. 6.4.1d).

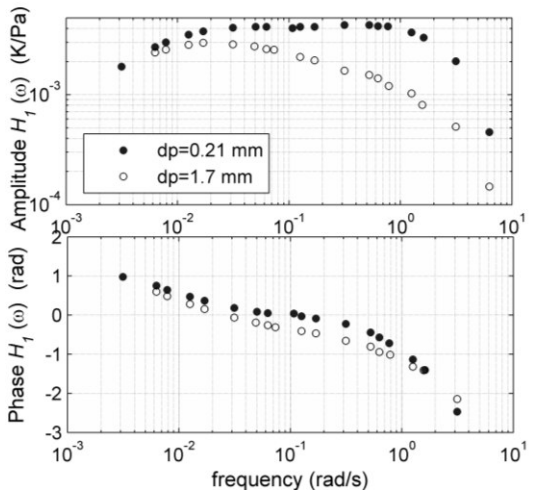

Fig. 6.5.7 First-order temperature FRFs $H_1(\omega)$

The obtained particle FRFs $F_1(\omega)$, $F_2(\omega,\omega)$ and $H_1(\omega)$ will be used for recognition of the governing kinetic mechanism and estimation of the equilibrium and kinetic parameters, as it will be presented in the following section.

6.6 Identification of the kinetic mechanism

Regarding the kinetic mechanism of adsorption of CO_2 on commercial zeolite 5A, Onyestyak et al. (1996), who have investigated this system by linear FR method, have reported isothermal macopore diffusion control as the governing mechanism for the temperatures higher than 373K, while for the lower temperatures it was not possible to fit the data to IMD model because the bimodal behavior was experimentally observed. It was supposed that the second peak of the phase lag at low frequencies corresponded to heat effects.

Therefore we have derived the FRFs up to the second order for NMD model (Chapter 5) as the suspected mechanism for adsorption of CO_2 on zeolite 5A particles at lower temperatures. The characteristic features of the experimental particle FRFs $F_1(\omega)$, $F_2(\omega,\omega)$ and $H_1(\omega)$, for particle diameters of 1.7mm and 0.21mm, are compared with those of the corresponding theoretical FRFs for NMD in Tables 6.6.1-6.6.3. Since the patterns of the real and imaginary part of the particle FRFs can give some additional insight in the process of mechanism identification, the particle FRFs, presented in Figs. 6.5.5-6.5.7 in the form of amplitude and phase characteristics, are also presented as the real and imaginary part vs. frequency in Figs. 6.6.1-6.6.3, respectively.

Table 6.6.1 Comparison of the characteristic features of the experimental functions $F_1(\omega)$ with the theoretical ones derived for the NMD model

	Theoretical for NMD	Experimental (d_p=1.7 mm)	Experimental (d_p=0.21 mm)
Amplitude $F_1(\omega)$	Changes slope once or twice	Changes slope once	Changes slope twice
Phase $F_1(\omega)$	Two inflections	Two inflections	Two inflections
Real $F_1(\omega)$	One or two inflections	One inflection	Two inflections
- Imag $F_1(\omega)$	One or two maxima	One maximum	Two maxima

Table 6.6.2 Comparison of the characteristic features of the experimental functions $F_2(\omega,\omega)$ with the theoretical ones derived for the NMD model

	Theoretical for NMD	Experimental (d_p=1.7 mm)	Experimental (d_p=0.21 mm)
Amplitude $F_2(\omega,\omega)$	Changes slope twice	Changes slope twice	Changes slope twice
Phase $F_2(\omega,\omega)$	Minimum followed by a maximum	Minimum followed by a maximum	Single minimum
Real $F_2(\omega,\omega)$	Changes slope twice	Changes slope twice	Changes slope twice
- Imag $F_2(\omega,\omega)$	Minimum followed by a very small maximum	Minimum followed by a very small maximum	Single minimum

Table 6.6.3 Comparison of the characteristic features of the experimental functions $H_1(\omega)$ with the theoretical ones derived for the NMD model

	Theoretical for NMD	Experimental (d_p =1.7 mm)	Experimental (d_p =0.21 mm)
Amplitude $H_1(\omega)$	One maximum	One maximum	Two maxima
Phase $H_1(\omega)$	Changes sign	Changes sign	Changes sign
Real $H_1(\omega)$	One maximum	One maximum	Two maxima
Imag $H_1(\omega)$	Maximum followed by a weak minimum	Maximum followed by a weak minimum	Maximum followed by inflection and deep minimum

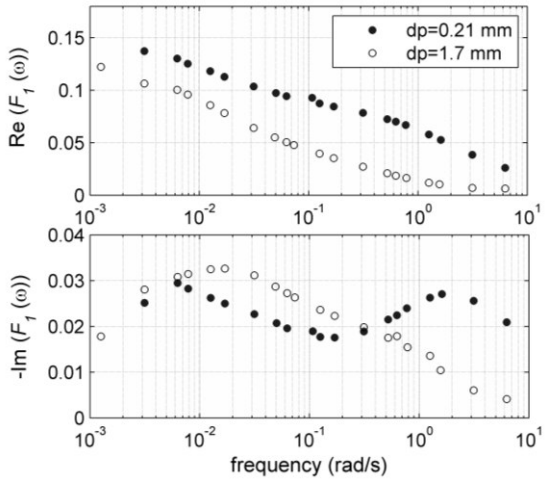

Fig. 6.6.1 First-order FRF $F_1(\omega)$

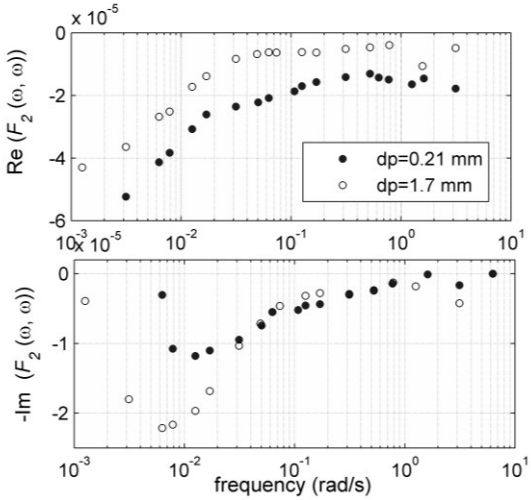

Fig. 6.6.2 Second-order FRF $F_2(\omega,\omega)$

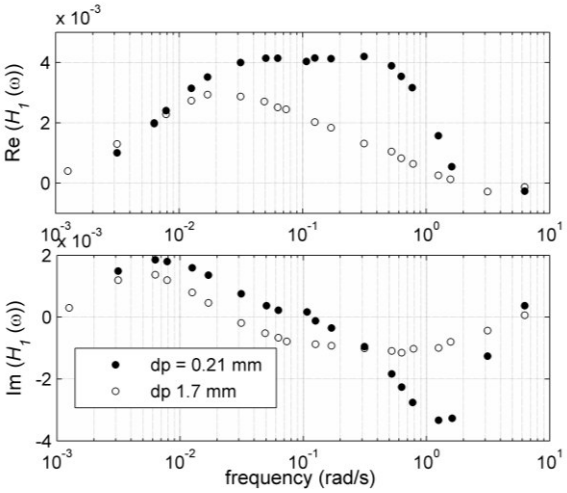

Fig. 6.6.3 First-order temperature FRF $H_1(\omega)$

Regarding the function $F_1(\omega)$, the pattern of the negative imaginary part of $F_1(\omega)$ is the most important for mechanism identification. Table 6.6.1. shows that the experimental $F_1(\omega)$ for the coarse particles exhibits one maximum and for the fine particles two maxima. Results of the theoretical studies show that $F_1(\omega)$ for the NMD model can exhibit one or two maxima of -Im ($F_1(\omega)$), depending on the parameters (Chapter 5, Section 5.4.3). The comparison given in Table 6.6.1 shows that, according to the function $F_1(\omega)$, the NMD could be considered as governing mechanism for both particle diameters. However, the unique feature of the NMD mechanism, the distinct minimum followed by a distinct maximum of the phase of $F_2(\omega,\omega)$,

is experimentally observed only for the coarse particles, while for the fine particles only a weak minimum of the phase $F_2(\omega,\omega)$ is present (Table 6.6.2). Inspection of Table 6.6.2 shows that all characteristics of the experimental $F_2(\omega,\omega)$ for the coarse particles coincide with those predicted by the NMD model. This result is very important since it is the first confirmation that all characteristic features of $F_2(\omega,\omega)$ can be experimentally observed.

Table 6.6.3 shows that the experimental temperature FRFs $H_1(\omega)$ for the coarse and fine particles have significantly different patterns. For the coarse particles the real part of $H_1(\omega)$ has a maximum and the imaginary part has a maximum followed by a weak minimum. These patterns agree with those of the theoretical $H_1(\omega)$ function for the NMD model. However, for the fine particles two maxima of the real part and a maximum followed by an inflection point and a deep minimum of the imaginary part of $H_1(\omega)$ is observed. Such patterns of $H_1(\omega)$ were reported by Bourdin et al. (1996) for the case of nonisothermal macropore diffusion with the significant surface barrier.

In summary, since all the characteristic features of the experimentally obtained functions, $F_1(\omega)$, $F_2(\omega,\omega)$ and $H_1(\omega)$ for the coarse particles are in accordance with the corresponding theoretical FRFs for the NMD model, NMD is recognized as the governing mechanism for the coarse particles. On the other hand, for the case of the fine particles, only the experimental $F_1(\omega)$ is in accordance with theoretical one for NMD, while $F_2(\omega,\omega)$ and $H_1(\omega)$ are not in accordance with the corresponding theoretical FRFs neither for NMD model nor for the nonisothermal micropore diffusion (Petkovska and Petkovska, 2003). Taking into account that with decrease of the particle radius, the surface barrier and micropore diffusion become more pronounced, the derivation of the second-order FRFs for nonisothermal macropore diffusion with surface barrier and nonisothermal micropore-macropore diffusion (and other possible complex mechanisms) would be needed for identification of the kinetic mechanism.

Furthermore, in the case of the fine particles the shape of the particles is not strictly spherical and there is a certain size distribution of the particles, which might cause the deviation of the experimental results from the model predictions. Apart from that, the shifting of the macropore diffusion time constant (maximum of the phase of $F_2(\omega,\omega)$) towards higher frequencies (where the results are less accurate) with decrease in the particle diameter may cause difficulties in identification of the kinetic mechanism.

6.7 Estimation of the model parameters

6.7.1 Equilibrium parameters

Estimation of the model parameters is the last step in the application of NFR method. It is based on the experimental FRFs and theoretical FRFs of the identified model. Since NMD is recognized as the governing mechanism for the coarse particles, the equilibrium and kinetic parameters are estimated according to the methodology proposed in Section 5.5. The equilibrium parameters, i.e. the first and second order derivatives of the adsorption isotherm are determined from the low-frequency asymptotic characteristic of $F_1(\omega)$ and $F_2(\omega,\omega)$:

$$\left.\frac{dQ}{dP}\right|_{Ps} = \lim_{\omega\to 0}(F_1(\omega)) = 0.124 \text{ mol/(m}^3\text{Pa)} \qquad (6.7.1)$$

$$\left.\frac{1}{2}\frac{d^2Q}{dP^2}\right|_{Ps} = \lim_{\omega\to 0}(F_2(\omega,\omega)) = 4.68\cdot 10^{-5} \text{ mol/(m}^3\text{Pa}^2\text{)} \qquad (6.7.2)$$

It should be noted that the obtained derivatives are actually effective values, which defines changes of the overall concentration in the particle with respect to the pressure. The comparison of these derivatives with the values based on the equilibrium relation obtained from gravimetric measurements (eq.6.2.1) is given in Table 6.7.1. The relative error of several percent may be caused with the fact that the asymptotic behavior at the low frequency end was not reached within the frequency range used in the experiments. It can be expected that these errors would be reduced by performing experiments at lower frequencies.

Table 6.7.1 Comparison of the first and second derivatives of the adsorption isotherms obtained from the NFR and gravimetric measurements

	NFR method	Gravimetric measurements (eq.6.2.1)	Rel. error, %
$\left.\frac{dQ}{dP}\right\|_{Ps}$ (mol/m^{3}Pa)	0.124	0.127	3.1
$\left.\frac{1}{2}\frac{d^2Q}{dP^2}\right\|_{Ps}$ (mol/m^{3}Pa^2)	$4.68\cdot10^{-5}$	$5.06\cdot10^{-5}$	7.5

6.7.2 Diffusion coefficient

The diffusion coefficient, D_p, is estimated from the frequency at which the phase of experimental $F_2(\omega,\omega)$ has the maximum, using the relation $\omega\tau_D = 13.6$ (Section 5.5.1). The phase of $F_2(\omega,\omega)$ for the coarse particles is presented in Fig.6.5.6b and the maximum lies at ω=0.18 rad/s. The corresponding diffusion time constant is τ_D=75.5 s and the diffusion coefficient D_p is calculated from the following equation:

$$D_p = \frac{R^2 e^*}{\tau_D} \tag{6.7.3}$$

where the parameter e^* is defined as:

$$e^* = \frac{\frac{(1-\varepsilon_p)}{R_g T_s}\left.\frac{dQ}{dP}\right|_{Ps} + \varepsilon_p}{\varepsilon_p} \tag{6.7.4}$$

and has a value $5.5\cdot10^{-6}$ m^2/s. Taking into account the dominant pore diameter of 250 nm (Table 6.2.1) and the mean free path of CO_2 at 2 kPa and 298 K of 2750 nm, the value of Knudsen number (K_n=11) indicates that the system at given conditions is in Knudsen regime of diffusion. The calculated effective diffusion coefficient $D_{eff} = D_{Kn}\varepsilon_p / \tau$ (D_{Kn} - Knudsen diffusivity, ε_p =0.35 and τ - tortuosity factor typically ≈3 for zeolites) is $3.49\cdot10^{-6}$ m^2/s, which is very close to the experimentally obtained D_p. Comparison of the diffusion coefficient obtained from the NFR method with the literature values for CO_2 on zeolite 5A obtained with other techniques, is given in Table 6.7.2, and shows good agreement.

Table 6.7.2 Comparison of the diffusion coefficient with literature values

	D_p (m^2/s)	technique	adsorbat/adsorbent	conditions
This work	$5.5\cdot10^{-6}$	NFR	CO_2- zeolite 5A	T_s=25°C, P_s=2kPa
Onyestyak et al. (1996)	$4.7\cdot10^{-7}$	FR	CO_2- zeolite 5A	T_s =150 °C P_s =0.133 kPa
Sargent and Whitford (1971)	$1\cdot10^{-6}$	tracer ($^{14}CO_2$)	CO_2- zeolite 5A	T_s =25 °C P_s = 101 kPa

6.7.3 Heat transfer coefficient

The heat transfer coefficient, h, is estimated from the frequency at which the imaginary part of the experimental function $H_1(\omega)/F_1(\omega)$ has a maximum, using the equation $\omega\tau_h = 1$ (Section 5.5.1). The function $H_1(\omega)/F_1(\omega)$ for the coarse particles is presented in Fig. 6.7.1, as the real and imaginary part. The imaginary part has the maximum at ω=0.0126 rad/s (Fig. 6.7.1), which corresponds to τ_h=79 s. The heat transfer coefficient is calculated from the following equation:

$$h = \frac{R(1-\varepsilon_p)\rho_p c_{ps}}{3\tau_h} = 2.56 \text{ W/m}^2\text{K} \qquad (6.7.5)$$

which is in the range of typical values for free convection (up to 10 W/m^{2}K).

6.7.4 Heat of adsorption

The heat of adsorption, (-ΔH), is estimated from the high-frequency asymptote of the real part of $H_1(\omega)/F_1(\omega)$ (Section 5.5.3), which represents the modified heat of adsorption, ξ^*, and from Fig.6.7.1 it is:

$$\lim_{\omega\to\infty}(\text{Re}(H_1(\omega)/F_1(\omega))) = \xi^* = 0.05 \text{ Km}^3/\text{mol} \qquad (6.7.6)$$

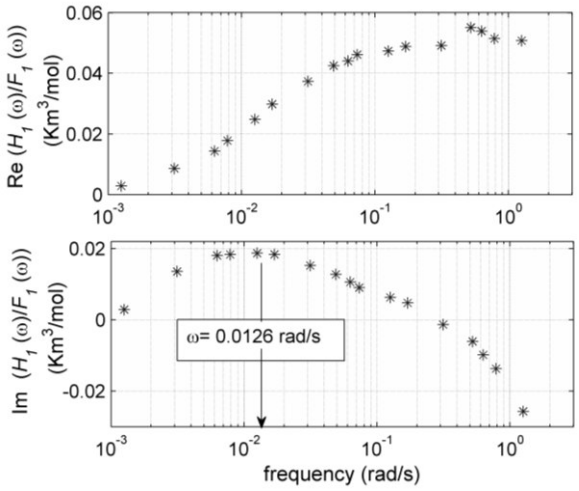

Fig. 6.7.1 Real and imaginary part of $H_1(\omega)/F_1(\omega)$

The heat of adsorption is than calculated as follows:

$$(-\Delta H) = \xi^* \rho_p c_{ps} = 29.5 \text{ kJ/mol} \qquad (6.7.7)$$

The obtained value is in good agreement with heats of adsorption for CO_2/zeolite 5A reported by Tlili et al.(2009) (30 kJ/mol) and Garces et al. (2013) (40 kJ/mol).

Summary

The new apparatus, described in this chapter, was succesfully used for validation of the NFR method for investigation of the gas adsorption. Satisfactorily good approximation of sinusoidal volume change was achieved by using the servomotor with linear actuator and feedback control of its position for driving the bellows. Measurements of the pressure responses by highly accurate Baratron pressure transducer provided determination of the experimental first- and second-order ***F***-functions. Infrared measurements of the particle temperature provided determination of the first order ***H***-function. Gas temperature measurements enable estimation whether the gas phase can be regarded as isothermal or not. For the investigated case, very small changes of the gas temperature were observed, so this temperature was regarded as constant. Based on the obtained FRFs the following parameters of the investigated system CO_2/zeolite 5A particles have been estimated: diffusion coefficient, heat transfer coefficient, first and second-order derivatives of the adsorption isotherm and the heat of adsorption. This results confirm that the NFR method is applicable regarding characterization of gas-solid adsorption and that it is advantageous compared to the classical FR method.

The results presented in this chapter have been published in the following article:

D. Brzić, M. Petkovska, Nonlinear frequency response measurements of gas adsorption equilibrium and kinetics: New apparatus and experimental verification, *Chem. Eng. Sci* 132 (2015), 9-21

7. CONCLUSIONS

The objective of this work was to explore the applicability of the concept of Nonlinear Frequency Response (NFR) for identification of the kinetic mechanism of adsorption of pure gases, since the commonly used linear FR method suffers from significant limitations. The NFR method represents an extension of the linear FR to the nonlinear range, by applying the concept of higher-order FRFs. The basic principle of the NFR method is determination of the experimental higher-order FRFs and their comparison with theoretical ones for different kinetic models. In this work FRFs up to the second order have been considered.

The most challenging issues regarding the application of the NFR approach for investigation of gas adsorption in the closed system were: 1) generation of the mechanical sine wave with variable amplitude, needed as the input excitation 2) accurate measurement of the second harmonic of the pressure response (which is typically low for weakly nonlinear adsorption systems) 3) lack of the theoretical higher-order FRFs for complex kinetic mechanisms.

The objective of this thesis was realized through three main parts of investigation: 1) applicability study based on numerical simulations of NFRs of a batch adsorber 2) design, constructing and evaluating of the experimental set-up for NFR measurements and 3) derivation of the theoretical FRFs up to the second order for nonisothermal adsorption controlled by macropore diffusion for spherical geometry. The most important results obtained from that investigations are summarized in the following text.

A) The applicability of the NFR concept for studying gas adsorption was evaluated by calculation of the first- and second-order particle FRFs ($F_1(\omega)$ and $F_2(\omega,\omega)$), using the simulated NFRs of a batch adsorption system as "quasi experimental" data. The simulation results have shown how the following parameters: mass of adsorbent, input amplitudes, frequency range and sampling rate, affect the possibility and accuracy of estimation of $F_1(\omega)$ and $F_2(\omega,\omega)$. Based on those results, the criteria which defines the optimal values of the mentioned parameters for efficient NFR experiments, have been ascertained. The values of those parameters can be determined for any adsorption system from several preliminary step response experiments according to the procedure developed in this work and summarized in a guideline given in Section 4.3.5. The input amplitude was found to be a critical issue for obtaining an accurate second-order FRF. The results have shown that input amplitude for

which the degree of nonlinearity (expressed as the ratio of the second and the first harmonic in the output) is about 3%, is the optimal for estimation of the second-order FRF. For the investigated system (CO_2/zeolite 5A) the optimal amplitude was 8-10 % of the steady-state volume. Since the satisfactory accuracy of $F_1(\omega)$ and $F_2(\omega,\omega)$ was obtained from "quasi experimental" NFRs for optimal parameters, it was concluded that constructing an experimental set-up is justified .

B) By deriving the first and second-order FRFs for the nonisothermal macropore diffusion (NMD) model, the existing library of theoretical FRFs have been extended. The NMD model under assumption of constant gas temperature is characterized by two series of FRFs (the ***F***-functions, which relate the adsorbed quantity to the pressure and the ***H***-functions, which relate the particle temperature to the pressure). For the first-order FRFs the analytical expressions were obtained, while the second order FRFs were obtained numerically. The analysis of the obtained FRFs, performed by simulations for different values of the non-isothermality coefficient (δ) and the ratio of the diffusional and heat transfer time constant (t_D/t_h), have shown the following:

- The second-order FRF ($F_2(\omega,\omega)$) exhibits specific bimodal pattern (a minimum followed by a maximum of the phase of $F_2(\omega,\omega)$), which allows reliable recognition of NMD mechanism
- The diffusion coefficient D_p can be estimated from the frequency at which the phase of the experimental $F_2(\omega,\omega)$ has a maximum, using the relation $\omega \cdot t_D=13.6$
- The heat transfer coefficient h can be obtained from the frequency at which the ratio $H_1(\omega)/F_1(\omega)$ has a maximum, using the relation $\omega \cdot t_h=1$
- The first- and second-order concentration derivatives of the adsorption isotherm can be obtained from the low-frequency asymptotes of $F_1(\omega)$ and $F_2(\omega,\omega)$, respectively
- The heat of adsorption ($-\Delta H$) can be obtained from the high-frequency asymptote of the ratio $H_1(\omega)/F_1(\omega)$.

The above results clearly show, that for estimation of both kinetic constants of the complex NMD model (t_D and t_h), three FRFs have to be determined: $F_1(\omega)$, $F_2(\omega,\omega)$ and $H_1(\omega)$.

C) The new apparatus for validation and exploiting of the NFR concept was constructed. The operating principle of the set up is modulation of the asdorption cell volume, around the steady-state value, as a sine wave of different amplitudes and frequencies and measurements

of the pressure, gas temperature and particle temperature responses with high accuracy and resolution. The sinusoidal modulations of the volume with amplitudes up to 10 % of the steady-state volume and frequencies up to 1 Hz were feasible. The apparatus was proven as capable of producing representative NFRs and their reliable measurements. Based on the measured NFRs for the CO_2/zeolite 5A system, the particle FRFs $F_1(\omega)$, $F_2(\omega,\omega)$ and $H_1(\omega)$ were obtained. It is the first evidence of obtaining the experimental second-order FRF which describes gas adsorption. Since the patterns of all those functions matched the theoretical ones for the NMD model, this model was accepted. The kinetic parameters: diffusion coefficient and heat transfer coefficient, the equilibrium parameters: the first- and second-order derivatives of the adsorption isotherm, as well as the heat of adsorption, were estimated. A conclusion follows that the investigated NFR method is applicable for identification of the kinetic mechanism and estimation of equilibrium and kinetic data of gas adsorption systems.

The main advantages of the NFR method compared to the linear FR are: 1) reliability of identification of the kinetic model based on the pattern of second-order FRF, 2) direct estimation of nonlinear model parameters based on the characteristics of the FRFs 3) estimation of the kinetic and equilibrium parameters from the same experimental data.

The main drawbacks of the NFR approach are related to experiments at very low and very high frequencies. At very low frequencies the experiments last very long and the initial steady-state conditions can be changed. At very high frequencies, the period of modulation is much shorter than the diffusion time constant and therefore the measured pressure signal does not differ much from the blank experiments. As a consequence, the errors due to the calculations with small numbers can arise. Apart of this, the frequencies higher than 1 Hz are not technically feasible by mechanical means.

Regarding further investigations on this topic, the following issues can be highlighted: 1) Improvement of the approximation of the sinusoidal volume change 2) Possibility of direct measurements of the adsorbed quantity instead of pressure 3) Extension of the frequency range above 1 Hz and 4) Derivation of the theoretical higher-order FRFs for complex kinetic models.

The scientific importance of this work lies in the fact that it represents the first evidence of the successful investigation of gas adsorption in the nonlinear range, which opens significant new perspectives in this field.

Literature cited

Baerlocher, Ch., McCusker, L.B. and Olson, D.H., 2007. Atlas of Zeolite Framework Types, Elsevier, Amsterdam

Bensmann, B., Petkovska, M., Vidaković-Koch, T., Hanke-Rauschenbach, R., Sundmacher, K., 2010. Nonlinear frequency response of electrochemical methanol oxidation kinetics: A theoretical analysis**.** *Journal of the Electrochemical Society* 157*,* B1279-B1289.

Birgham, E.O., 1988. The Fast Fourier Transform and its Applications, Prentice-Hall, Englewood Cliffs: NJ

Bourdin, V., Gray, P.G., Grenier, Ph., Terrier, M. F., 1998. An apparatus for adsorption dynamics studies using infrared measurement of the adsorbent temperature. *Rev. Sci Instrum.*, 69, 2130-2136.

Bourdin, V., Grenier, Ph., Meunier, F., Sun, L.M., 1996a. Thermal frequency response method for the study of mass-transfer kinetics in adsorbents. *AIChE J*. 42, 700-712.

Bourdin, V., Sun, L.M., Grenier, Ph., Meunier, F., 1996b. Analysis of the temperature frequency response for diffusion in crystals and biporous pellets. *Chem. Eng. Sci.*, 51 (2), 269-280.

Braunauer, S., Deming, L.S., Deming, W.E., Teller, E. J., 1940. On a Theory of of the van der Waals Adsorption of Gases. *Journal of the American Chemical Society*, 62, 1723-1732.

Brzić, D., Petkovska, M., 2015. Nonlinear frequency response measurements of gas adsorption equilibrium and kinetics: New apparatus and experimental verification, *Chem. Eng. Sci* 132, 9-21.

Camacho, B.C.R., Ribeiro, R. P. P. L., Esteves, I. A. A. C. and Mota, J. P. B., 2015. Adsorption equilibrium of carbon dioxide and nitrogen on the MIL-53(Al) metal organic framework. *Separation and Purification Technology*, 141, 150–159.

Conder, J.R., Young, C.L., 1979. Physicochemical Measurement by Gas Chromatography, John Wiley and Sons

Do, D.D., 1998. Adsorption Analysis: Equilibria and Kinetics, Imperial College Press, London

Dunne, J. A., Mariwala, R., Rao, M., Sircar, S., Gorte, R.J., Myers, A.L., 1996. Calorimetric heats of adsorption and adsorption isotherms. 1. O_2, N_2, Ar, CO_2, CH_4, C_2H_6, and SF_6 on silicalite. *Langmuir*, 12, 5888–5895.

Eić, M., Ruthven, D.M., 1988. A new experimental technique for measurement of intracrystalline diffusivity, *Zeolites*, 8, 40-45.

Garces, S. I., Villarroel-Rocha, J., Sapag, K., Korili, S.A., Gil, A., 2013. Comparative study of the adsorption equilibrium of CO_2 on microporous commercial materials at low pressures. *Ind. Eng. Chem. Res.*, 52, 6785-6793.

Giesy, J. T., Wang Y., LeVan M. D., 2012. Measurement of Mass Transfer Rates in Adsorbents: New Combined-Technique Frequency Response Apparatus and Application to CO_2 in 13X Zeolite. *Ind. Eng. Chem. Res.*, 51, 11509-11517.

Grenier Ph., Malka-Edery A., Bourdin V., 1999. A Temperature Frequency Response Method for Adsorption Kinetic Measurements. *Adsorption* 5, 135.

Grob, R.L., Barry, E.F., 2004. Modern Practice of Gas Chromatography, Fourth Edition, John Wiley and Sons

Humprey J.L., Keller G.E. , 1997. Separation Process Technology, McGraw-Hill

IAS home page, 1999. International Adsorption Society, http://ias.vub.ac.be/

Ilić, M., Petkovska, M., Seidel-Morgenstern, A., 2007a. Nonlinear frequency response method for estimation of single solute adsorption isotherms. Part I. Theoretical basis and simulations. *Chem. Eng. Sci*., 62, 4379-4393.

Ilić, M., Petkovska, M., Seidel-Morgenstern, A., 2007b. Nonlinear frequency response method for estimation of single solute adsorption isotherms. Part II. Experimental study. *Chem. Eng. Sci*., 62, 4394-4408.

Ilić, M., Petkovska, M., Seidel-Morgenstern, A., 2007c. Theoretical investigation of the adsorption of a binary mixture in a chromatographic column using the nonlinear frequency response technique. *Adsorption*, 13, 541-567.

Ilić, M., Petkovska, M., Seidel-Morgenstern, A., 2008. Estimation of single solute adsorption isotherms applying the nonlinear frequency response method using non-optimal frequencies. *Journal of Chromatography A*, 1200, 183-192.

Ilić, M., Petkovska, M., Seidel-Morgenstern, A., 2009. Determination of competitive adsorption isotherms applying the nonlinear frequency response method. Part II. Experimental demonstration. *Journal of Chromatography A*, 1216, 6108-6118.

Jentys, A., Tanaka, H., Lercher, J. A., 2005. Surface processes during sorption of aromatic molecules on medium pore zeolites. *Journal of Physical Chemistry B*, 109, 2254-2261.

Jordan D.W., Smith P., 2007. Non-Linear Ordinary Differential Equations: Introduction for Scientists and Engineers (4th ed.), Oxford University Press

Jordi, R. G., Do, D. D., 1994. Analysis of the frequency response method applied to non-isothermal sorption studies. *Chem. Eng. Sci*., 49, 957–979.

Kadyk, T., Hanke-Rauschenbach, R., Sundmacher, K., 2012. Nonlinear frequency response analysis of dehydration phenomena in polymer electrolyte membrane fuel cells. *International Journal of Hydrogen Energy*, 37, 7689-7701.

Karge, H.G., Weitkamp, J. (Eds.), 2008. Molecular Sieves Science and Technology 7, Adsorption and Diffusion, Springer

Katsanos, N.A., 1988. Flow Perturbation Gas Chromatography, Chromatographic Science Series 42, Marcel Dekker Inc.

Kärger, J., 2003. Measurement of Diffusion in Zeolites—A Never Ending Challenge, *Adsorption* 9, 29–35.

Kärger, J., Ruthven, D.M., 1992. Diffusion in Zeolites and Other Microporous Solids, John Wiley and Sons, New York

Keller, J., Staudt, R., 2005. Gas Adsorption Equilibria: Experimental Methods and Adsorption Isotherms, Springer Science + Business Media, Inc.

Keller J. U., 1995. Theory of Measurement of Gas-Adsorption Equilibria by Rotational Oscillations. *Adsorption*, 1 , 283-290.

Kiselev, A.V., Yashin, Y.I., 1969. Gas-Adsorption Chromatography, Plenum Press

Lee, G. M., 1997. Estimation of Nonlinear System Parameters Using Higher-Order Frequency Response Functions, *Mechanical Systems and Signal Processing*, 11, 219-228.

Leonaritis I.J., Billings, S.A., 1985. Input-output parametric models for non-linear systems, *International Journal of Control*, 41, 303-344.

LeVan, M.D., 1998. Adsorption processes and modeling: present and future, in: Fundamentals of Adsorption 6, F. Meunier (ed.), 19-29, Elsevier, Paris

Liu, J., Wang, Y., Benin, A. I., Jakubczak, P., Willis, R. R., LeVan, M. D., 2010. CO_2/H_2O adsorption equilibrium and rates on metal-organic frameworks: HKUST-1 and Ni/DOBDC. *Langmuir*, 26, 14301-14307.

MKS Product Catalogue *(www.mksins.com*)

Mofarahi, M., Bakhtyari, A., 2015. Experimental Investigation and Thermodynamic Modeling of CH4/N2 Adsorption on Zeolite 13X, *J. Chem. Eng. Data* 60, 683−696.

Naphtali, L.M., Polinski, L.M., 1963. A novel technique for characterisation of adsorption rates on heterogeneous surfaces. *J. Phys. Chem.* 67, 369-375.

Niessen, W., Karge, H.G., 1993. Diffusion of p-xylene in single and binary systems in zeolites investigated by FTIR spectroscopy, *Microporous Mater.* 1, 1-8.

Nikolić, D., Seidel-Morgenstern, A., Petkovska, M., 2014a. Nonlinear frequency response analysis of forced periodic operations of non-isothermal CSTR using single input modulations. Part I: Modulation of inlet concentration or flow-rate. *Chem. Eng. Sci.* 117, 71–84.

Nikolić, D., Seidel-Morgenstern, A., Petkovska, M., 2014b. Nonlinear frequency response analysis of forced periodic operations of non-isothermal CSTR with single input modulations. Part II: Modulation of inlet temperature or temperature of the cooling/heating fluid. *Chem. Eng. Sci.* 117, 31–44.

Nikolić, D., Seidel-Morgenstern, A., Petkovska, M., 2015. Nonlinear frequency response analysis of forced periodic operation of non-isothermal CSTR with simultaneous modulation of inlet concentration and inlet temperature. *Chem. Eng. Sci.* 137, 40–58.

Onyestyák, G., Shen, D., Rees, L.V.C., 1996. Frequency-response studies of CO_2 diffusion in commercial 5A powders and pellets. *Microporous Mater.* 5, 279-288.

Onyestyák, G., and Rees, L.V.C., 1999. Frequency response study of adsorbate mobilities of different character in various commercial adsorbents, *Journal of Physical Chemistry B* 103(35), 7469-7479.

Onyestyák, G., 2011. Comparison of dinitrogen, methane, carbon monoxide, and carbon dioxide mass-transport dynamics in carbon and zeolite molecular sieves. *Helvetica Chimica Acta* 94, 206-217.

Panić, V. V., Vidaković-Koch, T. R., Andrić, M., Petkovska, M., Sundmacher, K., 2011. Nonlinear frequency response analysis of the ferrocyanide oxidation kinetics. Part II. measurement routine and experimental validation. *Journal of Physical Chemistry C* 115, 17352-17358.

Park, I. S., Petkovska, M., Do, D. D., 1998. Frequency response of an adsorber with the modulationof the inlet molar flow-rate. Part II. A continuous flow adsorber. *Chem. Eng. Sci.* 53, 833-843.

Petkovska, M., 2000. Non-linear frequency response of non-isothermal adsorption controlled by micropore diffusion with variable diffusivity. *J. Serb. Chem. Soc.* 65, 939-961.

Petkovska, M., 2001. Nonlinear frequency response of nonisothermal adsorption systems. *Nonlinear Dynam.* 26, 351-370.

Petkovska, M., 2006. Nonlinear frequency response method for investigation of equilibria and kinetics in adsorption systems. In: Spasic, A.M., Hsu, J.P.(Eds.), Adsorption Systems in Finely Dispersed Particles: Micro Nano and Atto-Engineering. CRC Taylor & Francis, Boca Raton, 283–327.

Petkovska, M., Do, D. D., 1998. Nonlinear frequency response of adsorption systems: Isothermal batch and continuous flow adsorbers. *Chem. Eng. Sci.* 53, 3081-3097.

Petkovska, M., Do, D., 2000. Use of higher-order frequency response functions for identification of nonlinear adsorption kinetics: Single mechanisms under isothermal conditions. *Nonlinear Dynamics* 21, 353-376.

Petkovska, M., Petkovska, L. T., 2003. Use of nonlinear frequency response for discriminating adsorption kinetics mechanisms resulting with bimodal characteristic functions. *Adsorption* 9, 133-142.

Poole, C.F., 2012. Gas Chromatography, Elsevier

Rees, L.V.C., Shen, D., 1993. Characterization of microporous sorbents by frequency-response methods. *Gas Sep. Purif.* 7, 83-89.

Reyes, S.C., Iglesia E., 1994. Frequency Response Techniques for the Characterization of Porous Catalytic Solids, in: Catalysis (11), Spivey J.J., Agarwal, S.K. (Eds), Royal Society of Chemistry, London, 51-83.

Reyes, S.C., Sinfelt, J.H., DeMartin, G.J., Ernst, R.H., 1997. Frequency modulation methods for diffusion and adsorption measurements in porous solids. *J. Phys. Chem. B* 101, 614-622.

Ribeiro, R. P. P. L., Silva, R. J. S., Esteves, I. A. A. C., Mota, J. P. B., 2015. Development, Construction, and Operation of a Multisample Volumetric Apparatus for the Study of Gas Adsorption Equilibrium, *J. Chem. Educ.* 92, 757−761.

Roubani–Kalantzopoulou, F., 2004. Determination of isotherms by gas–solid chromatography- Applications, *Journal of Chromatography A*, 1037, 191–221.

Rouquerol, F., Rouquerol, J., Sing K., 1999. Adsorption by Powders and Porous Solids, Accademic Press, London

Rough, W., 1981. Nonlinear System Theory. The Volterra-Weiner Approach, John Hopkins University Press

Ruthven, D.M., 1984. Principles of adsorption and adsorption processes, John Wiley

Sargent, R.W.H., Whitford, C.J., 1971. Diffusion of carbon dioxide in type 5A molecular sieve. A*dv. Chem. Ser.* 102, 155-163.

Schemmert, U., Kärger, J., Weitkamp, J., 1999. Interference microscopy as a technique for directly measuring intracrystalline transport diffusion in zeolites, *Microporous Mesoporous Mater.* 32, 101-110.

Schetzen M., 1980. The Volterra and Wiener Theories of Non-Linear Systems. John Wiley, New York

Shen, D., Rees, L.V.C., 1991. Adsorption and diffusion of *n*-butane and 2-butyne in silicalite-I, *Zeolites* 11(7), 684-689.

Silva, J. A. C., Ferreira, A., Mendes, P. A. P., Cunha, A. F., Gleichmann, K., Rodrigues, A. E., 2015. Adsorption Equilibrium and Dynamics of Fixed Bed Adsorption of CH_4/N_2 in Binderless Beads of 5A Zeolite, *Ind. Eng. Chem. Res.* 54, 6390−6399.

Siperstein, F., R.J. Gorte, and A.L. Myers, Langmuir, 15, 1570–1576 (1999).

Sircar, S., 2006. Basic Research Needs for Design of Adsorptive Gas Separation Processes, *Ind. Chem. Res.* 45, 5435-5448.

Sircar S., Myers A.L., 2003. Gas separation by Zeolites, in: Handbook of zeolite science and technology, Auerbach, S. M., Carrado, K.A., Dutta,P.K., (Eds.), Marcel Dekker Inc.

Song L., Rees, L. V. C., 1997. Adsorption and transport of n-hexane in silicalite-1 by the frequency response technique*, J. Chem. Soc. Faraday Trans.* 93, 649-657.

Staudt, R., 1994. Analytische und experimentelle Untersuchungen von Adsorptipnsgleichgewichten von reinen Gasen und Gasgemischen an Aktivkohlen und Zeolithen. Dissertation at the Universität- Gesamthochschule-Siegen

Staudt R., Rave H., Keller J. U., 1999. Impedance Spectroscopic Measurements of Pure Gas Adsorption Equilibria on Zeolites, *Adsorption*, 5, 159-167.

Storer, D.M., 1991. Dynamic Analysis of Non-linear Structures Using Higher-order Frequency Response Functions, PhD Thesis, University of Manchester

Sun, L. M., Bourdin, V., 1993. Measurement of intracrystaline diffusion by the frequency response method: Analysis and interpretation of bimodal response curves. *Chem. Eng. Sci.* 48, 3783-3793.

Sun, L.M., Meunier F., Kärger J., 1993. On the heat effect in measurements of sorption kinetics by the frequency response method. *Chem. Eng. Sci.* 48, 715-722.

Sun, L.M., Meunier F., Grenier, Ph., Ruthven, D.M., 1994. Frequency response for nonisothermal adsorption in biporous pellets, *Chem. Eng. Sci.* 49(3), 373-381.

Suzuki, M., 1996. Application of Adsorption Technology for Environmental Control, in: Fundamentals of Adsorption, M.D. LeVan (Ed), Kluwer Acad. Pub., Boston, MA, 3-14.

Sward, B. K., LeVan, M. D., 2003. Frequency response method for measuring mass transfer rates in adsorbents via pressure perturbation. *Adsorption* 9, 37-54.

Thomas, W.J., Crittenden, B. Adsorption Technology and Design, Elsevier Science &Technology Books, 1998.

Tlili, N., Grevillot, G., Vallieres, C., 2009. Carbon dioxide capture and recovery by means of TSA and/or VSA. *Int. J. Greenhouse Gas Control* 3, 519-527.

Tranter, T.J., Herbst, R.S., Todd, T.A., Olson, A.L., Eldredge, H.B., 2003. Application of a second order kinetic model for the preliminary design of an adsorption bed system using ammonium molybdophosphate-polyacrylonitrile for the removal of 137Cs from acidic nuclear waste solutions, *Advances in Environmental Research* 7 (4), 913-923.

Turner M.D., Capron L., Laurence R. L., Conner Wm. C., 2001. The design and construction of a frequency response apparatus to investigate diffusion in zeolites. *Rev. Sci. Instrum.* 72, 4424-4433.

Vidaković-Koch, T. R., Panić, V. V., Andrić, M., Petkovska, M., Sundmacher, K., 2011. Nonlinear frequency response analysis of the ferrocyanide oxidation kinetics. Part I. theoretical analysis. *Journal of Physical Chemistry C* 115, 17341-17351.

Wang, Y., Sward, B.K., LeVan, M.D., 2003. New frequency response method for measuring adsorption rates via pressure modulation: Application to oxygen and nitrogen in a carbon molecular sieve. *Ind. Eng. Chem. Res.* 42(18), 4213-4222.

Weiner, D. D., Spina, J. F., 1980. Sinusoidal Analysis and Modelling of Weakly Nonlinear Circuits. Van Nostrand Reinhold Company, New York

Yang, J., Lee, C., Chang, Y., 1997. Separation of hydrogen mixtures by a two-bed pressure swing adsorption process using zeolite 5A. *Ind. Eng. Chem. Res.* 36, 2789-2798.

Yasuda, Y., 1989. Frequency response method for study of a heterogeneous catalytic reaction of gases. *Journal of Physical Chemistry* 93, 7185–7190.

Yasuda, Y., 1994. Frequency Response Method for Investigation of Gas/Surface Dynamic Phenomena. *Heterogen. Chem. Rev.* 1, 103–124.

Yasuda Y., Suzuki Y., Fukada H., 1991. Kinetic details of a gas/porous adsorbent system by the frequency response method. *Journal of Physical Chemistry* 95, 2486-2492.

Yasuda, Y., 1976. Frequency response method for study of the kinetic behaviour of a gas-surface system. 2. An ethylene-on-zinc oxide system. *J. Phys. Chem.* 80, 1870-1875.

Yasuda, Y., Nomura, K., 1993. Frequency response method for study of kinetic details of a heterogeneous catalytic reaction of gases. 2. A methanol conversion to olefins, *Journal of Physical Chemistry* 97, 3319–3323.

Young, D.M., Crowell, A.D., 1962. Physical Adsorption of Gases. London: Butterworths

Zhu, J., Jiang, L., Dai, C., Yang, N., Lei, Z., 2015. Gas adsorption in shaped zeolitic imidazolate framework-8, *Chinese Journal of Chemical Engineering* 23, 1275-1282.

Biography of the author

Danica V. Brzić was born on 22nd November 1973 in Belgrade, Serbia. She graduated from the Department of Chemical Engineering, Faculty of Technology and Metallurgy, University of Belgrade, in 1999, with average grade 9.03/10. She finished the postgraduate studies at the same Department in 2004, with *MSc* thesis entitled "*Partial oxidation of ethane in a fluidized bed*".

Danica Brzić has been employed at Faculty of Technology and Metallurgy, University of Belgrade, since the year 2000, as a teaching assistant. She has been involved in teaching of following subjects: *Unit operations*, *Transport Phenomena in Multiphase systems* and *Chemical Engineering Laboratory*. Besides teaching activities, she has participated in research projects regarding Transport Phenomena in Multiphase systems, funded by Ministry of Science and Technology (Republic of Serbia). In 2008-2009 she participated in a collaborative project between Faculty of Technology and Metallurgy and German company BASF SE*"Experimental investigation of mass transport limitations in adsorption, based on the Nonlinear Frequency Response method"*. In the frame of this project, she spent one year as a PhD student in the R&D Department of BASF SE in Ludwigshafen.

Danica Brzić was awarded a scholarship from German Service for Academic Exchange (DAAD) for research stay in duration of six months at Technical University in Dresden in 2006. She also spent six months (2003/2004) as a visiting scholar at Otto-von-Guericke University of Magdeburg in the frame of project *"Membrane supported reaction engineering"* funded by German Research Society (DFG).

Danica Brzić speaks English and German languages.

Danica Brzić is autor or co-author of nine highly rated scientific articles as well as several contributions to the international conferences in the field of Chemical Engineering.

Прилог 1.

Изјава о ауторству

Потписани-а Danica Brzić

број индекса _____

Изјављујем

да је докторска дисертација под насловом

"PRIMENA NELINEARNE FREKVENTNE METODE NA ISPITIVANJE RAVNOTEŽE I KINETIKE ADSORPCIONIH SISTEMA GAS-ČVRSTO"

"APPLICATION OF NONLINEAR FREQUENCY RESPONSE METHOD FOR INVESTIGATION OF EQUILIBRIUM AND KINETICS OF GAS-SOLID ADSORPTION ".

- резултат сопственог истраживачког рада,
- да предложена дисертација у целини ни у деловима није била предложена за добијање било које дипломе према студијским програмима других високошколских установа,
- да су резултати коректно наведени и
- да нисам кршио/ла ауторска права и користио интелектуалну својину других лица.

Потпис докторанда

У Београду, 07.04.2016.

_____

Прилог 2.

Изјава о истоветности штампане и електронске верзије докторског рада

Име и презиме аутора Danica Brzić

Број индекса _____

Студијски програм Hemija i hemijska tehnologija

Наслов рада: "PRIMENA NELINEARNE FREKVENTNE METODE NA ISPITIVANJE RAVNOTEŽE I KINETIKE ADSORPCIONIH SISTEMA GAS-ČVRSTO"

"APPLICATION OF NONLINEAR FREQUENCY RESPONSE METHOD FOR INVESTIGATION OF EQUILIBRIUM AND KINETICS OF GAS-SOLID ADSORPTION ".

Ментор Prof.dr Menka Petkovska

Потписани/а Danica Brzić

Изјављујем да је штампана верзија мог докторског рада истоветна електронској верзији коју сам предао/ла за објављивање на порталу **Дигиталног репозиторијума Универзитета у Београду.**

Дозвољавам да се објаве моји лични подаци везани за добијање академског звања доктора наука, као што су име и презиме, година и место рођења и датум одбране рада.

Ови лични подаци могу се објавити на мрежним страницама дигиталне библиотеке, у електронском каталогу и у публикацијама Универзитета у Београду.

Потпис докторанда

У Београду, 07.04.2016.

_____

Прилог 3.

Изјава о коришћењу

Овлашћујем Универзитетску библиотеку „Светозар Марковић“ да у Дигитални репозиторијум Универзитета у Београду унесе моју докторску дисертацију под насловом:

"PRIMENA NELINEARNE FREKVENTNE METODE NA ISPITIVANJE RAVNOTEŽE I KINETIKE ADSORPCIONIH SISTEMA GAS-ČVRSTO"

"APPLICATION OF NONLINEAR FREQUENCY RESPONSE METHOD FOR INVESTIGATION OF EQUILIBRIUM AND KINETICS OF GAS-SOLID ADSORPTION ".

која је моје ауторско дело.

Дисертацију са свим прилозима предао/ла сам у електронском формату погодном за трајно архивирање.

Моју докторску дисертацију похрањену у Дигитални репозиторијум Универзитета у Београду могу да користе сви који поштују одредбе садржане у одабраном типу лиценце Креативне заједнице (Creative Commons) за коју сам се одлучио/ла.

1. Ауторство

2. Ауторство - некомерцијално

3. Ауторство – некомерцијално – без прераде

4. Ауторство – некомерцијално – делити под истим условима

5. Ауторство – без прераде

6. Ауторство – делити под истим условима

(Молимо да заокружите само једну од шест понуђених лиценци, кратак опис лиценци дат је на полеђини листа).

Потпис докторанда

У Београду, 07.04.2016.

1. Ауторство - Дозвољавате умножавање, дистрибуцију и јавно саопштавање дела, и прераде, ако се наведе име аутора на начин одређен од стране аутора или даваоца лиценце, чак и у комерцијалне сврхе. Ово је најслободнија од свих лиценци.

2. Ауторство – некомерцијално. Дозвољавате умножавање, дистрибуцију и јавно саопштавање дела, и прераде, ако се наведе име аутора на начин одређен од стране аутора или даваоца лиценце. Ова лиценца не дозвољава комерцијалну употребу дела.

3. Ауторство - некомерцијално – без прераде. Дозвољавате умножавање, дистрибуцију и јавно саопштавање дела, без промена, преобликовања или употребе дела у свом делу, ако се наведе име аутора на начин одређен од стране аутора или даваоца лиценце. Ова лиценца не дозвољава комерцијалну употребу дела. У односу на све остале лиценце, овом лиценцом се ограничава највећи обим права коришћења дела.

4. Ауторство - некомерцијално – делити под истим условима. Дозвољавате умножавање, дистрибуцију и јавно саопштавање дела, и прераде, ако се наведе име аутора на начин одређен од стране аутора или даваоца лиценце и ако се прерада дистрибуира под истом или сличном лиценцом. Ова лиценца не дозвољава комерцијалну употребу дела и прерада.

5. Ауторство – без прераде. Дозвољавате умножавање, дистрибуцију и јавно саопштавање дела, без промена, преобликовања или употребе дела у свом делу, ако се наведе име аутора на начин одређен од стране аутора или даваоца лиценце. Ова лиценца дозвољава комерцијалну употребу дела.

6. Ауторство - делити под истим условима. Дозвољавате умножавање, дистрибуцију и јавно саопштавање дела, и прераде, ако се наведе име аутора на начин одређен од стране аутора или даваоца лиценце и ако се прерада дистрибуира под истом или сличном лиценцом. Ова лиценца дозвољава комерцијалну употребу дела и прерада. Слична је софтверским лиценцама, односно лиценцама отвореног кода.